Study of the Effects Produced by Time Modulation Applied to an Antenna Array in Digital Transmission Systems

Roberto Maneiro Catoira

Doctoral Thesis UDC / 2017

Advisors: Julio Claudio Brégains Rodríguez
José Antonio García Naya

PhD Program in Information Technology and Mobile Network Communication

Estudo dos Efectos Producidos pola Modulación Temporal Aplicada a unha Agrupación de Antenas en Sistemas de Transmisión Dixital

Roberto Maneiro Catoira

Tese de Doutoramento UDC / 2017

Directores: Julio Claudio Brégains Rodríguez
José Antonio García Naya

Programa de Doutoramento en Tecnoloxías da Información e das Comunicacións en Redes Móbiles

UNIVERSIDADE DA CORUÑA

Estudio de los Efectos Producidos por la Modulación Temporal Aplicada a una Agrupación de Antenas en Sistemas de Transmisión Digital

Roberto Maneiro Catoira

Tesis Doctoral UDC / 2017

Directores: Julio Claudio Brégains Rodríguez
José Antonio García Naya

Programa de Doctorado en Tecnologías de la Información y de las Comunicaciones en Redes Móviles

Roberto Maneiro Catoira

CERTIFICA / *CERTIFICA* / *CERTIFIES*

Que a presente memoria é o resultado do meu propio traballo de investigación e que o traballo doutros autores está citado axeitadamente.

Que la presente memoria es el resultado de mi propio trabajo de investigación y que el trabajo de otros autores está citado apropiadamente.

That the present report is the result of my own research work and that the work done by other authors is appropriately cited.

A Coruña, 6 de xuño de 2017 / *6 de junio de 2017* / *June 6th, 2017*

Roberto Maneiro Catoira

Julio Claudio Brégains Rodríguez
José Antonio García Naya

CERTIFICAN / *CERTIFICAN* / *CERTIFY*

Que a presente tese titulada "Estudo dos efectos producidos pola modulación temporal aplicada a unha agrupación de antenas en sistemas de transmisión dixital" foi realizada por Roberto Maneiro Catoira baixo a nosa dirección no Departamento de Enxeñaría de Computadores da Universidade da Coruña e preséntase para obter o grao de Doutor.

Que la presente tesis titulada "Estudio de los efectos producidos por la modulación temporal aplicada a una agrupación de antenas en sistemas de transmisión digital" fue realizada por Roberto Maneiro Catoira bajo nuestra dirección en el Departamento de Ingeniería de Computadores de la Universidade da Coruña y se presenta para obtener el grado de Doctor.

That the present thesis titled "Study of the effects produced by time modulation applied to an antenna array in digital transmission systems" was done by Roberto Maneiro Catoira under our supervision in the Department of Computer Engineering at the University of A Coruña and it is submitted to obtain the Ph.D. degree.

Os directores da tese / *Los directores de la tesis* / *The Ph.D. supervisors*.
A Coruña, 6 de xuño de 2017 / *6 de junio de 2017* / *June 6th, 2017*.

Dr. Julio Claudio Brégains Rodríguez
Prof. Contratado Doutor
Dpto. de Enxeñaría de Computadores
Universidade da Coruña

Associate Professor
Dept. of Computer Engineering
University of A Coruña

Dr. José Antonio García Naya
Prof. Contratado Doutor
Dpto. de Enxeñaría de Computadores
Universidade da Coruña

Associate Professor
Dept. of Computer Engineering
University of A Coruña

Tese de Doutoramento / *Tesis Doctoral* / *Doctoral Thesis*

Título:	Estudo dos efectos producidos pola modulación temporal aplicada a unha agrupación de antenas en sistemas de transmisión dixital
***Título*:**	*Estudio de los efectos producidos por la modulación temporal aplicada a una agrupación de antenas en sistemas de transmisión digital*
***Title*:**	*Study of the effects produced by time modulation applied to an antenna array in digital transmission systems*
Autor / *Autor* / *Author*:	Roberto Maneiro Catoira
Directores / *Directores* / *Supervisors*:	Julio Claudio Brégains Rodríguez José Antonio García Naya
Data / *Fecha* / *Date*:	6 de xuño de 2017 / *6 de junio de 2017* / *June 6th, 2017*

Tribunal / *Tribunal* / *Evaluation Committee*

Presidente / *Presidente* / *President*:	Ignacio Santamaría Caballero
Vogal / *Vocal* / *Member*:	Paolo Rocca
Secretaria / *Secretaria* / *Secretary*:	Nuria González Prelcic

To my family

Acknowledgements

In essence, this doctoral thesis has been possible thanks to the technical excellence, the meticulousness, the compromise and the great generosity of three people: my two thesis advisors, Julio Claudio Brégains Rodriguez and José Antonio García Naya, as well as the professor Luis Castedo Ribas. The three are co-authors of each and every one of the works associated with this thesis. Thanks to them, I have discovered and I can enjoy my true vocation: research. Gentlemen (that´s the way I use to address them), it is a privilege to be part of a quartet that already compose symphonies that fuse the nonlinearities of Time-Modulated (TMAs) with the always cult genre of digital communications...

I am aware, and I want to show my gratitude, for the opportunities given to present our works in such spectacular places as Memphis, Vancouver, Puerto Rico or San Diego, as well as for other extraordinary experiences derived from this thesis, like hiking, together with my children, through the Cimasera, in the Italian Alps, guided by the colleagues of the University of Trento.

Precisely, and in reference to my stays in Italy, I want to thank the Doctors Paolo Rocca and Lorenzo Poli, as well as the Professor Massa, their hospitality and all they have taught me at both human and technical levels.

Thanks to whom are my LIFE: my wife, Emilia, and my children, Alejandra and Roberto. I owe you time...

Thanks to my mother, to my father (who wherever may be, he will be emotional) and my brother Jorge, who although he does not have the capacity to read, I fervently wish that he was part of these lines. Walking with him through our Vilagarcía port, I discovered, in a wall dedicated to street art, a quote by Fernando Pessoa that identifies, largely and from a cosmogonic point of view, what this thesis has meant for me:

I am nothing.
I'll never be anything.
I couldn't want to be something.
Apart from that, I have in me all the dreams in the world . . .

Fernando Pessoa, The Tobacconist's, 1928.

Resumo

Os selos de identidade das comunicacións móbiles e sen fíos de hoxe en día son a demanda continua e crecente de mobilidade, capacidade e fiabilidade, xunto cun firme e definitivo compromiso coa sustentabilidade. Baixo estas premisas, as antenas intelixentes –capaces de *sensar* a contorna electromagnética e adaptar de xeito eficaz as súas características de radiación– están chamadas a xogar un papel crucial nas ditas comunicacións. Neste senso, os estándares sen fíos actuais consideran técnicas multi-antena encamiñadas a explotar a diversidade espacial, o multiplexado espacial e o conformado de feixe, acadando así mellores niveis de fiabilidade e capacidade.

Con todo, ditas vantaxes obtéñense a expensas dun incremento da complexidade do sistema, factor non sempre asumible en termos de tamaño e eficiencia enerxética. Consecuentemente, suscítanse unha serie de retos de cara a desenvolver tecnoloxías de antena axeitadas e capaces de dar resposta ás anteriores prestacións no espazo limitado que dita a mobilidade.

O concepto de agrupación de antenas modulada temporalmente (TMAs, do inglés *time-modulated arrays*) é unha técnica multi-antena que achega unha simplificación hardware significativa: o seu diagrama de radiación contrólase mediante a sinxela aplicación de pulsos periódicos de duración variable ás excitacións individuais da agrupación. A natureza non lineal desta operación causa a aparición de diagramas de radiación nas frecuencias harmónicas dos pulsos periódicos aplicados. A técnica pode empregarse para mellorar a topoloxía do nivel dos lóbulos secundarios do diagrama de radiación na frecuencia central e/ou para explotar de xeito proveitoso os diagramas dos harmónicos, dotando á antena de capacidades de antena intelixente.

Esta tese é o resultado dunha investigación das TMAs dende unha perspectiva interdisciplinaria, é dicir, non soamente dende a óptica do diagrama de radiación ou das agrupacións de antenas, senón tamén dende un punto de vista de procesado do sinal. Máis concretamente, a tese é unha análise en profundidade da aplicación das TMAs ás comunicacións dixitais, desenvolvida en catro etapas: 1) análise matemática da posibilidade de transmitir sinais dixitais mediante TMAs, identificando as restricións para salvagardar a integridade do sinal e cuantificando a potencia radiada, 2) caracterización da taxa de erro de bit dun sistema de comunicación dixital que incorpora un TMA en recepción explotando o seu modo fundamental e considerando canles con ruído branco Gaussiano, 3) estudo das prestacións das TMAs –explotando os harmónicos– na recepción de sinais de comunicación dixitais con diversidade angular en canles multitraxecto con esvaecemento, 4) caracterización de TMAs para conformado de feixe mediante o uso de pulsos de suma de cosenos ponderados no lugar de pulsos rectangulares, chegando ás denominadas TMAs melloradas, dotadas dunha resposta superior en termos de flexibilidade e eficiencia.

Resumen

Hoy en día, los sellos de identidad de las comunicaciones inalámbricas son la demanda continua y creciente de movilidad, capacidad y fiabilidad, junto con un firme y definitivo compromiso con la sostenibilidad. Bajo estas premisas, las antenas inteligentes –capaces de *sensar* el entorno electromagnético y adaptar de forma eficaz sus características de radiación– están llamadas a jugar un papel crucial en dichas comunicaciones. En este sentido, los estándares inalámbricos actuales consideran técnicas multiantena encaminadas a explotar la diversidad espacial, el multiplexado espacial o el conformado de haz, alcanzando así mejores niveles de fiabilidad y capacidad.

Sin embargo, dichas ventajas se obtienen a expensas de un incremento de la complejidad del sistema, factor no siempre asumible en términos de tamaño y eficiencia energética. En consecuencia, se plantean una serie de retos en el desarrollo de tecnologías de antena adecuadas, capaces de dar respuesta a las anteriores prestaciones en el espacio limitado que dicta la movilidad.

El concepto de agrupación de antenas modulada temporalmente (TMAs, del inglés *time-modulated arrays*) es una técnica multiantena que aporta una simplificación hardware significativa: su diagrama de radiación se controla mediante la sencilla aplicación de pulsos periódicos de duración variable a las excitaciones individuales de la agrupación. La naturaleza no lineal de esta operación causa la aparición de diagramas de radiación en las frecuencias armónicas de los pulsos periódicos aplicados. La técnica se puede utilizar para mejorar la topología del nivel de los lóbulos secundarios del diagrama de radiación en la frecuencia central y/o para explotar de forma beneficiosa los diagramas de armónicos, dotando a la antena de capacidades de antena inteligente.

Esta tesis es el resultado de una investigación de las TMAs desde una perspectiva interdisciplinar, es decir, no solamente desde la óptica del diagrama de radiación o de las agrupaciones de antenas, sino también desde un punto de vista de procesado de señal. Más concretamente, la tesis es un análisis en profundidad de la aplicación de las TMAs a las comunicaciones digitales, desarrollada en cuatro etapas: 1) análisis matemático de la factibilidad de transmitir señales digitales mediante TMAs, identificando las restricciones para salvaguardar la integridad de la señal y cuantificando la potencia radiada, 2) caracterización de la tasa de error de bit de un sistema de comunicación digital que incorpora una TMA en recepción explotando su modo fundamental y considerando canales con ruido blanco Gaussiano, 3) estudio de las prestaciones de las TMAs –explotando los armónicos– en la recepción de señales digitales con diversidad angular en canales multitrayecto con desvanecimiento, 4) caracterización de TMAs para conformado de haz mediante el uso de pulsos de suma de cosenos ponderados en lugar de pulsos rectangulares, llegando a las denominadas TMAs mejoradas, dotadas de una respuesta superior en términos de flexibilidad y eficiencia.

Abstract

An ever-increasing demand for higher mobility, capacity and reliability, together with a definitive compromise with sustainability, are the hallmarks of mobile and wireless communications systems nowadays. Under these premises, smart antenna devices –capable of sensing the electromagnetic environment and suitably adapting its radiation features– are correspondingly called to play a crucial role. In this sense, today's wireless standards consider multiple-antenna techniques in order to exploit space diversity, spatial multiplexing and beamforming to achieve better levels of reliability and capacity. Such advantages, however, are obtained at the expense of increased system complexity which may be unaffordable in terms of size and energy efficiency. Consequently, some technical challenges remain to develop the adequate antenna technologies capable of supporting the aforementioned features in a limited physical space that the mobility demand dictates.

The concept of time-modulated array (TMA) is a feasible multi-antenna technique that provides a significant hardware simplification: its radiated power pattern is controlled by the simple application of variable-width periodical pulses to the individual array excitations. The nonlinear nature of such an array operation causes the appearance of radiation patterns at the harmonic frequencies of the applied periodic pulses. The technique can be used for improving the side-lobe level topology of the radiation pattern at the central frequency and/or to profitably exploit the harmonic patterns in order to supply smart antenna capabilities.

This thesis is the result of an investigation of TMAs from an interdisciplinary perspective, i.e., not only under a radiation pattern or an antenna array outlook but also from a signal processing point of view. More specifically, the thesis deals with an in-depth analysis of the application of TMAs in digital communications developed in four stages: 1) mathematical analysis of the feasibility of transmission of digital signals over TMAs, identifying the restrictions to safeguard the integrity of the signal and quantifying the radiated power, 2) characterization of the bit error rate of a digital communication system that incorporates a receive-TMA exploiting its fundamental mode and considering additive white Gaussian noise channels, 3) study of the performance of TMAs –exploiting their harmonics– for the angle diversity reception of digital communication signals over multipath fading channels, 4) an approach to the characterization of beamforming TMAs which use sum of weighted cosines pulses instead of rectangular ones, leading to the so-called enhanced time-modulated arrays, which endows them with a better response in terms of flexibility and efficiency.

Table of Contents

List of Figures

List of Tables

Chapter 1

Introduction

Wireless services demanding more mobility, capacity, and robustness have placed wireless communications as the fastest growing sector of the telecommunication industry nowadays[1]. As a result, the increasingly limited wireless medium has to be smartly exploited and antennas are called to play an important role to achieve such a goal. A proper combination of antenna features and signal processing allows us to jointly and efficiently act in the space, frequency, and time domains in order to provide suitable alternatives to the complex task of faithfully receiving the desired signals and efficiently mitigating the unwanted ones.

One of the primary objectives of an intelligent system supported by a sensor network is its sustainability. The investigation of new technologies allowing for reducing the power consumption of sensor networks is aimed towards the design of smart antennas with low loss, muting and adaptive beamforming features. Additionally, such a smart antenna technology has to consider the hardware complexity, making the solution feasible in the context of sensors. Moreover, antenna devices pertaining to sensor networks must be capable of sensing the external electromagnetic environment, thus properly reconfiguring the radiation characteristics of the generated field to guarantee both the required quality of service of the communication link and a reduced power consumption.

However, some technical challenges remain when it comes to develop the adequate antenna technologies capable of supporting the aforementioned features in a limited physical space that the mobility demand dictates. In fact, today's wireless standards consider multiple-antenna techniques [RENZO 2014; HEATH 2016; MÉNDEZRIAL 2016] in order to exploit space diversity, spatial multiplexing and beamforming to achieve better levels of reliability and capacity. Such advantages, however, are obtained at the expense of increased system complexity, which may be unaffordable in small-size and low-cost sensor devices with a required low-power consumption.

The concept of time-modulated array (TMA) is a feasible multi-antenna technique that provides a significant hardware simplification. Furthermore, TMAs, typified among

[1] Sections 1.1 and 1.2 are based on the co-authored publication [MANEIROCATOIRA 2017c]

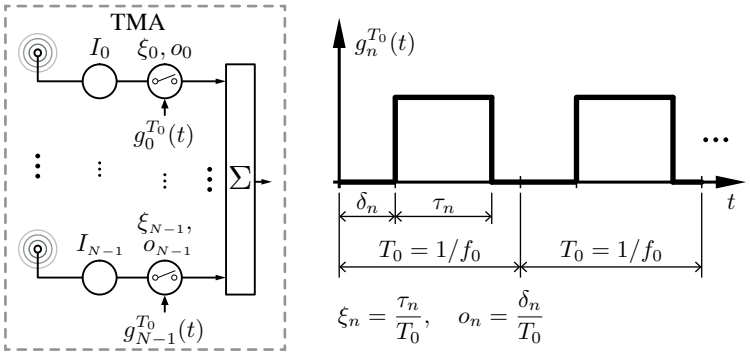

Figure 1.1: On the left hand side, the block diagram of a linear TMA with N elements implemented with radio frequency (RF) switches, with I_n being the static excitation of the n-th element of the array. On the right hand side, the periodic (T_0) pulse train that governs the n-th switch, $g_n^{T_0}(t)$, which is characterized by the normalized pulse duration ξ_n and the normalized switch-on instant o_n.

unconventional phased arrays architectures, have been intensively researched during the last years at an increasing pace [ROCCA 2016].

1.1 What is a TMA?

TMAs, in their simplest configuration, are antenna arrays whose radiated power patterns are controlled by periodically enabling and disabling the excitations of the individual array elements, as illustrated in Fig. 1.1. TMAs simplify considerably hardware implementations since they can be done with switches rather than the complex weight multiplications of conventional array feeding networks.

The TMA radiated field with N isotropic elements distributed along the z axis is given by [KUMMER 1963]

$$F(\theta, t) = \mathrm{e}^{j2\pi f_c t} \sum_{n=0}^{N-1} g_n^{T_0}(t) I_n \mathrm{e}^{jkz_n \cos\theta} \in \mathbb{C}, \tag{1.1}$$

where $g_n^{T_0}(t)$ is a periodic function with a fundamental period $T_0 = 1/f_0$, which governs the n-th array element, with $n = 0, \ldots, N-1$; $I_n = |I_n|\mathrm{e}^{j\varphi_n}$ and z_n represent the n-th antenna element complex static current excitation in its polar form ($|I_n|$ is its modulus and φ_n is its phase) and the position on the z axis, respectively; f_c is the carrier frequency of the incoming signal; θ is the angle with respect to the array main axis; and $k = 2\pi/\lambda$ is the wave number for a wavelength $\lambda = c/f_c$.

Since $g_n^{T_0}$ is a periodic signal, it can be represented by the following exponential Fourier series:

$$g_n^{T_0}(t) = \sum_{q=-\infty}^{\infty} G_{nq} \mathrm{e}^{jq2\pi f_0 t} \in \mathbb{R}, \tag{1.2}$$

where, in a conventional TMA, $g_n^{T_0}(t)$ is a periodic rectangular pulse train with duration τ_n and delay δ_n (see Fig. 1.1). In such a case, G_{nq} is given by [POLI 2011b]

$$G_{nq} = \xi_n \mathrm{sinc}(q\pi\xi_n)\mathrm{e}^{-jq\pi(\xi_n+2o_n)} \in \mathbb{C}, \tag{1.3}$$

where $\mathrm{sinc}(x) = \sin(x)/x$ denotes the sinc function, $\xi_n = \tau_n/T_0 \in (0,1) \subset \mathbb{R}$ are the normalized pulse durations, and $o_n = \delta_n/T_0 \in [0, 1-\xi_n] \subset \mathbb{R}$ are the normalized pulse delays[2]. Note that for $q = 0$ we have $G_{n0} = \xi_n$. Substituting Eq. (1.2) into Eq. (1.1) allows for rewriting the TMA radiated field as

$$F(\theta,t) = \underbrace{\left[\sum_{n=0}^{N-1} I_n \xi_n \mathrm{e}^{jkz_n\cos\theta}\right]}_{q=0} \mathrm{e}^{j2\pi f_c t} + \\ + \left[\sum_{n=0}^{N-1}\sum_{\substack{q=-\infty \\ q\neq 0}}^{\infty} I_n \underbrace{\xi_n \mathrm{sinc}(q\pi\xi_n)\mathrm{e}^{-jq\pi(\xi_n+2o_n)}}_{G_{nq},\, q\neq 0} \mathrm{e}^{jkz_n\cos\theta}\right] \mathrm{e}^{j2\pi(f_c+qf_0)t}. \tag{1.4}$$

Observe that the first term in Eq. (1.4) is the array factor at the fundamental mode ($q = 0$) frequency f_c, which shows that, by means of the normalized pulse durations ξ_n, we are able to reconfigure exclusively the magnitude of the excitations and thus control the radiation pattern. On the other hand, the second term in Eq. (1.4) reveals the existence of sideband radiation (SR) at frequencies $f_c + qf_0$ (harmonics). Note that by modifying ξ_n and/or o_n we can also control the radiation pattern at each sideband harmonic, in this case being able to simultaneously reconfigure the magnitude and the phase of the excitations. The SR can be either minimized or, as explained in the forthcoming sections, profitably exploited.

TMA Features

As shown above, the periodic modulation of a TMA is a nonlinear operation that generates sideband signals radiated at frequencies shifted from the carrier frequency at multiples of the time-modulation rate f_0. The time parameters which govern the TMA (specifically, the switch-on durations τ_n and the switch-on delays δ_n [TENNANT 2008; AKSOY 2012]) can be optimized to:

1. reconfigure the fundamental pattern only –at the carrier frequency f_c– with the aim of achieving ultra-low side-lobe levels (SLLs) while minimizing the SR, or
2. profitably exploit the harmonic patterns, endowing the TMA with smart antenna capabilities.

Hence, and according to the second point, by adapting the harmonic patterns to the wireless channel, and by combining its corresponding outputs, TMAs are able to perform adaptive

[2] In some cases, and according to the properties of the pulses $g_n^{T_0}(t)$, the dependency on o_n can be avoided, yielding $G_{nq} = \xi_n \mathrm{sinc}(q\pi\xi_n)\mathrm{e}^{-jq\pi\xi_n}$, but in this thesis we consider the general form.

beamforming with the benefit of using a single RF front-end. In this regard, the fact of avoiding the utilization of as many RF chains as the number of multipath components to be exploited, offers a series of key advantages:

- Hardware simplicity, with the subsequent impact on the size and the cost of the system.
- Reduction of power consumption, as it has been remarked and properly quantified in recent papers like [HEATH 2016, Table I] and [MÉNDEZRIAL 2016, Tables I and II], which have also proposed hybrid analog-digital architectures for beamforming. Indeed, in a fully digital implementation of a linear beamforming network (LBFN), the number of required RF chains, L, must be equal to the number of antenna elements N. In practice, however, a relationship $N \gg L$ is often preferable due to a number of reasons, being the power consumption per RF front-end one of the most important ones.
- Nonexistence of issues related to synchronization, phase coherence or coupling between different RF chains.

In summary, the application of periodic pulses at the antenna level has the effect of converting space diversity into frequency diversity and, thus, a single RF front-end is enough to exploit such a space diversity.

1.2 State of the Art

1.2.1 The Origin of the TMA Concept

The pioneering idea of using the time as an additional degree of freedom to control the radiation pattern of an antenna was proposed by Shanks and Bickmore, from the Microwave Laboratory at the Hughes Aircraft Company, California, in 1959 [SHANKS 1959]. The authors introduced theoretically this entirely new idea in antenna design and suggested several possible physical antenna configurations, such as a square wave switched linear array. However, in their first experimental tests, they employed a common parabolic dish antenna and applied a nutation movement to the primary horn with a frequency of 133 Hz. With this technique they achieved a multi-pattern operation obtaining simultaneously a sum diagram at the fundamental frequency and a difference diagram at the first sideband harmonic.

In 1963, Kummer et al. –also from Hughes Aircraft Company– experimentally extended the concept of "time-modulated antenna" to antenna arrays [KUMMER 1963], thus coining the term TMA. They obtained ultra-low side lobe patterns by inserting a set of RF switches –programmed according to a predetermined periodic time sequence– in the feed network of an 8-element waveguide slotted linear array working at the X-band. Kummer et al. stated that the higher the SLL improvement by applying time modulation, the higher the cost in the system gain. The source of this gain cost is the nonlinear nature of the periodic modulation, which inherently generates sideband radiated loss signals (see Eq. (1.4)). Consequently, SR had been primarily identified as a phenomenon that severely degrades the TMA gain. As a matter of

fact, Kummer et al. focused on two representative examples. On the one hand, they selected an initial static Dolph-Tschebyshev pattern with -30 dB SLL improved down to about -40 dB –by applying time modulation implemented by means of RF switches– at the expense of a modest loss in the antenna gain (0.3 dB). On the other hand, they considered a uniform static aperture distribution –with an SLL of -13 dB– improved down to -40 dB through time modulation with a much higher price to be paid (2.4 dB) in terms of the antenna gain. In this way, Kummer et al. have implicitly opened the door to future research that would be focused on minimizing the SR while improving the SLL through the application of suitable optimization processes to the TMA technique.

1.2.2 TMA Design under an (Exclusive) Antenna Perspective

Most of the research works involving TMAs have been developed under an antenna designer point of view. More specifically, they focus on the synthesis of an appropriate shape of the radiation pattern. We therefore classify such works depending on the patterns which are synthesized, i.e., fundamental or harmonics.

Fundamental Mode Pattern

Although it represents a natural and immediate area worth of investigation, the development of methods to minimize the SR did not start until the early 2000s when the first optimization algorithms emerged. The reason is that the sophisticated methods necessary to carry out this kind of optimization arrived simultaneously with the development of more powerful computers. In this sense, Yang et al. introduced in 2002 the TMA synthesis supported by systematic algorithms, capable of optimizing the SLL and the SR simultaneously by using differential evolution algorithms [YANG 2002]. In subsequent works, and with the same optimization objectives, other algorithms were considered: genetic algorithms [YANG 2005a], simulating annealing [FONDEVILA 2004; FONDEVILA 2006], particle swarm optimization [POLI 2010a], and artificial bee colony [MANDAL 2011]. Further works involved additional parameters in the multi-objective optimization, like the half power beam width [MANDAL 2013]. Other innovative –and structurally different– techniques have been recently proposed to minimize the SR based on modulating the RF switches with non-uniform [HE 2015b] or multiple [GUO 2016] time modulation periods.

Later on, an additional degree of freedom was introduced in the synthesis process by considering the switch-on instants of the periodic rectangular pulses –in addition to the pulse durations– applied to the antenna excitations [TENNANT 2008; POLI 2010b]. In [ZHU 2012a] the time modulation period was split into several time steps with variable lengths and, for each time step, the switch-on and switch-off times were optimized via the differential evolution algorithm to improve the SR radiation. In a further development, the impact of the periodic pulses time shift on the SR was theoretically analyzed [AKSOY 2012]. Likewise, hardware

solutions based on sub-arraying techniques [TONG 2011] or the use of fixed bandwidth elements [TONG 2012b], as well as the impact of pulse shaping [BEKELE 2013], were also investigated to reduce the SR.

In addition to linear geometrical configurations, planar and even conformal TMAs were also analyzed and optimized in terms of SLL and SR [YANG 2005b; POLI 2010b; AKSOY 2014; TENNANT 2009], as well as planar adaptive absorbers for radar based on phase-switched screen, whose design was modeled by means of the time-switched array theory [TENNANT 2009].

Another key aspect in the TMA technique is the antenna gain and how is affected by both the SR and the switching network. In [YANG 2004], Yang et al. characterized the TMA gain and quantified the TMA efficiency. More specifically, they separated the switching network efficiency (which accounts for the time fraction that the switches are off) and the TMA power efficiency (the ratio between the fundamental mode mean radiated power and the total mean radiated power, i.e., the useful radiated power divided by the total radiated power) being the total efficiency of the TMA the product of both. In order to improve the switching efficiency, [ZHU 2012b] proposed the utilization of single-pole double-throw (SPDT) switches in such a way that a single RF switch governs two adjacent elements of the array, so that, whenever complementary time sequences are synthesized, the off time is reduced to zero, and consequently the switching efficiency is set to an almost ideal value. More sophisticated structures based on the use of a reconfigurable power divider/combiner have been evaluated in [CHEN 2016a] in order to improve the switching network efficiency of the array.

On the other hand, since the fluctuations of the antenna gain –due to the application of a periodic on–off modulation to the static excitations– may severely affect the behavior of a received signal, some research works focused on the switching sequence, primarily to keep the instantaneous directivity of the main beam constant [MANICA 2009; ROCCA 2012a].

TMAs were also analyzed –exclusively from the radiation properties point of view– so as to be exploited in different applications, e.g., for the suppression of interferences and undesired signals impinging on the antenna aperture. Such a capability of adaptive nulling in time-varying scenarios was evaluated in [POLI 2011a] by Poli et al., and completed in [ROCCA 2012b]. Further examples are the synthesis of the so-called power-patterns for wide coverage purposes [YANG 2003; BALDERAS 2016], or radar applications [LI 2009b; EUZIÈRE 2014].

Apart from all of these applications, tools for a more accurate analysis of TMAs were also developed. In this sense, and in order to evaluate rigorously some nonlinear performance aspects of TMAs as a radiating system (e.g., the effects of mutual coupling between elements) a full-wave computation of the radiated far field was addressed by Masotti et al. in [MASOTTI 2013] by properly developing a multi-domain computer aided design platform. Aligned with this research topic, [YAO 2015a] is devoted to a full-wave analysis of the instantaneous and average behaviors of TMAs.

Harmonic Patterns

As already pointed out, the SR is not necessarily a damaging phenomenon and can be profitably exploited to improve the performance of a TMA. As a matter of fact, the exploitation of the harmonic patterns endows TMAs with smart-antenna capabilities. In this sense, the seminal work by Shanks [SHANKS 1961] theoretically introduced the beam-scanning capabilities of TMAs and, as an example, such features have been efficiently applied to an experimental prototype in [BOGDAN 2016b].

Adaptive beamforming was originally studied from a practical and simplified point of view by Li et al. [LI 2010a], focusing on the harmonic patterns synthesis in [POLI 2011b], and even taking advantage of time redundancy in [TONG 2012a]. Another strategy for beamforming through pulse splitting techniques was investigated in [POLI 2014]. In such a technique, based on particle swarm optimization, two patterns were simultaneously generated: the first one at the central frequency and the second one at a preselected harmonic with an arbitrary order, keeping the SR below a given level. An example of how harmonic beamforming with TMAs can be profitably applied, in this case to blanking in spectrometry and radar, was proposed in [BAROTT 2014].

Beam steering with TMAs was also introduced by Li et al. [LI 2009a], and a more elaborated version, with control of the side-lobe level, was addressed in [TONG 2010]. Applications of beam steering like direction finding or direction of arrival (DOA) estimation were analyzed in [LI 2010b; TENNANT 2010; HE 2015a].

Reflector arrays were also considered for being implemented using time modulation. Wang et al. introduced the concept of time-modulated reflector array (TMRA) in [WANG 2012], which was analyzed more deeply in [WANG 2014]. A TMRA makes use of the topology of a conventional reflector array, i.e., consists of a matrix of scattering elements which are illuminated by a feed horn but, instead of phase shifters, it uses discrete time switching to achieve beam steering or beamforming functions. As a result, the radiation pattern is controlled by adjusting the time-domain scattering. It was also shown that by employing double-layer designs [WANG 2016] it is possible to increase the energy efficiency of TMRAs.

Another interesting field for TMA applications is wireless power transmission, introduced by Masotti et al. in [MASOTTI 2016]. In this case, the real-time beamforming features of TMAs are properly exploited following a two-step procedure: firstly to precisely localize the tag to be powered and subsequently, to perform the directive wireless power transmission.

In recent investigations, the TMA philosophy was involved in more complex hybrid solutions contributing to improve the performance of the overall antenna system. In this way, time modulation was applied –together with I/Q modulation– to phased arrays in order to generate a scanning beam at the single positive sideband [YAO 2015b]. Time modulation was considered, jointly with *retrodirective* techniques, to synthesize *coaperture* antenna arrays [YAO 2016b] and also to obtain time-invariant spatial-fine-focusing beampatterns in frequency diverse arrays [YAO 2016a].

1.2.3 TMA Design under a Signal Processing Perspective

Most of the above-referenced investigations exclusively focus on the synthesis of the antenna patterns. The fundamental and/or the harmonic components are manipulated in some way, without considering the interaction between the TMA technique and the signals sent or received by such an antenna. This subsection is devoted to those works that apply TMAs to wireless communications.

As a starting point, it is necessary to find the signal frequency restrictions, i.e., the relationship between the time modulation frequency, the signal bandwidth, and the carrier frequency that must be satisfied in order to keep the integrity of the signals that are transmitted/received over the TMA. Those restrictions were initially stated by Shanks and Bickmore [SHANKS 1959], and completed by Brégains et al. [BRÉGAINS 2008], where additional closed-form expressions for the total mean SR power and for the TMA power efficiency were properly derived.

The transmission of narrowband amplitude modulation (AM) and frequency modulation (FM) signals was theoretically analyzed by Li et al. [LI 2009c] and, for the case of AM, experimentally demonstrated in [ZHU 2013]. Other specific cases were also investigated like a dual-channel AM receiver [YAVUZ 2015], the transmission of linearly frequency modulated (LFM) signals [GUO 2015], or the feasibility of implementing a dual function of radar and communication [EUZIÈRE 2015; EUZIÈRE 2016].

The TMA technology was also proposed –originally by Zhu et al. –to transmit direction-dependent signals in the context of secure communications [ZHU 2014; ROCCA 2014; HANNAN 2016]. The idea is based on generating a null level of SR in some desired directions and a high level of SR on other directions in order to distort the signal. Conditions of frequency overlapping between the signal replicas placed in adjacent harmonic frequencies must be satisfied, paradoxically contrary to those ones established in [SHANKS 1959].

A first study on the signal-to-noise ratio (SNR) in a system with a receiver TMA was presented in [ZHU 2015] by Zhu et al. This work describes a specific case exploiting the fundamental pattern and the first positive harmonic to receive two different binary phase shift-keying (BPSK) signals over additive white Gaussian noise (AWGN) channels. The multibeam characteristics of TMAs were also proposed for spatial multiplexing by He et al. [HE 2015c], although the performance with broadband signals was not analyzed. More recent works focus on the hardware design of TMAs applied to spatial filtering of signals [BOGDAN 2016a], and even for interference suppression in mm-Wave communications [YASHCHYSHYN 2015].

Note that, although the TMA topic has been mainly considered from a theoretical point of view, several prototypes have already been described in the literature [BOGDAN 2016b; LI 2010a; LI 2009a; TENNANT 2010; HE 2015a; YAO 2016b; ZHU 2013; HE 2015c; BOGDAN 2016a].

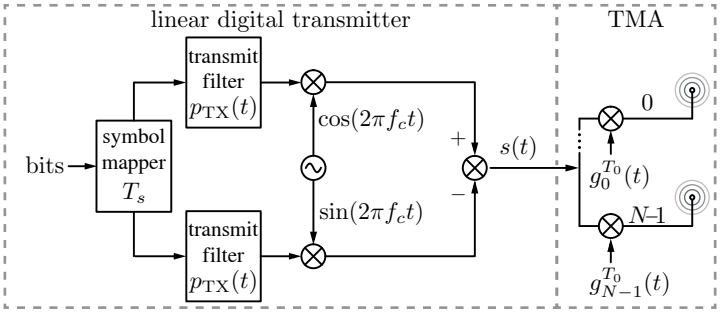

Figure 1.2: Transmitter block diagram considering a linearly modulated digital signal radiated through a TMA exploiting its fundamental pattern: $p_{\mathrm{TX}}(t)$ is the transmit filter, f_c is the carrier frequency, $s(t)$ is the TMA input signal, and $g_0^{T_0}(t), \ldots, g_{N-1}^{T_0}(t)$ are the periodic (T_0) functions governing the N array elements.

1.3 Main Contributions and Organization of this Thesis

None of the above-referenced works analyze in depth, and in a theoretical way, the influence of TMAs on digital communication wireless systems, which is the main motivation of this thesis. In this sense, Chapter 2 (based on [MANEIROCATOIRA 2014a]) investigates the feasibility of TMAs for digital communications. This first insight towards the study of the impact of the TMA technique on the transmission of digital signals focuses on a particular family: linear modulations [GOLDSMITH 2005, Chapter 5]. The main reason for this choice is that these signals exhibit the simplest schemes to be considered in any analysis pertaining to digital signal transmission systems. On the other hand, a TMA by itself imposes a nonlinear transformation – derived from the application of periodic pulses to the antenna excitations, as mentioned above– and therefore, linear modulations avoid the introduction of additional nonlinearities in the communication system. The block diagram in Fig. 1.2 illustrates the continuous-time version of the system under study, in which a linearly modulated digital signal $s(t)$ is first generated by means of an in-phase and quadrature modulator at carrier f_c, and next $s(t)$ is radiated through a TMA that exploits its fundamental pattern assuming a fast decay of the harmonics. Note that we confine the study to the continuous-time model (thus the digital-to-analog converter (DAC) is not included) and that the digital information symbols are generated at a symbol period T_s. Accordingly, the restrictions to safeguard the integrity of the signal and the radiated power (useful and SR) under those conditions are mathematically analyzed and quantified, both in the time and frequency domains.

- The referred restrictions are the following:
  1. $f_0 \ll f_c$, with $f_0 = 1/T_0$ being the TMA fundamental frequency and f_c the carrier frequency of the TMA input signal $s(t)$ (see Fig. 1.2).
  2. $f_0 > B_s$, where $B_s = (1+\rho)/T_s$ is the bandwidth of the TMA input signal $s(t)$, T_s is the symbol period and $\rho \in [0, 1]$ is the so-called roll-off factor when the transmit filter $p_{\mathrm{TX}}(t)$ corresponds to the well known raised cosine filter [PROAKIS 2008].

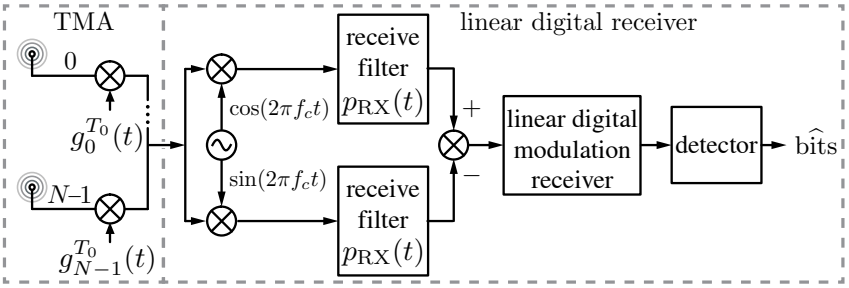

Figure 1.3: Receiver block diagram based on a linear digital modulation scheme incorporating a TMA. The notation is the same as in Fig. 1.2 except $p_{\mathrm{RX}}(t)$, which denotes the receive filter.

- The radiated power through the TMA is given by:

$$P_{\text{rad}} = \mathcal{G}_{\text{TMA}} P_{u\text{i}} = \left(\mathcal{G}_{\text{TMA}_0} + \mathcal{G}_{\text{TMA}_{\text{SR}}}\right) P_{u\text{i}}, \tag{1.5}$$

  where $P_{u\text{i}} = 4\pi\mathcal{D}_u$ (expressed in watts) represents the power radiated by an isotropic antenna transmitting a linearly modulated equivalent baseband digital signal $u(t) \in \mathbb{C}$ with a power density $\mathcal{D}_u$ (it is possible to consider $\mathcal{D}_u = E_s(4-\rho)/4$, with E_s being the average transmit symbol energy and ρ the roll-off factor of the raised cosine filter), whereas $\mathcal{G}_{\text{TMA}}$ represents the TMA power transfer function (dimensionless) accounting for both the array geometry and the time-modulated elements radiating a carrier signal. The $\mathcal{G}_{\text{TMA}}$ expression coincides with the array total power in [BRÉGAINS 2008, Eq. (30)] and is employed to separate the useful power for $q = 0$ ($\mathcal{G}_{\text{TMA}_0}$) from the harmonic SR losses for $q \neq 0$ ($\mathcal{G}_{\text{TMA}_{\text{SR}}}$).

Once the conditions for faithfully transmitting digital signals over a TMA have been stated, as well as the SR losses characterized, the next step consists in investigating the impact of a TMA on the performance of a digital communication system. Aligned with this idea, Chapter 3 (based on [MANEIROCATOIRA 2015a; MANEIROCATOIRA 2014b]) studies the performance –or quality– of the communication link in which the TMA is involved. In Chapter 3 the TMA exclusively exploits its fundamental pattern (a pencil beam pattern in this case). The block diagram of the corresponding digital communication system under study is shown in Fig. 1.3. Chapter 3 characterizes, for the first time and from a theoretical point of view, the bit error ratio (BER) [GOLDSMITH 2005, Chapter 6, p. 171] of a linearly modulated digital communication system with a TMA at the receiver for the simplest case of an AWGN channel model [SKLAR 2001, Chapter 1, p. 33].

However, the major potentialities of TMAs for wireless communications are unavoidably related to the exploitation of their harmonic patterns. In this sense, most works available in the literature address the harmonic beamforming capability exhibited by TMAs focusing exclusively on a radiation point of view. Accordingly, different scenarios of harmonic beamforming have been properly investigated, e.g., the conversion of spatial diversity into frequency diversity [LI 2010a; POLI 2011b; TONG 2012a; POLI 2014; BAROTT 2014], the mitigation of interfering signals [LI 2010a; POLI 2011b], the orthogonality between

patterns [ROCCA 2014; HE 2015c], and the advantages of time redundancy [TONG 2012a]. However, all of those works have neglected a crucial aspect in the system performance when communications signals are involved: the TMA efficiency. Therefore, a more ambitious extension of the analysis in Chapter 3 (based on [MANEIROCATOIRA 2015a; MANEIROCATOIRA 2014b]) is undertaken, by involving the TMA in a multipath fading communication where the antenna efficiency plays a key role. Hence, the true challenge at this point is the synthesis of an efficient harmonic beamforming where it is not enough to satisfy certain conditions in terms of locations of maxima and nulls, but to safeguard the TMA efficiency and, consequently, the average SNR at the receiver (recall that the gain per beam path is proportional to the TMA efficiency [YANG 2004]). The pioneering work involving the efficiency in the TMA beamforming design is detailed in Chapter 4 (based on [MANEIROCATOIRA 2017d; MANEIROCATOIRA 2015b]), which is devoted to the performance analysis of TMAs for the angle diversity reception of digital communication signals. Fig. 1.4 shows the system block diagram whose performance is analyzed in Chapter 4: a narrowband wireless communication system using a conventional M-ary linear digital modulation assuming an omnidirectional antenna at the transmitter, and a TMA, together with a maximum ratio combining (MRC) at the receiver, to exploit the channel diversity through the beamforming with the first $L-1$ positive TMA harmonic patterns.

According to Fig. 1.4, once the transmitted signal $s(t)$ arrives through a multipath channel at the receiver, we obtain L different replicas $y_0(t), \ldots, y_{L-1}(t)$ constituting the TMA input. Each of the L replicas at the TMA output appears at a different (harmonic) frequency $f_l = f_c + l \cdot f_0$, with $l = 0, \ldots, L-1$. Assuming that f_0 has been correctly selected according to the bandwidth B_s of $s(t)$, the TMA output signal occupies a total bandwidth $B_{\text{TMA}} \geq \sum_{l=0}^{L-1} B_s = L \cdot B_s$. After the RF down-conversion at a frequency $f_c - f_I$ (being f_I the lowest intermediate frequency), the obtained signal is sampled at a frequency $f_s^{\text{TMA}} > 2B_{\text{TMA}}$ (fulfilling the Nyquist criterion) and each of the resulting L digital signals is I/Q decomposed (including the corresponding receive filter) at a different intermediate frequency $f_{l_{IF}} = f_I + l \cdot f_0$, with $l = 0, \ldots, L-1$. Finally, the obtained L complex-valued signals are combined in an MRC and the resulting signal is demodulated to obtain the received bits. Notice that, for the sake of simplicity, channel estimation and equalization are assumed to be perfect. Note also that the non-linear operation carried out by the TMA allows for employing a single RF branch (with increasing bandwidth) followed by a single analog-to-digital converter (ADC) (with a higher sampling rate) to exploit L signal replicas impinging at the TMA. Consequently, the complexity of the receiver structure is simplified and, above all, its power consumption is reduced.

The investigations in Chapter 4 show the limitations of rectangular pulses when the aim is to achieve a flexible and efficient beamforming with TMAs. Such vulnerabilities are directly related to the frequency response of rectangular pulses [PRABHU 2014, Chapter 3, p89]: a minimum main-lobe width and a modest side-lobe level (-13 dB), together with a slow (first order) asymptotic side-lobe decay. In fact, in Chapter 5 (based on [MANEIROCATOIRA 2017a;

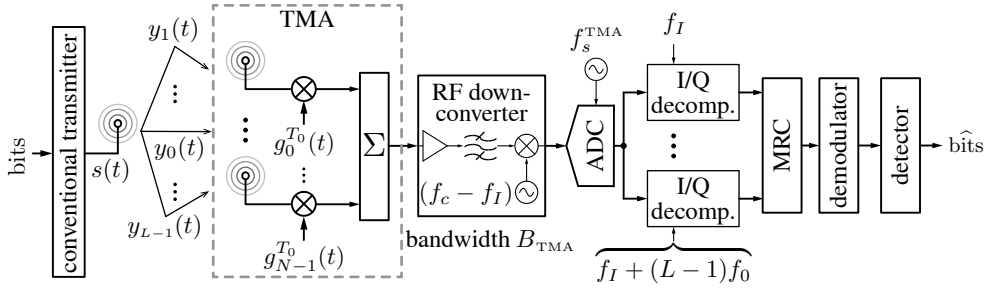

Figure 1.4: Block diagram of a system consisting of a conventional linear digital transmitter equipped with an omni-directional antenna and a receiver with a TMA designed for exploiting channel diversity at the receiver through MRC.

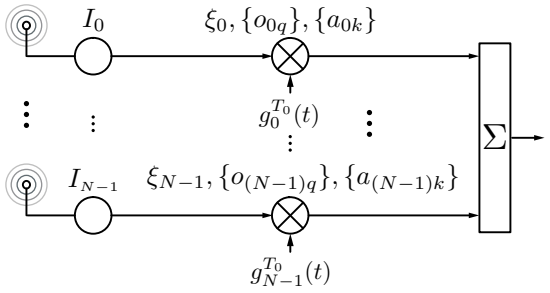

$$g_n^{T_0}(t) = \sum_{q=-\infty}^{\infty} \frac{\xi_n^2 q}{\pi} \sin(\pi \xi_n q) \sum_{k=0}^{K} \frac{(-1)^k a_{nk}}{\xi_n^2 q^2 - k^2} \mathrm{e}^{-jq2\pi o_{nq}}$$

Figure 1.5: Block diagram of a TMA governed by periodical SWC pulses $g_n^{T_0}(t)$.

MANEIROCATOIRA 2016], taking as the starting point the weaknesses of rectangular pulses when applied to harmonic beamforming, the proposals are:

- A type of pulses that are more suitable for harmonic beamforming with TMAs: the so-called sum-of-weighted-cosine (SWC) pulses [NUTTALL 1981].
- Based on the previous pulses, a new family of beamforming TMAs, termed enhanced time-modulated array (ETMA), is characterized and evaluated in terms of efficiency by properly comparing it to conventional beamforming TMAs based on rectangular pulses.

Fig. 1.5 shows the block diagram of an ETMA where the static excitations $I_0, \ldots, I_{N-1}$ of the array are time-modulated by more sophisticated periodical waveforms parametrized by ξ_n (normalized pulse durations), o_{nq} (normalized pulse time shifts), and a_{nk} (pulse weights), $n \in \{0, 1, \ldots, N-1\}$, $q \in \{0, \pm 1, \ldots, \pm L\}$, and $k \in \{0, 1, \ldots, K\}$, where N is the number of antenna elements, L is the order of the highest exploited harmonic, and K is the order of the pulse.

A common denominator of the investigations detailed along this thesis [MANEIROCATOIRA 2014a; MANEIROCATOIRA 2015a; MANEIROCATOIRA 2017d; MANEIROCATOIRA 2017a], and summarized in Chapter 6, is that TMAs are analyzed and evaluated not only from an antenna outlook, but also from a signal processing perspective

applied to wireless communications. Finally, Chapter 6 also introduces the future research lines involving TMAs.

1.4 Thesis Methodology and Resources

With respect to the methodology, due to the theoretical character of the thesis, it is really quite simple to describe. It is based on three fundamental points and under the following chronological order:

- A proper research and a meticulous study of the state of the art.
- A mathematical investigation based on communications theory and signal processing in order to model and/or analyze the novel concepts introduced.
- A set of exemplifications of the results through numerical simulations.

The resources employed were

- The bibliography.
- The necessary software for symbolic (Mathematica) or numerical (Matlab) simulation, as well as for document edition (LaTeX).

Regarding the formal aspects, it is remarkable that a transversal idea is present throughout this thesis: all chapters are almost self-contained. With this strategy, it is intended that the reader has a greater fluidity in spite of the multidisciplinary character of the contents. Aligned with this philosophy, sometimes it is more convenient to repeat a particular concept or equation across different chapters, particularizing it for the specific topics addressed in each one.

1.5 Co-authored Publications

The study presented in this thesis led to the publication of five JCR-indexed journal papers and four conference papers which are included in the lists below.

Journal Papers

1. R. Maneiro-Catoira, J. Brégains, J. A. García-Naya, and L. Castedo. "**On the feasibility of time-modulated arrays for digital linear modulations: a theoretical analysis**". *IEEE Transactions on Antennas and Propagation*, vol. 62, no. 12, 2014, pp. 6114–6122. ISSN: 0018-926X.
   DOI: 10.1109/TAP.2014.2365827
2. R. Maneiro-Catoira, J. Brégains, J. A. García-Naya, and L. Castedo. "**Impact of time-modulated arrays on the BER of linear digital modulations**". *Journal of Electromagnetic Waves and Applications*, vol. 29, no. 16, 2015, pp. 2147–2154. ISSN: 0920-5071.
   DOI: 10.1080/09205071.2015.1075908

3. R. Maneiro-Catoira, J. Brégains, J. A. García-Naya, L. Castedo, P. Rocca, and L. Poli. "**Performance analysis of time-modulated arrays for the angle diversity reception of digital linear modulated signals**". *IEEE Journal of Selected Topics in Signal Processing*, vol. 11, no. 2, 2017, pp. 247–258. ISSN: 1932-4553.
DOI: 10.1109/JSTSP.2016.2609852
4. R. Maneiro-Catoira, J. Brégains, J. A. García-Naya, and L. Castedo. "**Enhanced time-modulated arrays for harmonic beamforming**". *IEEE Journal of Selected Topics in Signal Processing*, vol. 11, no. 2, 2017, pp. 259–270. ISSN: 1932-4553.
DOI: 10.1109/jstsp.2016.2627178
5. R. Maneiro-Catoira, J. Brégains, J. A. García-Naya, and L. Castedo. "**Time modulated arrays: from their origin to their utilization in wireless communication systems**". *Sensors*, vol. 17, no. 3, 2017. ISSN: 1424-8220.
DOI: 10.3390/s17030590

Conference Papers

1. R. Maneiro-Catoira, J. Brégains, J. A. García-Naya, and L. Castedo. "**Time-modulated arrays for digital communications**". *Proc. of IEEE International Symposium on Antennas and Propagation and USNC-URSI Radio Science Meeting (2014 IEEE AP-S and USNC-URSI)*. Memphis, Tennessee, USA, 2014, pp. 1760–1761.
DOI: 10.1109/APS.2014.6905206
2. R. Maneiro-Catoira, J. Brégains, J. A. García-Naya, and L. Castedo. "**Time-modulated arrays for digital communications in multipath scenarios**". *Proc. of 2015 IEEE International Symposium on Antennas and Propagation and North American Radio Science Meeting (2015 IEEE AP-S & USNC-URSI)*. Vancouver, BC, Canada, 2015, pp. 816–817. ISBN: 9781479978168.
DOI: 10.1109/APS.2015.7304795
3. R. Maneiro-Catoira, J. Brégains, J. A. García-Naya, and L. Castedo. "**Time-modulated arrays with sum of weighted cosine pulses**". *Proc. of 2016 IEEE International Symposium on Antennas and Propagation and USNC-URSI Radio Science Meeting (2016 IEEE AP-S & USNC-URSI)*. Fajardo, Puerto Rico, 2016, pp. 697–698.
DOI: 10.1109/APS.2016.7696057
4. R. Maneiro-Catoira, J. Brégains, J. A. García-Naya, and L. Castedo. "**Frequency-domain synthesis of time-modulated arrays**". *Proc. of 2017 IEEE International Symposium on Antennas and Propagation & USNC/URSI National Radio Science Meeting (accepted for publication)*. San Diego, California, USA, 2017

Chapter 2

Feasibility of TMAs for Digital Communications

As stated in Sections 1.2 and 1.3, no previous works have addressed an in-depth theoretical study considering the influence of a time-modulated array (TMA) on a digital communication system, which is precisely the main aim of this chapter.

This chapter is mainly based on the following co-authored publications:

- R. Maneiro-Catoira, J. Brégains, J. A. García-Naya, and L. Castedo. "**On the feasibility of time-modulated arrays for digital linear modulations: a theoretical analysis**". *IEEE Transactions on Antennas and Propagation*, vol. 62, no. 12, 2014, pp. 6114–6122. ISSN: 0018-926X.
  DOI: 10.1109/TAP.2014.2365827
- R. Maneiro-Catoira, J. Brégains, J. A. García-Naya, and L. Castedo. "**Time-modulated arrays for digital communications**". *Proc. of IEEE International Symposium on Antennas and Propagation and USNC-URSI Radio Science Meeting (2014 IEEE AP-S and USNC-URSI)*. Memphis, Tennessee, USA, 2014, pp. 1760–1761.
  DOI: 10.1109/APS.2014.6905206

This chapter is structured as follows. In Section 2.2 after describing the mathematical fundamentals of both TMAs and linearly modulated digital signals, a dual time-frequency domain analysis is performed in order to identify the restrictions for faithfully transmitting digital signals over TMAs. A step further is taken in Section 2.3, where an analysis –with the same dual character– to quantify the power radiated by a TMA is carried out considering that the TMA is combined with linear digital modulation schemes. As a result, aspects like the generalized TMA power response or the TMA efficiency are also properly characterized in this section and exemplified in Section 2.4. Finally, Section 2.5 is devoted to the conclusions.

2.1 Introduction

Digital modulation is the process of translating bits into analog waveforms suitable for being transmitted over a physical channel. The input bit stream is grouped into blocks of k bits and such blocks are referred to as symbols. For each symbol, a different signal of duration T_s is chosen. Hence, each symbol is mapped into one of $M = 2^k$ different waveforms.

Linear modulation methods in which the transmitted signal depends linearly on the information symbols to be sent are the most widely used forms of digital modulations. In such cases the digital information is coded in the amplitude and/or the phase of a carrier sinusoidal signal. Among the factors influencing the choice of a digital modulation, spectral efficiency (bit rate per bandwidth unit, expressed in bit/s/Hz) and power efficiency are of great importance.

Nonlinear modulations such as frequency-shift keying (FSK) [SKLAR 2001] and its variants are power efficient and very robust against both channel impairments and non-linearities. However, they exhibit worse spectral efficiency than their linear counterparts. Linear modulations such as amplitude-shift keying (ASK), phase-shift keying (PSK), and qauadrature amplitude modulation (QAM) are spectral efficient but not power-efficient by themselves [SKLAR 2001]. Nevertheless, when combined with channel coding, linear modulations can also be made power-efficient and this is the reason why they are being used in most of today's wireless communication standards.

ASK modulation presents a poor noise protection as the alphabet size M increases. Both ASK and QAM modulations do not have a constant envelope, so the performance degrades in the presence of non-linearities. PSK overcomes such a limitation because the signal envelope is kept constant.

For high values of M QAM is preferred to PSK. Even though both offer the same spectral efficiency, QAM is more resilient to noise. QAM will be the usual modulation when M is high (i.e., 16, 64, or 256), and for this reason they are usually called high-order modulations [PROAKIS 2008]. QAM provides both high data rates and high spectral efficiency. Consequently, it is particularly suitable for those applications in which bandwidth is limited and high data rates are demanded, as for example in satellite systems or mobile wireless communications [SKLAR 2001]. Apart from the above reasons, linear modulation is one of the simplest schemes to be considered in any analysis pertaining signal transmission systems. Those conditions represent an ideal frame to start with, and it is the one chosen in this branch of our work.

By incorporating a TMA (whose primary purpose is to adjust the radiated power pattern) to a radio system based on a linear digital modulation scheme (see Fig. 2.1) we will show that it is possible to obtain an adequate system performance under certain restrictions. To accurately analyze the control of the power radiation pattern obtained through a TMA when linearly modulated signals are transmitted, we provide a mathematical analysis with two different objectives. First, we determine the TMA restrictions in terms of the parameters of the linearly

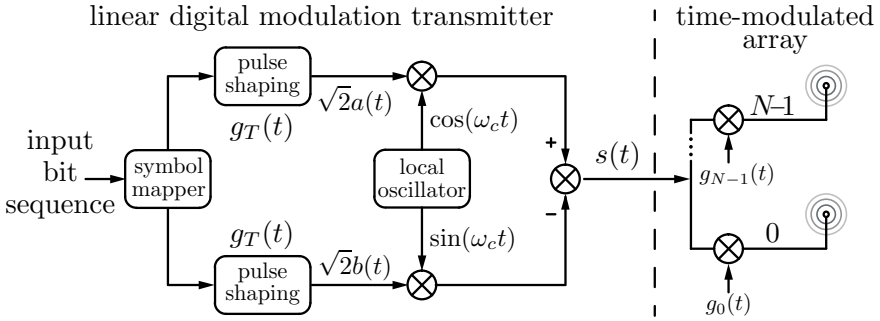

Figure 2.1: Transmitter block diagram of a TMA incorporated to a radio system based on a linear digital modulation scheme.

modulated digital signal to guarantee the integrity of the information transmitted. Second, we derive an expression for both the total power and the useful power radiated when a linearly modulated signal is transmitted by the TMA. The special motivation for the last objective is to model theoretically the power-radiated efficiency of the TMA when it is combined with digital linear modulation schemes. In other words, we want to know how much of the radiated power is lost because of the TMA.

2.2 Mathematical Fundamental Analysis

2.2.1 Time-Modulated Array Fundamentals

The radiated field of a linear TMA composed of N isotropic elements distributed along the z axis is given by the following expression [BRÉGAINS 2008; AKSOY 2012; YANG 2004; LI 2009c]

$$F(\theta, t) = \mathrm{e}^{j\omega_c t} \sum_{n=0}^{N-1} g_n(t) I_n \mathrm{e}^{jkz_n \cos\theta} \in \mathbb{C}, \tag{2.1}$$

where $g_n(t)$ is a periodic function (with period $T_0 = 2\pi/\omega_0$) usually considered to be a rectangular pulse train governing the n-th switch; $I_n = |I_n|\mathrm{e}^{j\varphi_n}$ and z_n are respectively the complex current excitation in polar form (φ_n is its phase) and the position on the z-axis for the n-th array element; the θ variable corresponds to the angle with respect to the z-axis (notice that, for such an array geometrical configuration, the φ coordinate is not necessary); $k = 2\pi/\lambda$ represents the wavenumber for a carrier wavelength $\lambda = 2\pi c/\omega_c = c/f_c$; and $\mathbb{C}$ is the set of complex numbers.

Let us consider the Fourier series expansion of the n-th array element modulating pulse:

$$g_n(t) = \sum_{q=-\infty}^{\infty} G_{nq} \mathrm{e}^{jq\omega_0 t} \in \mathbb{R}, \tag{2.2}$$

being $\omega_0 = 2\pi/T_0 = 2\pi f_0$, and $\mathbb{R}$ the set of real numbers.

By substituting Eq. (2.2) in Eq. (2.1) we have:

$$F(\theta,t)=\left[\sum_{n=0}^{N-1}I_nG_{n0}\mathrm{e}^{jkz_n\cos\theta}\right]\mathrm{e}^{j\omega_c t}\;+\left[\sum_{n=0}^{N-1}\sum_{\substack{q=-\infty\\q\neq 0}}^{\infty}I_nG_{nq}\mathrm{e}^{jkz_n\cos\theta}\right]\mathrm{e}^{j(\omega_c+q\omega_0)t}. \tag{2.3}$$

The first term in Eq. (2.3) is the array factor at ω_c, which allows for controlling the radiated pattern through the G_{n0} coefficients. When $g_n(t)$ is a periodic train of rectangular pulses of duration τ_n (i.e., the array elements are controlled by on-off switches), then G_{n0} corresponds to the normalized duration $\xi_n=\tau_n/T_0$ [FONDEVILA 2004].

The second term in Eq. (2.3) reveals the presence of harmonics located at frequencies $\omega_c+q\omega_0$, which can be either minimized using TMA optimization techniques [YANG 2002; YANG 2003; YANG 2005a; FONDEVILA 2004; FONDEVILA 2006; POLI 2010b; TENNANT 2008; AKSOY 2011; POLI 2010a; POLI 2010c] or used profitably [ROCCA 2012b; POLI 2011b; LI 2010a; LI 2009a; LI 2010b]. Note that the G_{nq} coefficients will influence the amplitude level –and thus the topology– of the main pattern ($q=0$) and also the decay rate of the harmonics (increasing $|q|$ values) levels. In the analyses that follow, we will consider that the G_{nq} lead to relatively fast decaying rates of the harmonics maximum levels as, for example, in those cases of the above-mentioned optimized configurations.

2.2.2 Linear Digital Modulation Fundamentals

A generalized linear modulation scheme may be viewed as a system in which the message is inserted in the amplitude $A(t)$ and/or in the phase $\alpha(t)$ of the transmitted signal $s(t)\in\mathbb{R}$ whose carrier frequency is $\omega_c=2\pi f_c$ (see Fig. 2.1). Therefore, a linearly modulated signal can be written as

$$s(t)=\sqrt{2}A(t)\cos(\omega_c t+\alpha(t))=\mathrm{Re}\left\{\sqrt{2}u(t)\mathrm{e}^{j\omega_c t}\right\}, \tag{2.4}$$

where

$$u(t)=A(t)\mathrm{e}^{j\alpha(t)}=a(t)+jb(t)\in\mathbb{C} \tag{2.5}$$

is the so-called complex-valued envelope or equivalent baseband signal of $s(t)$, and with

$$a(t)=A(t)\cos(\alpha(t)),\text{ and }b(t)=A(t)\sin(\alpha(t)).$$

The term $\sqrt{2}$ in Eq. (2.4) is included to ensure that the bandpass signal $s(t)$ and the equivalent baseband signal $u(t)$ have the same mean power, as shown in the forthcoming analysis results (see Eqs. Eq. (2.39) and Eq. (2.53)). According to Eqs. (2.4) and (2.5), the signal under consideration can also be written as

$$s(t)=\sqrt{2}a(t)\cos(\omega_c t)-\sqrt{2}b(t)\sin(\omega_c t), \tag{2.6}$$

with

$$a(t) = \sum_{k=-\infty}^{\infty} a_k g_T(t - kT_s) \text{ and}$$
$$b(t) = \sum_{k=-\infty}^{\infty} b_k g_T(t - kT_s) \tag{2.7}$$

being the so-called in-phase (I) and quadrature (Q) signal components, respectively. The complex numbers $a_k + jb_k$ represent symbols to be transmitted and taken from a constellation mapping; T_s is the duration (period) of each symbol; and $g_T(t)$ is the transmit pulse-shaping filter chosen to be, in our case, a raised cosine shaping filter with roll-off factor ρ [SKLAR 2001].

2.2.3 Restrictions for Single-Carrier Transmission: Frequency and Time-Domain Analysis

Let us consider that a linearly-modulated digital signal is radiated through a TMA. From Eqs. (2.1) and (2.5), the signal radiated by the n-th array element is given by (see Fig. 2.1)

$$s_n(\theta, t) = \sqrt{2}A(t)|I_n|g_n(t) \cdot \cos\left(\omega_c t + \varphi_n + kz_n \cos\theta + \alpha(t)\right). \tag{2.8}$$

In order to simplify the subsequent analysis, let us take the complex-valued representation of $s_n(t)$ given by

$$\begin{aligned}\tilde{s}_n(\theta, t) &= \left[\sqrt{2}u(t)g_n(t)I_n \mathrm{e}^{jkz_n \cos\theta}\right] \mathrm{e}^{j\omega_c t} \\ &= r_n(\theta, t)\mathrm{e}^{j\omega_c t} \in \mathbb{C},\end{aligned} \tag{2.9}$$

where $r_n(\theta, t) = \sqrt{2}u(t)g_n(t)I_n \mathrm{e}^{jkz_n \cos\theta}$ is the complex envelope of the analytic signal $\tilde{s}_n(\theta, t)$.

The signal radiated by the TMA results from the sum of the contributions from all N array elements

$$\begin{aligned}\tilde{s}_{\text{rad}}(\theta, t) &= \sum_{n=0}^{N-1} \tilde{s}_n(\theta, t) \\ &= \left[\sqrt{2}u(t) \sum_{n=0}^{N-1} g_n(t)I_n \mathrm{e}^{jkz_n \cos\theta}\right] \mathrm{e}^{j\omega_c t} \\ &= \sqrt{2}u(t)F(\theta, t),\end{aligned} \tag{2.10}$$

with $F(\theta, t)$ defined in Eq. (2.1) whereas $\tilde{s}_{\text{rad}}(\theta, t)$ is the analytic representation of the radiated signal. Note now that the Fourier transform (FT) of $g_n(t) = \sum_{q=-\infty}^{\infty} G_{nq}\mathrm{e}^{jq\omega_0 t}$ is

$$G_n(\omega) = \mathrm{FT}[g_n(t)] = 2\pi \sum_{q=-\infty}^{\infty} G_{nq}\delta(\omega - q\omega_0), \tag{2.11}$$

which is expressed in terms of the frequency $\omega = 2\pi f$.

On the other hand, according to the FT properties, a multiplication in the time domain corresponds to a convolution (denoted here by $\star$) in the frequency domain, which for two given signals $x(t)$ and $y(t)$ yields

$$\mathrm{FT}\left[x(t)\,y(t)\right] = \frac{1}{2\pi} X(\omega) \star Y(\omega). \tag{2.12}$$

Applying Eq. (2.12) to $u(t)g_n(t)$, considering the linearity of the FT, and that $U(\omega) = \mathrm{FT}\left[u(t)\right]$, the FT of $r_n(t)$ is

$$\begin{aligned} R_n(\theta,\omega) &= \mathrm{FT}\left[r_n(\theta,t)\right] \\ &= \sqrt{2}\sum_{q=-\infty}^{\infty} I_n \mathrm{e}^{jkz_n\cos\theta} G_{nq} U(\omega - q\omega_0). \end{aligned} \tag{2.13}$$

Now, since $\mathrm{FT}\left[r_n(\theta,t)\mathrm{e}^{j\omega_c t}\right] = R_n(\theta,\omega-\omega_c)$, considering Eq. (2.13) we obtain

$$\tilde{S}_n(\omega) = \sqrt{2}\sum_{q=-\infty}^{\infty} I_n \mathrm{e}^{jkz_n\cos\theta} G_{nq} U(\omega - (\omega_c + q\omega_0)), \tag{2.14}$$

and then, the spectrum of $\tilde{s}_{\text{rad}}(t)$ is expressed as

$$\begin{aligned} \tilde{S}_{\text{rad}}(\omega) &= \sum_{n=0}^{N-1} \tilde{S}_n(\omega) \\ &= \sqrt{2}\sum_{n=0}^{N-1}\sum_{q=-\infty}^{\infty} I_n \mathrm{e}^{jkz_n\cos\theta} G_{nq} U(\omega - (\omega_c + q\omega_0)). \end{aligned} \tag{2.15}$$

By observing Eq. (2.15) we conclude that

1. The desired radiated signal is the one corresponding to $q = 0$ (the so-called fundamental mode) and it is given by:

$$\tilde{S}_{\text{rad}}(\omega)\Big|_{q=0} = \sqrt{2}\sum_{n=0}^{N-1} I_n G_{n0} \mathrm{e}^{jkz_n\cos\theta} U(\omega - \omega_c), \tag{2.16}$$

   with $G_{n0} = \xi_n$ when $g_n(t)$ is a periodic train of rectangular pulses. Eq. (2.16) has the same spectrum topology as if $s(t)$ were radiated through a conventional array but now having control over the dynamic excitations $I_n G_{n0} = I_n \xi_n$.
2. The terms corresponding to $q \neq 0$ are signal replicas centered at the frequencies $\omega_c + q\omega_0$. To avoid interferences between the TMA (carrier at ω_0) and the linearly-modulated digital signal $s(t)$ centered at ω_c, an immediate requirement is mandatory:

$$\omega_0 \ll \omega_c \Leftrightarrow f_0 \ll f_c \Leftrightarrow T_0 \gg 1/f_c \quad \textbf{(restriction 1)}. \tag{2.17}$$

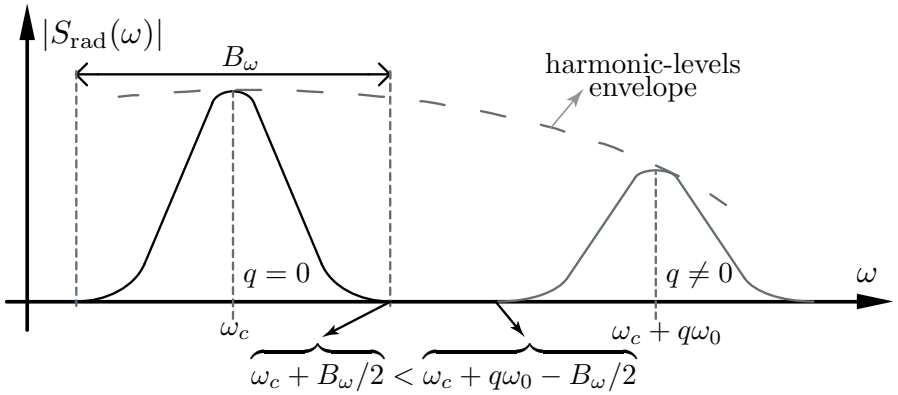

Figure 2.2: Non-overlapping condition between the replicas and the fundamental mode of the transmitted signal.

As the linearly-modulated digital signal has a limited bandwidth B_ω [rad/s], an additional restriction is necessary to avoid overlapping between the signal replicas and the fundamental mode. Figure 2.2 is a simplified graphical representation of Eq. (2.15), which is helpful for deriving the following condition

$$\omega_c + q\omega_0 - \frac{B_\omega}{2} > \omega_c + \frac{B_\omega}{2} \Rightarrow q\omega_0 > B_\omega. \tag{2.18}$$

By selecting the closest harmonic to the carrier frequency (i.e., choosing $|q| = 1$), the restriction becomes

$$\omega_0 > B_\omega. \tag{2.19}$$

Inequalities in Eqs. (2.17) and (2.19) were previously derived in [BRÉGAINS 2008], but we restate them again under the more rigorous view of the Fourier transforms and to provide uniformity to our reasoning line.

The bandwidth of a linearly-modulated digital signal is determined by the transmit pulse-shaping filter $g_T(t)$ (see Fig. 2.1). A suitable solution to minimize the inter-symbol interference (ISI) is the raised cosine filter [PROAKIS 2008]

$$G_T(f) = \begin{cases} T_s & |f| < f_1 \\ \dfrac{T_s}{2}\left[1 + \cos\left(\dfrac{\pi(|f| - f_1)}{\frac{1}{Ts} - 2f_1}\right)\right] & f_1 \leq |f| \leq f_2 \\ 0 & |f| > f_2, \end{cases} \tag{2.20}$$

with $f_1 = (1-\rho)/(2T_s)$; $f_2 = (1+\rho)/(2T_s)$; $\rho \in [0, 1]$ is the roll-off factor which determines the smoothness of its frequency response. The signal bandwidth is given by [PROAKIS 2008]

$$B = \frac{1+\rho}{T_s}\ \text{[Hz]}, \quad \text{with } B = \frac{B_\omega}{2\pi}. \tag{2.21}$$

When the restriction in Eq. (2.19) is expressed in terms of the TMA period, we have $(1/T_0) > B$, which together with Eq. (2.21) leads to

$$T_0 < \frac{T_s}{1+\rho} \quad \textbf{(restriction 2)}. \tag{2.22}$$

According to the scheme in Fig. 2.1, if the bit rate at the input of the symbol mapper is $R_b = J/T_s$ bit/s (with J being the number of bits per symbol) and Eq. (2.21) is taken into account, the modulation spectral efficiency is given by

$$\frac{R_b}{B} = \frac{J/T_s}{B} = \frac{J}{1+\rho} = \frac{\log_2 M}{1+\rho} \text{ [(bit/s)/Hz]}, \tag{2.23}$$

which reveals that the spectral efficiency is maximized when ρ takes small values and/or the alphabet order, M, is large.

Let us now analyze, in the time domain, the effects of a TMA on the transmission of a linearly modulated digital signal. Substituting Eq. (2.2) into Eq. (2.9), the signal transmitted by the n-th antenna element can be rewritten as

$$\tilde{s}_n(\theta,t) = \left[\sqrt{2}u(t)\sum_{q=-\infty}^{\infty} G_{nq}\mathrm{e}^{jq\omega_0 t} I_n \mathrm{e}^{jkz_n\cos\theta}\right]\mathrm{e}^{j\omega_c t}. \tag{2.24}$$

Again, the expression of the radiated signal in the time domain corresponds to the contribution of the N elements

$$\begin{aligned}\tilde{s}_{\text{rad}}(\theta,t) &= \sum_{n=0}^{N-1}\tilde{s}_n(\theta,t)\\ &= \left[\sqrt{2}u(t)\sum_{n=0}^{N-1}\sum_{q=-\infty}^{\infty} G_{nq} I_n \mathrm{e}^{jkz_n\cos\theta}\right]\mathrm{e}^{j(\omega_c+q\omega_0)t}.\end{aligned} \tag{2.25}$$

In view of Eq. (2.25), it is immediate the need of the first restriction in Eq. (2.17) in order to avoid the interference between the carrier and the fundamental frequency of the array pulse modulation. At the same time, the second restriction in Eq. (2.22) is also mandatory in order that the unwanted harmonics outside the bandwidth of the information signal $u(t)$ be filtered out.

Recall that the desired signal is the one corresponding to $q = 0$, which is given by

$$\tilde{s}_{\text{rad}}(\theta,t)\Big|_{q=0} = \sqrt{2}u(t)\left[\sum_{n=0}^{N-1} I_n G_{n0}\mathrm{e}^{jkz_n\cos\theta}\right]\mathrm{e}^{j\omega_c t}. \tag{2.26}$$

From the equation above we are able to ensure that, under the two restrictions in Eqs. (2.17) and (2.22), such a signal could be processed at the receiver as a conventional linearly modulated digital signal so that after I/Q demodulation, low-pass filtering and detection, the transmitted symbols would be properly recovered.

2.3 Analysis of the Radiated Power

Our aim in this section is to obtain the total power radiated by the TMA when a linearly modulated digital signal is transmitted. We will start by considering the analysis of the signal

time-varying power, making use of the mean power density concept. Then we will continue with the analogous density function considered in the frequency domain, and built on Parseval's identity. Although both analysis will lead to the same results, we will see that the paths followed in each case will enlighten some different, yet complementary, features.

2.3.1 Analysis of the Radiated Power: Time Domain

Since the real part of the radiated signal Eq. (2.10) ultimately represents the real-valued magnitude of the electric field vector in the far region of the antenna array, its square will be a real-valued number proportional to the magnitude of the Poynting's vector[1], which will represent the power density (measured in W/m^2) of the signal evaluated at the angular point θ and at time t. The power (spatial) density averaged over time will consequently be

$$\mathcal{D}_{\text{rad}}(\theta) = \lim_{\mathcal{T}\to\infty} \frac{1}{\mathcal{T}} \int_{-\mathcal{T}/2}^{\mathcal{T}/2} s_{\text{rad}}^2(\theta, t)dt \quad \left[\frac{\text{W}}{\text{m}^2}\right]. \tag{2.27}$$

By considering Eq. (2.9) and Eq. (2.10), we can write

$$\begin{aligned} s_{\text{rad}}(\theta, t) &= \text{Re}\left\{\tilde{s}_{\text{rad}}(\theta, t)\right\} = \text{Re}\left\{\sum_{n=0}^{N-1} \tilde{s}_n(\theta, t)\right\} \\ &= \text{Re}\left\{\sum_{n=0}^{N-1} r_n(\theta, t)\text{e}^{j\omega_c t}\right\}. \end{aligned} \tag{2.28}$$

For a clearer analysis, we can express the above as

$$\begin{aligned} s_{\text{rad}}(\theta, t) &= \text{Re}\left\{|r(\theta, t)|\, \text{e}^{j\psi(t)}\text{e}^{j\omega_c t}\right\} \\ &= |r(\theta, t)| \cos\left(\omega_c t + \psi(t)\right), \text{ where} \end{aligned} \tag{2.29}$$

$$r(\theta, t) = \sum_{n=0}^{N-1} r_n(\theta, t) = |r(\theta, t)|\text{e}^{j\psi(t)} \tag{2.30}$$

is the complex envelope of $s_{\text{rad}}(\theta, t)$ –and thus $|r(\theta, t)|$ represents the real-valued envelope of $s_{\text{rad}}(\theta, t)$.

Substituting Eq. (2.29) into Eq. (2.27), and taking into account that $\cos^2(x) = [1 + \cos(2x)]/2$, we have

$$\mathcal{D}_{\text{rad}}(\theta) = \frac{1}{2} \lim_{\mathcal{T}\to\infty} \frac{1}{\mathcal{T}} \int_{-\mathcal{T}/2}^{\mathcal{T}/2} |r(\theta, t)|^2 dt \; + \frac{1}{2} \lim_{\mathcal{T}\to\infty} \frac{1}{\mathcal{T}} \int_{-\mathcal{T}/2}^{\mathcal{T}/2} |r(\theta, t)|^2 \cos\left(2\omega_c t + 2\psi(t)\right) dt. \tag{2.31}$$

[1]We can depart from the Poynting's (real-valued) vector $\vec{P}_v = \mu_0^{-1}\vec{E} \times \vec{B}$ (μ_0 is the vacuum magnetic permeability). Since at far distances from the antenna $\vec{E}$ and $\vec{B}$ are perpendicular to each other and their magnitudes satisfy the relationship $E = cB$ –being c the speed of light in vacuum–, then $\vec{P}_v = (\mu_0 c)^{-1}E^2\vec{k}$, where $\vec{k}$ is the wave vector pointing in the direction of the advancing electromagnetic plane wave. Finally, $P_v \propto E^2$, i.e., $P_v \propto s_{\text{rad}}^2(\theta, t)$. By adjusting the constant of proportionality to be equal to one, we can obtain a quantity which is measured in W/m^2, as indicated in Eq. (2.27).

In view of Eq. (2.9) and Eq. (2.30), and considering the two restrictions in Eqs. (2.17) and (2.22), we can conclude that the real-valued envelope $|r(\theta,t)|^2$ varies slowly relative to the rapid variations (twice the carrier frequency plus slow variations in phase due to $2\psi(t)$) of the cosine function. Then the net area contributed by the right-hand-side integral in Eq. (2.31) is very small compared to the value of the left-hand-side term and, hence, it can be neglected [PROAKIS 2008]. We can then safely write

$$\mathcal{D}_{\text{rad}}(\theta) = \frac{1}{2}\lim_{\mathcal{T}\to\infty}\frac{1}{\mathcal{T}}\int_{-\mathcal{T}/2}^{\mathcal{T}/2}|r(\theta,t)|^2 dt. \tag{2.32}$$

We now develop the integrand. From Eq. (2.30) we find that

$$\begin{aligned}|r(\theta,t)|^2 &= r(\theta,t)r^*(\theta,t)\\ &= \sum_{n=0}^{N-1}|r_n(\theta,t)|^2 + \sum_{n=0}^{N-1}\sum_{\substack{m=0\\m\neq n}}^{N-1} r_n(\theta,t)r_m^*(\theta,t),\end{aligned} \tag{2.33}$$

but with the help of Eq. (2.9) and Eq. (2.2) the sum over the squared amplitude terms becomes

$$\begin{aligned}\sum_{n=0}^{N-1}|r_n(\theta,t)|^2 &= 2\sum_{n=0}^{N-1}|I_n|^2|u(t)|^2|g_n(t)|^2\\ &= 2\sum_{n=0}^{N-1}|I_n|^2|u(t)|^2\left[\sum_{q=-\infty}^{\infty}G_{nq}\mathrm{e}^{jq\omega_0 t}\sum_{p=-\infty}^{\infty}G_{np}^*\mathrm{e}^{-jp\omega_0 t}\right]\\ &= 2\sum_{n=0}^{N-1}|I_n|^2\left[\sum_{q=-\infty}^{\infty}|G_{nq}|^2 + \sum_{p=-\infty}^{\infty}\sum_{\substack{q=-\infty\\q\neq p}}^{\infty}G_{np}G_{nq}^*\mathrm{e}^{j(p-q)\omega_0 t}\right]|u(t)|^2,\end{aligned} \tag{2.34}$$

whereas

$$\begin{aligned}&\sum_{m=0}^{N-1}\sum_{\substack{n=0\\n\neq m}}^{N-1} r_m(\theta,t)r_n^*(\theta,t) =\\ &= 2\sum_{m=0}^{N-1}\sum_{\substack{n=0\\n\neq m}}^{N-1}|u(t)|^2 I_m I_n^*\mathrm{e}^{jk(z_m-z_n)\cos\theta}\cdot\left[\sum_{q=-\infty}^{\infty}G_{mq}\mathrm{e}^{jq\omega_0 t}\cdot\sum_{p=-\infty}^{\infty}G_{np}^*\mathrm{e}^{-jp\omega_0 t}\right]\\ &= 2\sum_{m=0}^{N-1}\sum_{\substack{n=0\\n\neq m}}^{N-1} I_m I_n^*\mathrm{e}^{jk(z_m-z_n)\cos\theta}\left[\sum_{q=-\infty}^{\infty}G_{mq}G_{nq}^* + \sum_{p=-\infty}^{\infty}\sum_{\substack{q=-\infty\\q\neq p}}^{\infty}G_{mp}G_{nq}^*\mathrm{e}^{j(p-q)\omega_0 t}\right]|u(t)|^2.\end{aligned} \tag{2.35}$$

On the other hand, if we consider the integral

$$I = \int_{-\infty}^{\infty}|u(t)|^2\mathrm{e}^{-j(q-p)\omega_0 t}dt, \tag{2.36}$$

with $p \neq q$, we can see that it coincides with $\mathrm{FT}\left[|u(t)|^2\right]$ evaluated at a non-zero integer multiple of ω_0 frequency. As a consequence of the convolution property Eq. (2.12)[2], $\mathrm{FT}\left[|u(t)|^2\right]$ has a bandwidth equal to B_ω. Therefore, it does not have any components at frequencies away from the $[-B_\omega, B_\omega]$ range. Under the restriction in Eq. (2.19) the integral I then vanishes.

If we substitute Eqs. (2.34) and (2.35) into Eq. (2.33), and then integrate Eq. (2.32) considering that the integral in Eq. (2.36) is equal to zero, we arrive at

$$\mathcal{D}_{\text{rad}}(\theta) = \sum_{q=-\infty}^{\infty} \left[\sum_{n=0}^{N-1} |I_n|^2 |G_{nq}|^2 + \sum_{m=0}^{N-1} \sum_{\substack{n=0 \\ n\neq m}}^{N-1} I_m I_n^* G_{mq} G_{nq}^* \mathrm{e}^{jk(z_m - z_n)\cos\theta} \right] \cdot \mathcal{D}_u, \tag{2.37}$$

where

$$\mathcal{D}_u = \mathcal{D}_s = \lim_{\mathcal{T}\to\infty} \frac{1}{\mathcal{T}} \int_{-\mathcal{T}/2}^{\mathcal{T}/2} |u(t)|^2 dt \tag{2.38}$$

is referred to isotropic elements. Therefore it is constant with respect to the spatial coordinates (the dependency is not explicitly shown) and represents the baseband-equivalent signal mean power density which, as a matter of fact, equals the baseband counterpart. Let us show this last point. To compute the mean power density of $s(t)$ as defined in Eq. (2.4) we have to take the integral of $s^2(t)$:

$$\begin{aligned} \mathcal{D}_s &= \lim_{\mathcal{T}\to\infty} \frac{1}{\mathcal{T}} \int_{-\mathcal{T}/2}^{\mathcal{T}/2} s^2(t) dt \\ &= \lim_{\mathcal{T}\to\infty} \frac{1}{\mathcal{T}} \int_{-\mathcal{T}/2}^{\mathcal{T}/2} 2A^2(t) \cos^2\left(\omega_c t + \alpha(t)\right) dt \\ &= \lim_{\mathcal{T}\to\infty} \frac{1}{\mathcal{T}} \int_{-\mathcal{T}/2}^{\mathcal{T}/2} |u(t)|^2 dt = \mathcal{D}_u, \end{aligned} \tag{2.39}$$

with $|u(t)| = A(t)$, and where the first three equalities were obtained by reasoning analogously to the steps from Eq. (2.27) to Eq. (2.32). The last identity was obtained from the definition of the mean power of a complex-valued signal [PROAKIS 2008][3].

The total mean power P_{rad} is computed by integrating $\mathcal{D}_{\text{rad}}$ over a sphere of constant large

[2]The frequency range of $U(\omega)$ and $U(-\omega)$ is $[-B_\omega/2, B_\omega/2]$, determined by $G_T = \mathrm{FT}[g_T(t)]$ (see Eq. (2.20)). $\mathrm{FT}\left\{|u(t)|^2\right\} = \mathrm{FT}\left\{u(t)u^*(t)\right\} = \frac{1}{2\pi} U(\omega) \star U^*(-\omega)$, whose frequency range can be easily deduced from the convolution properties, yielding $[-B_\omega, B_\omega]$.

[3]The equivalent baseband signal $u(t)$ is defined in Eq. (2.5) as the superposition of two orthogonal signals $a(t)$ and $b(t)$ satisfying: $\int_{-\infty}^{\infty} a(t)b(t)dt = 0$. The power of $u(t)$ will be given by: $P_u = \lim_{\mathcal{T}\to\infty} \frac{1}{\mathcal{T}} \int_{-\mathcal{T}/2}^{\mathcal{T}/2} \left(a(t) + b(t)\right)^2 dt = \lim_{\mathcal{T}\to\infty} \frac{1}{\mathcal{T}} \int_{-\mathcal{T}/2}^{\mathcal{T}/2} \left(a^2(t) + b^2(t)\right) dt = \lim_{\mathcal{T}\to\infty} \frac{1}{\mathcal{T}} \int_{-\mathcal{T}/2}^{\mathcal{T}/2} |u(t)|^2 dt$.

(far field) radius[4], i.e.,

$$\begin{aligned} P_{\text{rad}} &= \int_0^{2\pi}\int_0^{\pi} \mathcal{D}_{\text{rad}}(\theta)\sin(\theta)d\theta d\varphi \\ &= 2\pi\int_0^{\pi} \mathcal{D}_{\text{rad}}(\theta)\sin(\theta)d\theta \qquad [\text{W}]. \end{aligned} \tag{2.40}$$

Since $\int_0^{\pi} \mathrm{e}^{jK\cos\theta}\sin\theta d\theta = 2\mathrm{sinc}(K)$, we obtain

$$P_{\text{rad}} = \sum_{q=-\infty}^{\infty}\left[\sum_{n=0}^{N-1}|I_n|^2|G_{nq}|^2 + \sum_{m=0}^{N-1}\sum_{\substack{n=0\\n\neq m}}^{N-1} I_m I_n^* G_{mq}G_{nq}^*\mathrm{sinc}(k(z_m-z_n))\right]4\pi\mathcal{D}_u. \tag{2.41}$$

Note that we can associate every couple of summands in

$$\sum_{m=0}^{N-1}\sum_{\substack{n=0\\n\neq m}}^{N-1} I_m I_n^* G_{mq}G_{nq}^*\mathrm{sinc}(k(z_m-z_n)),$$

which have crossed m and n indexes as illustrated below:

$$\begin{aligned} &I_m I_n^* G_{mq}G_{nq}^*\mathrm{sinc}(k(z_m-z_n)) + I_n I_m^* G_{nq}G_{mq}^*\mathrm{sinc}(k(z_n-z_m)) \\ &= 2\,\mathrm{Re}\{I_m I_n^* G_{mq}G_{nq}^*\}\mathrm{sinc}(k(z_m-z_n)). \end{aligned}$$

Since sinc is an even function, the first term above is the complex conjugate of the second one and the sum leads to a real value. Therefore, we can simplify Eq. (2.41) yielding:

$$\begin{aligned} P_{\text{rad}} &= \sum_{q=-\infty}^{\infty}\left[\sum_{n=0}^{N-1}|I_n|^2|G_{nq}|^2 + 2\sum_{m=0}^{N-1}\sum_{\substack{n=0\\n\neq m}}^{N-1}\mathrm{Re}\{I_m I_n^* G_{mq}G_{nq}^*\}\mathrm{sinc}(k(z_m-z_n))\right]\cdot 4\pi\mathcal{D}_u \\ &= \mathcal{G}_{\text{TMA}}P_{u\text{i}}, \end{aligned} \tag{2.42}$$

where $P_{u\text{i}} = 4\pi\mathcal{D}_u$ (measured in W) represents the power radiated by an isotropic antenna transmitting a linearly modulated equivalent baseband digital signal $u(t) \in \mathbb{C}$ with a power density $\mathcal{D}_u$, whereas $\mathcal{G}_{\text{TMA}}$ represents the TMA power transfer function (dimensionless) accounting for both the array geometry and the time-modulated elements radiating a carrier signal. The $\mathcal{G}_{\text{TMA}}$ expression coincides with the array total power in [BRÉGAINS 2008, Eq. (30)] and, as expressed there, such a factor can be used to separate the useful power ($q = 0$) from the harmonic sideband radiation (SR) ($q \neq 0$) losses in a similar way than that described in this work. By splitting up those terms we have

$$P_{\text{rad}} = \left(\mathcal{G}_{\text{TMA}_0} + \mathcal{G}_{\text{TMA}_{\text{SR}}}\right)P_{u\text{i}}, \tag{2.43}$$

where $\mathcal{G}_{\text{TMA}_0} = \mathcal{G}_{\text{TMA}}\big|_{q=0}$ and $\mathcal{G}_{\text{TMA}_{\text{SR}}} = \mathcal{G}_{\text{TMA}}\big|_{q\neq 0}$.

[4]Notice that the implicit factor $\mathrm{e}^{j\vec{k}\cdot\vec{R}}/R$, being $\vec{R}$ the field point vector, in the array factor Eq. (2.1) allows us to assign W/m^2 units to both $\mathcal{D}_u$ and $\mathcal{D}_{\text{rad}}$.

2.3.2 Analysis of the Radiated Power: Frequency Domain

The power radiated density in the frequency domain can be found by applying Parseval's theorem [SKLAR 2001; PROAKIS 2008] to Eq. (2.27):

$$\mathcal{D}_{\text{rad}}(\theta) = \frac{1}{2\pi} \lim_{\mathcal{W}\to\infty} \frac{1}{\mathcal{W}} \int_{-\mathcal{W}/2}^{\mathcal{W}/2} |S_{\text{rad}}(\theta,\omega)|^2 d\omega, \tag{2.44}$$

where $|S_{\text{rad}}(\theta,\omega)|^2 = |\text{FT}\left[s_{\text{rad}}(\theta,t)\right]|^2$ is the energy spectral density of the signal transmitted by the array that is a function of both angular spherical coordinates and frequency.
By considering the relationship between the radiated signal Eq. (2.28) and its complex-valued representation Eq. (2.10)

$$s_{\text{rad}}(\theta,t) = \text{Re}\left\{\tilde{s}_{\text{rad}}(\theta,t)\right\} = \frac{\tilde{s}_{\text{rad}}(\theta,t) + \tilde{s}^*_{\text{rad}}(\theta,t)}{2}, \tag{2.45}$$

and applying the FT we obtain

$$S_{\text{rad}}(\theta,\omega) = \frac{\tilde{S}_{\text{rad}}(\theta,\omega) + \tilde{S}^*_{\text{rad}}(\theta,-\omega)}{2}. \tag{2.46}$$

Taking Eqs. (2.15), (2.17) and (2.22) into account we can obtain[5]

$$|S_{\text{rad}}(\theta,\omega)|^2 = \frac{1}{4}\left[|\tilde{S}_{\text{rad}}(\theta,\omega)|^2 + |\tilde{S}_{\text{rad}}(\theta,-\omega)|^2\right]. \tag{2.47}$$

Substituting Eq. (2.47) into Eq. (2.44) we have

$$\begin{aligned}
&\frac{1}{2\pi} \lim_{\mathcal{W}\to\infty} \frac{1}{\mathcal{W}} \int_{-\mathcal{W}/2}^{\mathcal{W}/2} \frac{1}{4}\left[|\tilde{S}_{\text{rad}}(\theta,\omega)|^2 + |\tilde{S}_{\text{rad}}(\theta,-\omega)|^2\right] d\omega \\
&= \frac{1}{4\pi} \lim_{\mathcal{W}\to\infty} \frac{1}{\mathcal{W}} \int_{-\mathcal{W}/2}^{\mathcal{W}/2} |\tilde{S}_{\text{rad}}(\theta,\omega)|^2 d\omega \\
&= \mathcal{D}_{\text{rad}}(\theta).
\end{aligned} \tag{2.48}$$

We now calculate

$$\begin{aligned}
|\tilde{S}_{\text{rad}}(\theta,\omega)|^2 &= \left[\sum_{n=0}^{N-1} \tilde{S}_n(\theta,\omega)\right]\left[\sum_{n=0}^{N-1} \tilde{S}^*_n(\theta,\omega)\right] \\
&= \sum_{n=0}^{N-1} |\tilde{S}_n(\theta,\omega)|^2 + \sum_{m=0}^{N-1} \sum_{\substack{n=0 \\ n\neq m}}^{N-1} \tilde{S}_m(\theta,\omega)\tilde{S}^*_n(\theta,\omega).
\end{aligned} \tag{2.49}$$

[5] In the expansion $|S_{\text{rad}}(\theta,\omega)|^2 = \frac{1}{4}\{\tilde{S}_{\text{rad}}(\theta,\omega)\tilde{S}^*_{\text{rad}}(\theta,\omega)$
$+\tilde{S}_{\text{rad}}(\theta,\omega)\tilde{S}_{\text{rad}}(\theta,-\omega) + \tilde{S}^*_{\text{rad}}(\theta,-\omega)\tilde{S}^*_{\text{rad}}(\theta,\omega) + \tilde{S}^*_{\text{rad}}(\theta,-\omega)\tilde{S}_{\text{rad}}(\theta,-\omega)\}$
the terms $\tilde{S}_{\text{rad}}(\theta,\omega)\tilde{S}_{\text{rad}}(\theta,-\omega)$ and $\tilde{S}^*_{\text{rad}}(\theta,-\omega)\tilde{S}^*_{\text{rad}}(\theta,\omega)$ will vanish. This is readily seen with the help of Fig. 2.2: $|\tilde{S}_{\text{rad}}(\theta,\omega)|$ is centered at ω_c, so $|\tilde{S}_{\text{rad}}(\theta,-\omega)|$ will be centered at $-\omega_c$ (because $|\tilde{S}_{\text{rad}}(\theta,-\omega)|$ will be obtained by reflecting $|\tilde{S}_{\text{rad}}(\theta,\omega)|$ with respect to the $\omega = 0$ axis). Thus, the larger amplitudes of $\tilde{S}_{\text{rad}}(\theta,\omega)$ (i.e., ω around ω_c) will fall into the region where $|\tilde{S}_{\text{rad}}(\theta,-\omega)|$ is zero (due to the fact that $\omega_c \gg \omega_0$ (see Eq. (2.17) and comments below Eq. (2.3)), and vice versa, the relevant nonzero values of $|\tilde{S}_{\text{rad}}(\theta,-\omega)|$ will fall into the regions where $|\tilde{S}_{\text{rad}}(\theta,\omega)|$ is zero. Therefore, their multiplication will be zero for $-\infty < \omega < \infty$. The same reasoning applies to the other product. Besides, $|\tilde{S}^*_{\text{rad}}(\theta,-\omega)|^2 = |\tilde{S}_{\text{rad}}(\theta,-\omega)|^2$.

The two sums above are easily determined from Eq. (2.15) and the two restrictions in Eqs. (2.17) and (2.19). Indeed,

$$\sum_{n=0}^{N-1} |\tilde{S}_n(\theta,\omega)|^2 = \sum_{n=0}^{N-1} \left[\sum_{q=-\infty}^{\infty} |I_n|^2 |G_{nq}|^2 V(\omega,q) \right], \tag{2.50}$$

and

$$\sum_{m=0}^{N-1} \sum_{\substack{n=0 \\ n\neq m}}^{N-1} \tilde{S}_m(\theta,\omega)\tilde{S}_n^*(\theta,\omega) = \sum_{m=0}^{N-1} \sum_{\substack{n=0 \\ n\neq m}}^{N-1} \sum_{q=-\infty}^{\infty} I_m I_n^* G_{mq} G_{nq}^* \mathrm{e}^{jk(z_m-z_n)\cos\theta} V(\omega,q), \tag{2.51}$$

where $V(\omega,q) = 2|U(\omega-(\omega_c+q\omega_0))|^2$. Substituting Eqs. (2.50) and (2.51) in Eq. (2.49), and the result in the integral in Eq. (2.44) we have:

$$\mathcal{D}_{\text{rad}}(\theta) =$$
$$\frac{1}{4\pi} \lim_{\mathcal{W}\to\infty} \frac{1}{\mathcal{W}} \int_{-\mathcal{W}/2}^{\mathcal{W}/2} \sum_{q=-\infty}^{\infty} \left[\sum_{n=0}^{N-1} |I_n|^2 |G_{nq}|^2 + \sum_{m=0}^{N-1} \sum_{\substack{n=0 \\ n\neq m}}^{N-1} I_m I_n^* G_{mq} G_{nq}^* \mathrm{e}^{jk(z_m-z_n)\cos\theta} \right] V(\omega,q) d\omega. \tag{2.52}$$

For each index q, we must solve:

$$\begin{aligned} &\frac{1}{2\pi} \lim_{\mathcal{W}\to\infty} \frac{1}{\mathcal{W}} \int_{-\mathcal{W}2}^{\mathcal{W}/2} |U(\omega-(\omega_c+q\omega_0))|^2 d\omega \\ &= \frac{1}{2\pi} \lim_{\mathcal{W}\to\infty} \frac{1}{\mathcal{W}} \int_{-\mathcal{W}/2}^{\mathcal{W}/2} |U(\omega)|^2 d\omega \\ &= \frac{1}{2\pi} \lim_{\mathcal{W}\to\infty} \frac{1}{\mathcal{W}} \int_{-\mathcal{W}/2}^{\mathcal{W}/2} |S(\omega)|^2 d\omega \\ &= \mathcal{D}_S = \mathcal{D}_U, \end{aligned} \tag{2.53}$$

where $\mathcal{D}_S = \mathcal{D}_U$ is the power density of the linearly modulated digital signal. By considering Parseval's theorem in Eq. (2.39), the equality $\mathcal{D}_U = \mathcal{D}_u$ is satisfied. Also, the first equality in Eq. (2.53) is true because, according to the two restrictions in Eqs. (2.17) and (2.22), signals inside the respective integrals in Eq. (2.52) (independently from q) are replicas of $|U(\omega)|^2$. Consequently, each of the areas under them over their respective frequency range for a given q is exactly the same as the one centered at the origin.

Furthermore, according to Eqs. (2.5) and (2.7), $u(t)$ is given by

$$u(t) = \sum_{k=-\infty}^{\infty} c_k g_T(t-kT_s), \tag{2.54}$$

where $c_k = a_k + jb_k$ are complex-valued symbols. Hence, $u(t)$ is an infinite sequence of symbols which we will assume zero-mean and uncorrelated. Recall that every T_s

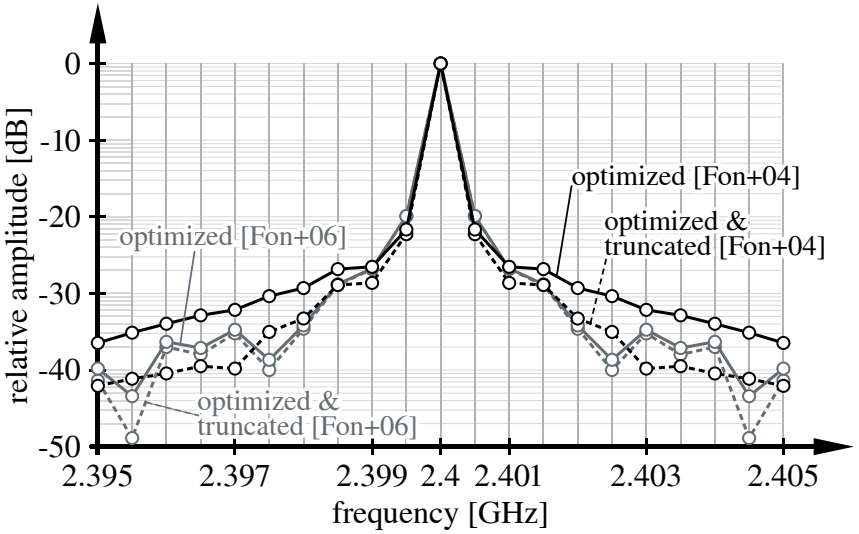

Figure 2.3: TMA total mean normalized radiated power (mapping the first $\mathcal{G}_{\text{TMA}}$ meaningful terms) for the example in Section 2.4.

seconds we send a pulse of the form $c_k g_T(t - kT_s)$ with an average energy spectral density $E_s|G_T(\omega/2\pi)|^2 = E_s|G_T(f)|^2$, with E_s being the average symbol energy of the sequence. Therefore, the power spectral density of $u(t)$ is obtained as $E_s|G_T(f)|^2/T_s$. Consequently, the integral in Eq. (2.53) in terms of the energy spectral density of $u(t)$ can be expressed as

$$\mathcal{D}_U = \frac{1}{2\pi} \lim_{\mathcal{W}\to\infty} \int_{-\mathcal{W}/2}^{\mathcal{W}/2} \frac{E_s|G_T(\omega/2\pi)|^2}{T_s} d\omega = \frac{E_s\|g_T\|^2}{T_s}, \tag{2.55}$$

where $\|g_T\|^2$ is the energy of the shaping pulse in Eq. (2.20):

$$\|g_T\|^2 = \frac{1}{2\pi} \lim_{\mathcal{W}\to\infty} \int_{-\mathcal{W}/2}^{\mathcal{W}/2} |G_T(\omega/2\pi)|^2 d\omega = \frac{T_s(4-\rho)}{4}, \tag{2.56}$$

which leads to a simple expression for $\mathcal{D}_U$:

$$\mathcal{D}_U = \frac{E_s}{4}(4-\rho). \tag{2.57}$$

Therefore, by considering Eq. (2.53) and the equality $\mathcal{D}_U = \mathcal{D}_u$, Eq. (2.52) takes exactly the form of Eq. (2.37). Then, by integrating Eq. (2.52) over the whole space according to Eq. (2.40), and taking into account the definition of $\mathcal{G}_{\text{TMA}}$ in Eq. (2.42) we arrive at

$$P_{\text{rad}} = \mathcal{G}_{\text{TMA}} 4\pi \mathcal{D}_U = \mathcal{G}_{\text{TMA}} P_{ui} \quad [\text{W}], \tag{2.58}$$

which is, as expected, the same result as the one given in Eq. (2.42).

2.4 Example

As a numerical example we consider two TMAs optimized through simulated annealing (SA) and published in [FONDEVILA 2004, Fig. 2] and [FONDEVILA 2006, Table 3]. We also

consider –without impact in terms of maximum side-lobe level (SLL) of the $q = 0$ power pattern– an inter-element distance $d = \lambda/2$ (instead of $d = 0.7\lambda$ used in [FONDEVILA 2004; FONDEVILA 2006]). Both TMAs transmit a M-QAM signal with $M = 256$ and $R_b = 1$ Mbit/s. Given that $R_b = J/T_s$, with $J = \log_2(M) = 8$, the symbol period is $T_s = J/R_b = 8\,\mu$s. The modulator has a shaping filter with $\rho = 0.2$, yielding a signal bandwidth $B = (1 + \rho)/T_s = 150$ kHz according to Eq. (2.21).

We plot in Fig. 2.3 the distribution of the total mean normalized radiated power at the carrier frequency $f_c = 2.4$ GHz and at the first ten multiples of $f_0 = 500$ kHz, i.e., the mapping of the corresponding terms of the $\mathcal{G}_{\text{TMA}}$ defined in Eq. (2.42). The curves labeled as "optimized" corresponds directly to the above-mentioned pulse distribution, while "optimized & truncated" curves consider permanently in off-state those elements whose normalized pulse durations are very close to zero (elements 1, 3, 4, and 5 in [FONDEVILA 2004]), while those elements whose normalized pulse durations are very close to one (elements 23 and 29 in [FONDEVILA 2004]; and elements 14 and 15 in [FONDEVILA 2006]) are set permanently to on-state. The TMA power efficiency [BRÉGAINS 2008] is improved from 96.7 % to 98 % for [FONDEVILA 2004] (lowering the overall SR level), and from 96.8 % to 97 % for [FONDEVILA 2006], keeping the main ($q = 0$) power pattern SLL topology almost unchanged (for [FONDEVILA 2004], the maximum SLL equals -20.02 dB for the non-truncated case, and -19.43 dB for the truncated one; -15.91 dB and -15.90 dB for [FONDEVILA 2006], respectively).

2.5 Conclusion

The possible impact on the information content caused by TMAs when used for transmission of linearly modulated signals can be overridden if constraints in Eqs. (2.17) and (2.22) are applied. Under those conditions, together with the assumption of a fast decaying rate of the harmonics level as a function of q, a generalized TMA power response is accurately derived and given by the product of its power transfer function and the equivalent baseband signal power. The TMA transfer power function is presented as its canonical response. In other words, the TMA radiated power when a single carrier at its center frequency is transmitted.

Both time and frequency domain analyses have been carried out to quantify the power-radiated efficiency of the TMA when it is combined with digital linear modulation schemes, hence allowing for the use of conditioned TMAs in wireless communication systems.

Chapter 3

Impact of TMAs on the BER of Linear Digital Modulations

Once demonstrated the feasibility of the time-modulated array (TMA) technique applied to a digital communication in Chapter 2, in this chapter we investigate the quality of such a communication expressed in terms of bit error ratio (BER).

This chapter is mainly based on the following co-authored publication:

- R. Maneiro-Catoira, J. Brégains, J. A. García-Naya, and L. Castedo. "**Impact of time-modulated arrays on the BER of linear digital modulations**". *Journal of Electromagnetic Waves and Applications*, vol. 29, no. 16, 2015, pp. 2147–2154. ISSN: 0920-5071.
  DOI: 10.1080/09205071.2015.1075908

The structure of the chapter is the following. In Section 3.2, a closed form for the TMA gain is derived. Such an expression allows for quantifying the power balance of a wireless communication system that uses an M-ary linear digital modulation scheme with a conventional array at the transmitter and a TMA at the receiver side. Section 3.3 models a generalized discrete-time receiver based on a linear digital modulation scheme incorporating a TMA. As a result, the closed form expressions for the bit error rate can be properly derived. Next, in Section 3.4, results obtained by means of numerical simulations –considering different distributions for the antenna excitations– are shown in order to illustrate the impact of TMAs on the performance of linear digital communication systems. Finally, the conclusions of the chapter are compiled in Section 3.5.

3.1 Introduction

The possibility of transmitting communication signals using TMAs has been studied in [BRÉGAINS 2008; ZHU 2013; MANEIROCATOIRA 2014a]. The investigations corresponding to this chapter of the thesis go a step further and analyzes the impact of TMAs on the system

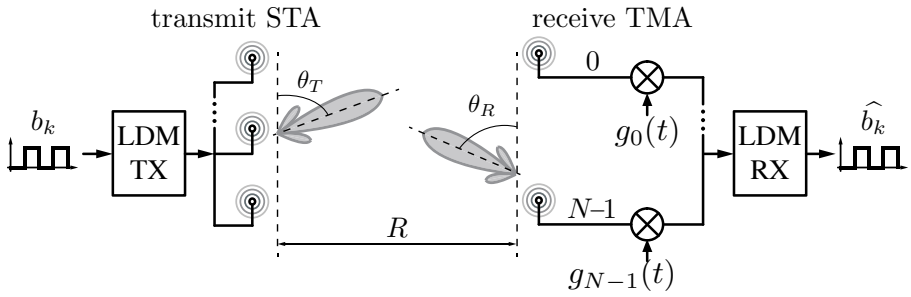

Figure 3.1: Digital communication system based on an M-ary linear modulation scheme with a conventional transmit-STA and a receive-TMA synthesizing pencil beam radiation patterns.

BER when linear digital modulation (LDM) signals are transmitted. In other words, due to the nature of TMAs, it is relevant here to link the classical array synthesis trade-off among side-lobe level (SLL), gain, and half-power beamwidth (HPBW), to a key figure of merit in digital communication systems such as the BER. It is also useful to include a less quantitative parameter, the complexity of the array feeding network.

Antenna arrays with non-uniform amplitude excitation distributions provide radiation patterns with a desired SLL value. For the case of a conventional static array (STA), since the dynamic range[1] of the amplitude distribution is higher, the SLL decreases. Furthermore, the STA feeding network becomes more complex and thus more difficult to design and construct. However, the TMA philosophy is not based in amplitude control through the feeding geometric configuration. A TMA feeding network makes use of pure time control; in fact, as indicated in previous sections, its usual circuitry consists of simple ON/OFF periodical switching of the antenna elements [KUMMER 1963]. Therefore, from an engineering point of view, a comparison between a TMA solution and its STA counterpart should unequivocally include the complexity of the feeding network.

In this work we take, as a design premise, a STA with a relatively low level of complexity; in other words, not very restrictive in terms of SLL. In this case, and for simplicity, we consider a real-valued amplitude distribution on a linear array. We will apply time modulation to the previous STA –thus introducing a modest extra cost in terms of complexity– in order to achieve a previously specified SLL level [KUMMER 1963]. As a novelty, we quantify theoretically the system BER as a function of the TMA normalized pulse durations, providing closed-form expressions to compare TMAs and STAs for different scenarios in wireless communications.

3.2 Power Balance

Let us calculate the power balance of the wireless communication system shown in Fig. 3.1. Such a system uses an M-ary linear digital modulation scheme [PROAKIS 2008] with a conventional STA at the transmitter side and a TMA at the receiver side, separated from the

[1]The dynamic range can be defined as $|I_n|_{\max}/|I_n|_{\min}$.

transmitter by a distance R. Both transmit-STA and receive-TMA exhibit synthesizing pencil-beam patterns whose maximums are pointed into directions θ_T and θ_R radians off the z-axis, respectively (see Fig. 3.1)[2].

Recall now that the radiated field of a linear TMA composed of N isotropic elements distributed along the z axis is given by [KUMMER 1963; BRÉGAINS 2008; ZHU 2013]

$$F(\theta,t) = \mathrm{e}^{j\omega_c t}\sum_{n=0}^{N-1}\sum_{q=-\infty}^{\infty} G_{nq}\mathrm{e}^{jq\omega_0 t} I_n \mathrm{e}^{jkz_n\cos\theta} = \sum_{q=-\infty}^{\infty} F_q(\theta,t), \tag{3.1}$$

where G_{nq} are the Fourier series expansion coefficients of periodic functions (usually rectangular pulses with period $T_0 = 2\pi/\omega_0$) applied to the array n-th element; $I_n = |I_n|\mathrm{e}^{j\phi_n}$ and z_n are, respectively, the complex current excitation and the position on the z-axis for such an element; the θ variable corresponds to the angle with respect to the z-axis; and $k = 2\pi/\lambda$ is the wavenumber for a carrier wavelength $\lambda = c/f_c$.

The maximum gain of the receive-TMA is given by [ZHU 2013]

$$G_{\text{TMA}} = \eta_s 4\pi |F_0(\theta,t)|^2_{\text{max}}/P_{\text{rad}}, \tag{3.2}$$

where η_s corresponds to the efficiency of the switches of the feeding network including the power absorption of their off-state; $F_0(\theta,t)$ is $F_q(\theta,t)$ given in Eq. (3.1) for $q = 0$; and P_{rad} is the average radiated power by the TMA when a sinusoidal carrier is transmitted and is given by [MANEIROCATOIRA 2014a]

$$P_{\text{rad}} = 4\pi\sum_{q=-\infty}^{\infty}\left\{\sum_{n=0}^{N-1}|I_n|^2|G_{nq}|^2 + 2\sum_{n=0}^{N-1}\sum_{\substack{m=0\\m\neq n}}^{N-1}\mathrm{Re}\{I_m I_n^* G_{mq} G_{nq}^*\}\mathrm{sinc}(k(z_m - z_n))\right\} \tag{3.3}$$

A simplified expression for Eq. (3.2) is obtained when the inter-element spacing is set to $\lambda/2$, the element excitations are real-valued $I_n \in \Re$ (thus $I_n = |I_n|$), and the pulse modulations $g_n(t)$ are (e.g. in [BRÉGAINS 2008]) even rectangular pulses. This last hypothesis allows for the representation of $g_n(t)$ by means of a Fourier series expansion with real coefficients of the form

$$G_{nq} = \xi_n \mathrm{sinc}(q\pi\xi_n), \tag{3.4}$$

where ξ_n is the normalized pulse time duration of the n-th element. In such a case, the maximum squared amplitude can be simplified to

$$|F_0(\theta,t)|^2_{\text{max}} = [F_0(\theta,t)F_0^*(\theta,t)]_{\theta=\frac{\pi}{2}} = \left[\sum_{n=0}^{N-1} I_n\xi_n\right]^2 \tag{3.5}$$

[2]It can be seen from that figure that the main axes of the antennas are considered to be both parallel to the z-axis of a global coordinate system.

We now plug Eqs. (3.3) to (3.5) into Eq. (3.2) to rewrite the receive-TMA gain as

$$G_{\text{TMA}} = \frac{\eta_s \left[\sum_{n=0}^{N-1} I_n \xi_n\right]^2}{\sum_{n=0}^{N-1} I_n^2 \xi_n^2 + \sum_{n=0}^{N-1} \left[\sum_{\substack{q=-\infty \\ q\neq 0}}^{\infty} I_n^2 \xi_n^2 \text{sinc}^2(q\pi\xi_n)\right]}, \tag{3.6}$$

Having in mind that for all $\xi_n \in (0,1)$ the sinc-squared infinite series converges to $1/\xi_n$, then

$$\sum_{\substack{q=-\infty \\ q\neq 0}}^{\infty} \text{sinc}^2(q\pi\xi_n) = \frac{1}{\xi_n} - 1, \tag{3.7}$$

and we can simplify Eq. (3.6) to obtain

$$G_{\text{TMA}} = \frac{\eta_s \left[\sum_{n=0}^{N-1} I_n \xi_n\right]^2}{\sum_{n=0}^{N-1} I_n^2 \xi_n} = \frac{\eta_s \left[\sum_{n=0}^{N-1} I_{\text{TMA}_n}\right]^2}{\sum_{n=0}^{N-1} I_n^2 \xi_n}, \tag{3.8}$$

where $I_{\text{TMA}_n} = I_n \xi_n$ is the n-th dynamic excitation [BRÉGAINS 2008].

Since the transmitting antenna is considered to be a conventional N-element STA with a $\lambda/2$ inter-element spacing and the same static excitations I_n, we can find the maximum gain of the transmit-STA in a completely analogous way. We will then arrive at

$$G_{\text{STA}} = \frac{\left[\sum_{n=0}^{N-1} I_n\right]^2}{\sum_{n=0}^{N-1} I_n^2}. \tag{3.9}$$

Finally, we apply the well-known Friis Transmission Equation [BALANIS 2005] to determine the received-to-transmitted power ratio,

$$\frac{P_R}{P_T} = \left(\frac{\lambda}{4\pi R}\right)^2 G_{\text{STA}} G_{\text{TMA}}, \tag{3.10}$$

where the transmit and receive antennas are considered to be perfectly aligned[3], i.e., $\theta_T = \theta_R = \pi/2$.

3.3 Discrete-Time Receiver: System BER

Fig. 3.2 shows the block diagram of a M-ary LDM receiver with an embedded TMA. Such a receiver is able to detect, with minimum error probability,[4] the waveform sent at every symbol

[3] In this case, as the array elements are isotropic, the polarization matching factor is tacitly regarded as unity.

[4] The minimum error probability (P_e) criterion [KAY 1998] is applied in Detection Theory when a multiple hypothesis test H_i is present ($H_i \in \{\text{True, False}\}$ being True if s_i was sent and False otherwise), with $i \in \Psi = \{0, 1, \cdots, M-1\}$ for an M-ary scheme. In addition, both a priory probabilities $p(H_i)$ and probability density functions $p(x/H_i)$ are assumed to be known for the indices $i \in \Psi$. The detector chooses the H_i that maximizes $p(H_i/x)$ which is equivalent to minimize $P_e = \sum_{i=0}^{M-1} \sum_{j=0}^{M-1} \delta_{ij} p(H_i/H_j) p(H_j)$, where δ_{ij} is the Kronecker delta.

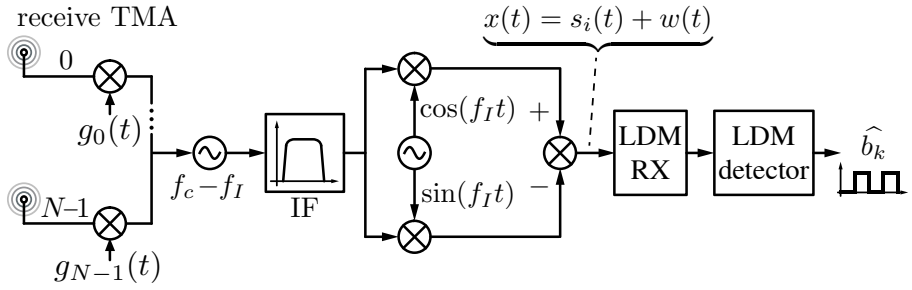

Figure 3.2: Generalized receiver based in a linear digital modulation scheme incorporating a TMA.

interval T_s from a set of M possible transmit waveforms, with M being the order of the LDM signal constellation. We also assume that the received signal is distorted by additive white Gaussian noise (AWGN). Therefore, after down-conversion of the signal received by the TMA (which, depending on the receiver architecture, involves operations such as band-pass filtering, I/Q demodulation or low-pass filtering) at every T_s seconds, the signal

$$x(t) = s_i(t) + w(t), \text{ with } i \in \Psi = \{0, 1, \dots M-1\} \tag{3.11}$$

is available at the input of the LDM detector (see Fig. 3.2). If the frequencies of both the TMA and the signal satisfy [BRÉGAINS 2008] the restrictions (see Eqs. (2.17) and (2.22) in pages 20 and 21, respectively)

$$T_0 \gg 1/f_c \quad \text{and} \quad \omega_0 > B_\omega, \tag{3.12}$$

with ω_0 the angular frequency of the TMA periodic pulses, f_c the carrier frequency of the LDM signal, and B_ω its bandwidth, then the signals $s_i(t)$, $i \in \Psi$ (see Fig. 3.2) will be deterministic. On the other hand, $w(t)$ represents AWGN with zero mean and variance σ^2. Under these circumstances, the BER expressions for the system in Fig. 3.2 can be obtained through the derivations found in [PROAKIS 2008]. All BER expressions can be obtained as particular cases of the following closed-form expression with a common structure [PROAKIS 2008]:

$$\text{BER}_{\text{mod}}(E_N) = f_{\text{mod}}(M) Q\Big(\sqrt{g_{\text{mod}}(M) E_N}\Big), \tag{3.13}$$

where f_{mod} and g_{mod} are two scalar parameters that depend on the constellation size M and on the linear modulation type (ASK, PSK, and QAM); $Q(\cdot)$ is the well-known Gaussian error function; and $E_N = E_b/N_0$ is the ratio between energy per bit and power spectral density of the thermal noise at the receiver, being given by [PROAKIS 2008] $E_N = B_\omega \text{SNR}/(2\pi f_s \log_2 M)$ with SNR, B_ω, and f_s the signal-to-noise ratio (SNR), the bandwidth, and the symbol rate of the received LDM signal.

Since our aim is to compare the performance of the system when incorporating a receive-TMA with respect to its STA counterpart, we introduce the following TMA cost function (see Eqs. (3.8) and (3.9)):

$$\alpha = \alpha(I_n, \xi_n) = \frac{G_{\text{TMA}}}{G_{\text{STA}}} = \frac{E_N|_{\text{TMA}}}{E_N|_{\text{STA}}}. \tag{3.14}$$

Table 3.1: Comparison between a TMA uniform optimized distribution –built from a static uniform distribution– and its STA counterpart (see the text for the definition of the parameters).

	TMA SLL $= -19.43$ dB; $N = 30$ HPBW $= 3.6°$; $\lvert F_1\rvert_{\text{max}} = -32.24$ dB			
	α	ΔSLL	ΔHPBW	$\Delta\{\Delta\lvert I_n\rvert\}$
STA uniform	0.82	6.19 dB	0.36°	0.00%
STA uniform optimized	0.98	0.00 dB	0.00°	93.65%

Taking as a reference channel the one corresponding to a scenario with a conventional STA at the receiver, with gain given by Eq. (3.9), we can evaluate, over a reference range of E_N denoted by $E_{N\text{ref}} = E_N|_{\text{STA}}$, the BER for the complete family of LDM signals involving a receive-TMA solution with respect to the STA counterpart by substituting $E_N|_{\text{TMA}} = \alpha E_N|_{\text{STA}}$ from Eq. (3.14) in Eq. (3.13) writing, finally,

$$\text{BER}_{\text{mod}}|_{\text{TMA}} = f_{\text{mod}}(M) Q\left(\sqrt{g_{\text{mod}}(M)\alpha(I_n,\xi_n)E_{N\text{ref}}}\right). \tag{3.15}$$

3.4 Numerical Examples

This section presents the results of numerical examples to quantify the impact on the performance of a QAM digital communication system [PROAKIS 2008] when using a TMA at the receiver and a STA at the transmitter side. We consider the excitation amplitudes of the static feeding network corresponding to two cases: uniform [FONDEVILA 2004], and Dolph-Tschebyscheff [BALANIS 2005; KUMMER 1963] distributions, as explained below.

3.4.1 Optimized Uniform Distribution

Let us consider a 30-element array with uniform current excitations, i.e., $I_n = I_{U_n} = 1$. By means of time modulation (TM) we determine a new pattern with a better maximum SLL whose coefficients are I_{TMA_n}. Such coefficients can be obtained by applying the normalized TM widths ξ_n to the uniform excitations, i.e.,

$$I_{\text{TMA}_n} = I_{\text{U}_n}\xi_n = \xi_n. \tag{3.16}$$

We consider the optimized values for ξ_n obtained in [FONDEVILA 2004][5], which lower the SLL from -13.24 dB to -19.43 dB (hence giving a $\Delta\text{SLL}_{\text{dB}} = |\text{SLL}_{\text{TMA}} - \text{SLL}_{\text{U}}| = 6.19$ dB)

[5] In fact, it corresponds to a simplified version of the distribution given in [FONDEVILA 2004], where the very small (close to 0) and very large (close to 1) ξ_n are replaced by 0 and 1, respectively. Such a simplification, which

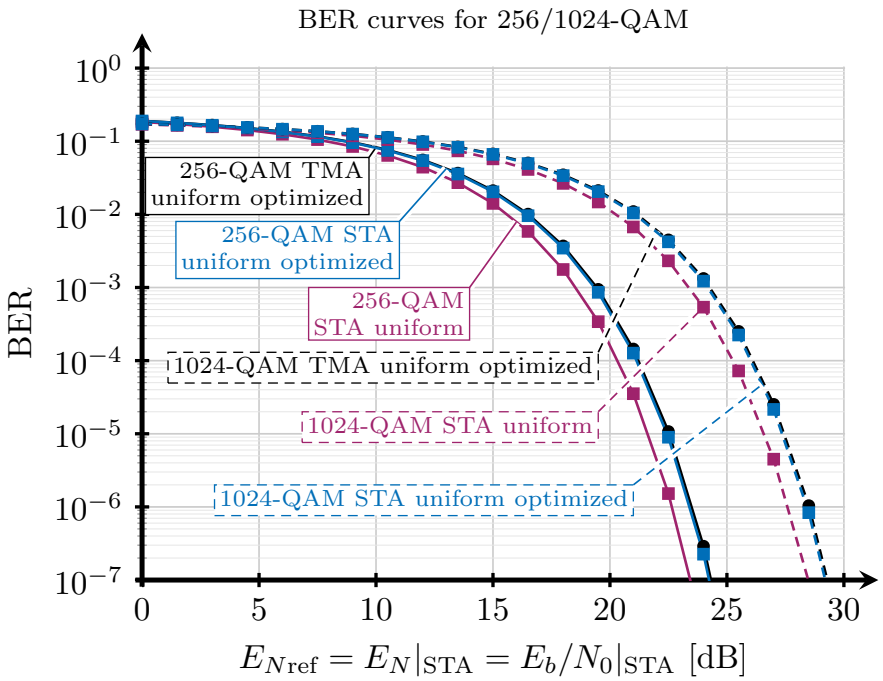

Figure 3.3: BER curves for 256- and 1024-QAM signals received through the arrays outlined in Table 3.1. For a reference BER $= 10^{-6}$ the TMA SNR loss with respect to the STA uniform optimized is 0.1 dB for both 256-QAM and 1024-QAM; and with respect to the STA uniform is 0.9 dB for both 256-QAM and 1024-QAM.

and provide a first side-band maximum harmonic level below $|F_{\text{TMA}_1}|_{\max} = -30\,\text{dB}$. We then compute the gain cost (see Eqs. (3.8), (3.9) and (3.16)) with $\eta_s = 1$ (ideal switches [ZHU 2013]), the HPBW percentage variation $\Delta\text{HPBW} = \text{HPBW}_{\text{TMA}} - \text{HPBW}_{\text{U}}$, and the dynamic range ratio of the static normalized amplitude distribution, defined as a percentage, i.e.,

$$\Delta|I_n|_{\%} = \max\{100(I_{n+1} - I_n)\} \text{ for } n = 0, \ldots, N-2 \tag{3.17}$$

Finally, we repeat the comparison by changing the static amplitude distribution to $I_n = I_{\text{TMA}_n}$, which would lead to the case where the STA has the same pattern than the optimized TMA. Table 3.1 shows the results derived from the mentioned comparisons.

Fig. 3.3 compares the same systems as those given in Table 3.1 but now in terms of the BER curves when QAM signals are sent. Notice that in the first case a considerable improvement in terms of SLL is achieved with a modest degradation on both the beamwidth and gain, resulting in a slight degradation of the BER curves. Recall that in the second case the power pattern is the same for TMA and STA. This indicates that the STA can be replaced by TMA hence showing that the less complex TMA feeding network fully compensates a practically negligible gain cost reduction.

further reduces the first harmonic level and does not change the SLL significantly, is done also in view of the fact that very small or very large time durations would lead to technical problems (too fast switches). This is similar to what has been done in the example given in Section 2.4, see page 29.

Table 3.2: Comparison between a TMA_{DT} with $\text{SLL} = 40\,\text{dB}$ –built from a STA_{DT} with $\text{SLL} = 30\,\text{dB}$– and its STA counterparts.

	TMA $\text{SLL} = -40\,\text{dB}$; $N = 16$ $\text{HPBW} = 8.98°$; $\lvert F_1\rvert_{\text{max}} = -19.94\,\text{dB}$			
	α	ΔSLL	ΔHPBW	$\Delta\{\Delta\lvert I_n\rvert\}$
STA_{DT} SLL=30 dB	0.83	10.00 dB	0.72°	0.00%
STA_{DT} SLL=40 dB	0.93	0.00 dB	0.00°	148.30%

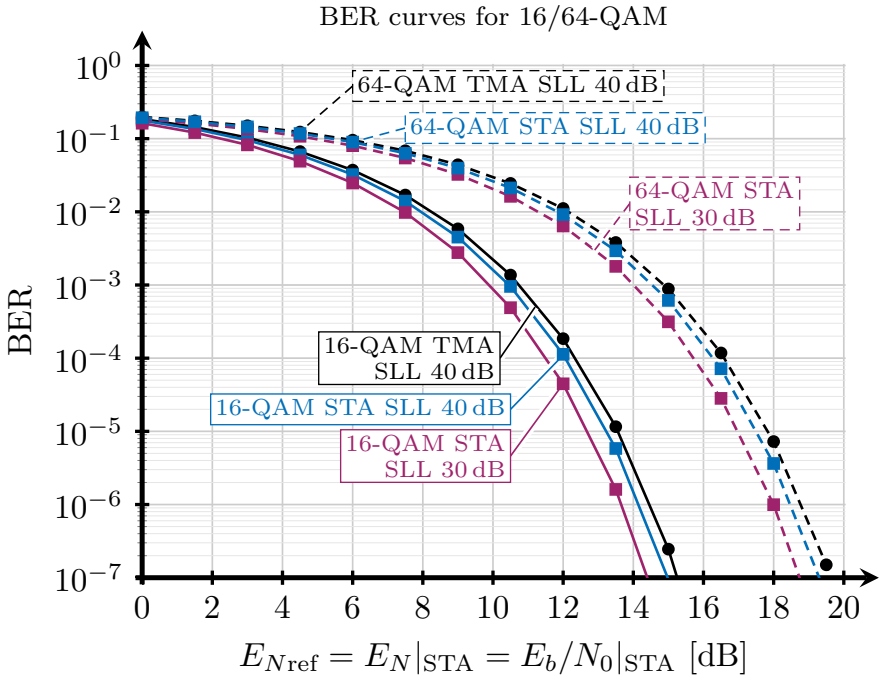

Figure 3.4: BER curves for 16- and 64-QAM signals received through the arrays outlined in Table 3.2. For a reference $\text{BER} = 10^{-6}$ the TMA SNR loss with respect to the STA with $\text{SLL} = 40\,\text{dB}$ is $0.3\,\text{dB}$ for both 16-QAM and 64-QAM; and with respect to the STA with $\text{SLL} = 30\,\text{dB}$ is $0.8\,\text{dB}$ for both 16-QAM and 64-QAM.

3.4.2 Dolph-Tschebyscheff Distribution

We now consider a 16-element array with $I_n = I_{DT_n}$ corresponding to a $-30\,\text{dB}$ DT normalized excitation distribution [BALANIS 2005; KUMMER 1963]. We then apply TM to achieve a new pattern with an $\text{SLL} = -40\,\text{dB}$.

Table 3.2 and Fig. 3.4 show that, when compared to the $\text{STA}_{\text{DT}} = -30\,\text{dB}$, the TMA provides an SLL improvement ($-10\,\text{dB}$) that still could compensate for a relatively low impact on gain (0.826) and, consequently in BER. However, when compared to a STA with the same power pattern, the TMA provides a clear solution according to its modest gain cost and the

reduction of the dynamic range of the excitations. Note that, according to Eq. (3.15) and taking $E_N = E_N|_{\text{STA}}$ in Eq. (3.13), the difference between the absolute values of the slopes of the BER curves for TMA and its STA counterpart can be quantified through

$$m_{\text{TMA}} - m_{\text{STA}} = C_1 \sqrt{\frac{\alpha}{E_N}} \left(\frac{1}{\mathrm{e}^{C_2 E_N}} - \frac{1}{\mathrm{e}^{\alpha C_2 E_N}} \right), \tag{3.18}$$

with $C_1 = f_{\text{mod}}(M)\sqrt{g_{\text{mod}}(M)/(8\pi)}$ and $C_2 = g_{\text{mod}}(M)/2$ observing that, as $0 < \alpha < 1$, then $m_{\text{TMA}} < m_{\text{STA}}$.

3.5 Conclusion

We have characterized the BER of a linearly modulated digital communication system that incorporates a receive-TMA to synthesize pencil beam radiation patterns. The system BER is properly connected to the classical trade-off antenna variables for TMA synthesis purposes. The analysis shows the benefits provided by the TMA technique, namely the reconfigurability of the power pattern while achieving ultra-low levels of SLL with a less complex feeding network, are obtained with minimal impact on the BER.

Chapter 4

Performance Analysis of TMAs to Exploit Angle Diversity at the Receiver

In Chapters 2 and 3 we investigated, respectively, the feasibility and the performance of digital communications when time-modulated arrays (TMAs) were employed, exploiting exclusively the TMA fundamental pattern. However, further investigations should consider the exploitation of harmonic patterns with the aim of increasing the potentialities of TMAs for wireless communications. More specifically, the investigations provided in this chapter focus on the application of the harmonic beamforming capacity of a TMA to a multipath fading digital communication.

This chapter is mainly based on the following co-authored publications:

- R. Maneiro-Catoira, J. Brégains, J. A. García-Naya, L. Castedo, P. Rocca, and L. Poli. "**Performance analysis of time-modulated arrays for the angle diversity reception of digital linear modulated signals**". *IEEE Journal of Selected Topics in Signal Processing*, vol. 11, no. 2, 2017, pp. 247–258. ISSN: 1932-4553.
  DOI: 10.1109/JSTSP.2016.2609852
- R. Maneiro-Catoira, J. Brégains, J. A. García-Naya, and L. Castedo. "**Time-modulated arrays for digital communications in multipath scenarios**". *Proc. of 2015 IEEE International Symposium on Antennas and Propagation and North American Radio Science Meeting (2015 IEEE AP-S & USNC-URSI)*. Vancouver, BC, Canada, 2015, pp. 816–817. ISBN: 9781479978168.
  DOI: 10.1109/APS.2015.7304795

The structure of the chapter is the following. Section 4.1 motivates and introduces the problem. Section 4.2 introduces the considered TMA, its radiation characteristics, and the equivalent baseband model for each multipath component. Such a model is used in Section 4.3 to quantify the average signal-to-noise ratio (SNR) per symbol at each maximum ratio combining (MRC) input branch. Next, Section 4.4 characterizes the symbol error ratio (SER) of such a system when M-ary linear digital modulation (LDM) signals are transmitted, thus allowing for comparing the performance of the system with respect to other approaches

based on conventional arrays. Section 4.5 analyzes the trade-off between the TMA efficiency and the number of multipath components to be exploited. The systems included for comparison purposes are described in Section 4.6. More specifically, the receiver shown in Fig. 4.1 is compared firstly to a single input single output (SISO) system (which does not exploit channel diversity) using a conventional array that has a radiation pattern with the same spatial shape as that of the TMA fundamental mode, but provided with a higher gain because it is not affected by any sideband radiation; and then to a single input multiple output (SIMO) system equipped with a conventional array and an adaptive linear beamforming network (LBFN) capable of synthesizing simultaneously a set of spatial radiation patterns with the same shapes as those generated by the TMA in its operating frequencies (fundamental and harmonics) but, in this case, at a single frequency f_c. Section 4.7 presents the results from numerical simulations. Finally, Section 4.8 is devoted to the conclusions.

4.1 Introduction

According to the state of the art presented in Chapter 1, no previous study has addressed a performance comparison of TMAs with respect to other conventional beamforming adaptive arrays when applied to an LDM communication system over fading channels. Under this approach, the contribution of this chapter is three-fold:

1. The introduction of key aspects for signal transmission (e.g., SNR per path or antenna efficiency) in the synthesis of harmonic beamforming with TMAs.
2. The derivation of closed-form expressions for the SNR per path, the average SNR, and the SER at reception, as functions of the TMA parameters, allowing for synthesizing ad-hoc TMAs for multipath narrowband communication purposes.
3. The comparison of TMAs both in terms of performance and complexity with respect to other conventional beamforming adaptive arrays when applied to an LDM communication system over a realistic fading channel.

LDMs are widely used because of their high spectral efficiency, especially when the number of modulation levels is large [GOLDSMITH 2005, Chapter 5, p. 140]. In addition, LDMs are often combined with powerful error correction codes to become power efficient. On the other hand, TMAs can be used to perform adaptive beamforming, exploiting the multipath channel diversity without the need of phase shifters [ROCCA 2014].

In this chapter we consider a narrowband wireless communication system using an M-ary LDM as shown in Fig. 4.1. We assume an omni-directional antenna at the transmitter and a TMA at the receiver. The signal propagates over different paths (with distinct lengths) and arrives at the receiver from multiple directions. Therefore, the receiver observes multiple replicas of the transmitted signal with different amplitudes and time-delays. In such a scenario, a TMA allows for obtaining an equivalent SIMO system that exploits the angle diversity of the channel by means of adaptive beamforming. Under certain assumptions, this receiver

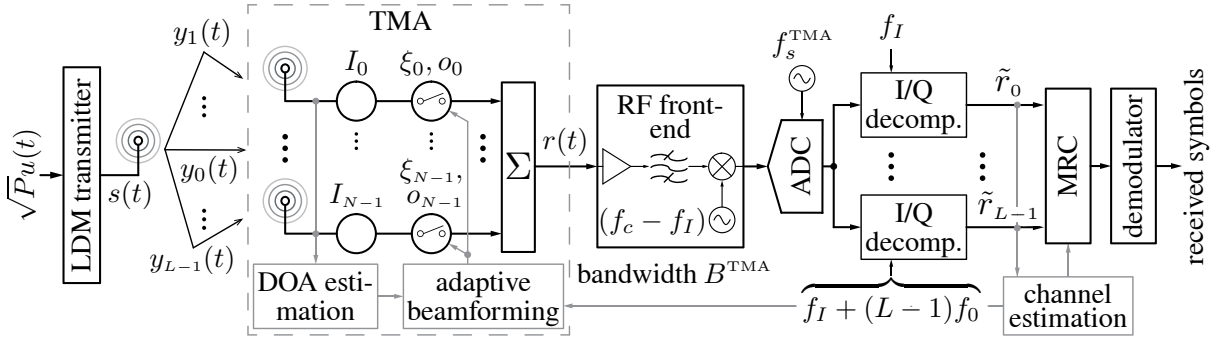

Figure 4.1: Block diagram of a wireless system with an LDM transmitter equipped with an omnidirectional antenna and a TMA for exploiting channel diversity at the receiver. A superheterodyne transceiver architecture is assumed for the receiver, although a direct-conversion design is also possible. The signal at the TMA output $r(t)$ (with a bandwidth B^{TMA}) is first down-converted to f_I and digitized by the analog-to-digital converter (ADC) (with a sampling frequency f_s^{TMA}). Next, for each of the L branches, the signals are I/Q decomposed (the I/Q digital decomposition frequency corresponding to the i-th branch is $f_I + mf_0$), filtered, and decimated. Finally, the obtained discrete-time $\tilde{r}_i$ symbols are forwarded to the MRC, producing an improved version of the received symbol $\tilde{r}$ which is finally sent to the digital demodulator to estimate the transmitted symbol from the received one.

faithfully recovers L multipath replicas of the transmitted signal, making a profitable use of them. Although we will see in detail those assumptions in the forthcoming analysis, we next present an overview of the whole system.

We consider a multipath wireless channel. The different path gains are modeled as zero-mean complex-valued statistically-independent Gaussian-distributed random variables. Such a channel is referred to as Rayleigh fading channel (RFC) and is an adequate model for non-line-of-sight (NLOS) scenarios [M K SIMON 2005, Chapter 2, p. 18]. According to this model, each wireless fading path introduces a random change on the amplitude and on the delay of the transmitted signals. Given that we are considering narrowband communications, such time-delays are assumed to be small enough compared to the symbol duration in order to avoid inter-symbol interference (ISI). We assume that at the receiver we have knowledge of the direction of arrival (DOA) of the L signal replicas to make feasible the TMA adaptive beamforming capabilities (see Fig. 4.1). More specifically, the beamforming is done with the first $L-1$ positive harmonic patterns of the TMA (excluding the fundamental mode), i.e., those at frequencies $f_c \pm mf_0, m = 1, \ldots, L-1$, where f_0 is the TMA pulse frequency, and f_c the carrier frequency. We also assume that the signal replica $y_0(t)$ has a DOA that coincides with the maximum of the TMA fundamental mode pattern and hence there is no need for beamforming with the fundamental mode. The beamforming will satisfy the spatial orthogonality among all the TMA radiation patterns (fundamental and harmonics) in the directions of their respective maximums to avoid interference between the replicas [ROCCA 2014]. On the other hand, we assume perfect channel state information (CSI) [M K SIMON 2005, Chapter 7, p. 159] at the

receiver when determining the MRC parameters. Regarding the frequencies involved in the data transmission process, the TMA pulse frequency (f_0) and the signal bandwidth (B) must satisfy the condition $f_0 > 2B$ to avoid overlapping [MANEIROCATOIRA 2014a]. We also assume, for the sake of simplicity, that there are no interference signals impinging on the TMA at $f_c + mf_0$. Finally, the noise at the receiver is modeled as additive white Gaussian noise (AWGN) [SKLAR 2001, Chapter 1, p. 33].

4.2 Characterization of the Diversity Paths

Let us consider that the receive antenna in Fig. 4.1 is a linear TMA with N isotropic elements distributed along the z axis. Let $g_n(t)$ be the periodic pulse train (with fundamental period T_0 and fundamental frequency $f_0 = 1/T_0$) that controls the n-th array element. Since $g_n(t)$ is a periodic signal, it can be represented by its Fourier series expansion. For rectangular pulses, the q-th coefficient of such a series is given by [POLI 2011b]

$$G_{nq} = \xi_n \mathrm{sinc}(q\pi\xi_n)\mathrm{e}^{-jq\pi(\xi_n+2o_n)}, \tag{4.1}$$

where $\mathrm{sinc}(x) = \sin(x)/x$ denotes the sinc function, $n \in \Upsilon = \{0, \ldots, N-1\}$, $\xi_n \in (0,1) \subset \mathbb{R}$ are the normalized pulse time durations and $o_n \in [0, 1-\xi_n] \subset \mathbb{R}$ the switch-on instants, respectively. On the other hand, the array factor with the term $\mathrm{e}^{j2\pi(f_c+qf_0)t}$ explicitly included, $F_q^{\mathrm{TMA}}(\theta, t)$, corresponding to the harmonic frequency $q\omega_0$ is given by [ZHU 2013]

$$F_q^{\mathrm{TMA}}(\theta, t) = \mathrm{e}^{j2\pi(f_c+qf_0)t} \sum_{n=0}^{N-1} G_{nq} I_n \mathrm{e}^{jkz_n \cos\theta}, \tag{4.2}$$

where z_n represents the n-th array element position on the z-axis, $I_n = |I_n|\mathrm{e}^{j\varphi_n}$ is the complex static current excitation in polar form ($|I_n|$ is its modulus and φ_n is its phase), θ is the angle with respect to the array main axis, k is the wavenumber, and f_c is the carrier frequency.

The optimization of the periodic pulse trains $g_n(t)$ often focuses on the generation of suitable harmonic beams. Notice that when only the fundamental beam ($q = 0$) is exploited, the TMA will acquire the desired signal over the pattern $F_0^{\mathrm{TMA}}(\theta, t)$. However, TMAs are able to simultaneously receive multiple replicas arriving from different directions over the higher order harmonic patterns $F_q^{\mathrm{TMA}}(\theta, t)$ with $q \neq 0$.

Fig. 4.1 shows a block diagram of a wireless digital communication system capable of exploiting channel diversity. At the receiver, the signals $y_m(t)$ (with $m \in \Psi = \{0, 1, \ldots, L-1\}$), each one corresponding to the m-th multipath signal component, are acquired through a TMA that performs beamforming with the first $L-1$ harmonic patterns. At the output of the TMA, each multipath signal component appears at its own carrier frequency $f_c + mf_0$ (with $m \in \Psi$). Assuming $f_0 > 2B$, being B the signal bandwidth, implies that there is no overlapping in the frequency domain between the multipath signals and they can be down-converted to an intermediate frequency f_I by a conventional RF front-end with the only requirement of

supporting the additional bandwidth required by the $L-1$ signal multipath components. After the down-converter, multipath signal components appear at frequencies $f_I + mf_0$.

In the next step, the signals are converted to the digital domain by means of a single ADC configured with a sampling frequency f_s^{TMA} high enough, given the bandwidth B^{TMA} occupied by all multipath signal components. At each demodulator branch, the digital signal is first I/Q decomposed (i.e., the passband signal at the ADC output is converted to its equivalent baseband representation), and finally, the demodulation (including the decimation) takes place. As a result, $\tilde{r}_m[n]$ symbols (with $m \in \Psi$) corresponding to the L multipath signal components are obtained.

Next, the signals are forwarded to the MRC, which optimally combines the L multipath replicas and produces an improved version of the received signals to be forwarded to the LDM demodulator. Notice that the main objective of the MRC is to maximize the SNR of the received symbol [M K SIMON 2005, Chapter 9, p. 262]. Note also that the approach typically followed by multiple-antenna receivers based on MRC requires a complete receiver chain (antenna, RF front-end, and ADC) for each of the L branches, while the TMA approach allows for using a single receiver chain although requiring a larger bandwidth.

4.2.1 Baseband Model for the Diversity Paths

In this subsection we derive the baseband-equivalent model for each of the L multipath signal components in Fig. 4.1. We assume an LDM transmit signal

$$s(t) = \sqrt{P}u(t)\mathrm{e}^{j2\pi f_c t}, \tag{4.3}$$

where P represents the transmit power, and $u(t)$ is the equivalent baseband representation of $s(t)$ [MANEIROCATOIRA 2014a]. The transmit signal $s(t)$ propagates over an L-path wireless channel, arriving at the TMA along the directions θ_m, with $m \in \Psi$. Let $y_m(t)$ be the signal impinging on the TMA over the multipath angle θ_m after being attenuated and time-delayed, i.e.,

$$y_m(t) = \alpha_m s(t-\tau_m) = \alpha_m\sqrt{P}u(t-\tau_m)\mathrm{e}^{j2\pi f_c(t-\tau_m)}, \tag{4.4}$$

where α_m and τ_m are the attenuation factor and time-delay of the m-th multipath, respectively.

With respect to the wireless channel, the TMA, and the receiver, we assume the following:

- the directions θ_m, the attenuations α_m, and the delays τ_m are statistically independent random variables for each path m, with $m \in \Psi$, and known to the system designer to ensure a fair performance comparison between the considered systems regardless channel estimation errors;
- given that we are considering narrow-band communications, the time-delays satisfy $\tau_m \ll 1/B$. Hence, $u(t-\tau_m) \approx u(t)$ and Eq. (4.4) can be rewritten as

$$y_m(t) = \alpha_i\sqrt{P}u(t)\mathrm{e}^{j2\pi f_c t}\mathrm{e}^{-j2\pi f_c\tau_m} = \alpha_m\mathrm{e}^{-j\phi_m}s(t), \tag{4.5}$$

  with $\phi_m = 2\pi f_c\tau_m$ being the phase shift introduced by τ_m;

- the m-th path channel response $h_m = \alpha_m \mathrm{e}^{-j\phi_m}$ is modeled as a complex normal zero-mean circularly-symmetric random variable. This model is particularly valid when considering a multipath clustered environment, in which case the channel response is the result of the sum of all the multipath responses within a cluster. Hence, by virtue of the central limit theorem, it is reasonable to model h_m as a complex normal zero-mean circularly-symmetric random variable [TSE 2005, Chapter 2, p. 36]. Consequently, α_m is Rayleigh-distributed with a mean square value

$$\Omega_m = \mathrm{E}[|h_m|^2], \tag{4.6}$$

  where $E[x]$ stands for the expectation of x, and ϕ_m is uniformly distributed in $[0, 2\pi)$. This channel model is known in the literature as RFC [M K SIMON 2005, Chapter 2, p. 18];
- it is possible to synthesize the TMA radiation patterns such that $|F_m^{\mathrm{TMA}}(\theta_m, t)1$, with $m \in \Psi$, is maximized along the m-th path direction θ_m, while the remaining paths are filtered-out, i.e., $|F_m^{\mathrm{TMA}}(\theta_l, t) \approx 0 \; \forall m \neq l|$ with $m, l \in \Psi$ [ROCCA 2014]. As a consequence, the $r_m(t)$ signals at the output of the TMA are orthogonal in frequency;
- the signal replica $y_0(t)$ impinges on the TMA through the direction corresponding to the maximum of the TMA fundamental mode pattern;
- $|F_q^{\mathrm{TMA}}(\theta_m, t)|^2 \ll |F_l^{\mathrm{TMA}}(\theta_m, t)|^2$, for $m, l \in \Psi$ and $q \geq L$, i.e., only the first L patterns of the TMA are considered while the rest are minimized;
- in order to avoid spectral signal overlapping, the bandwidth B of $u(t)$ and the TMA frequency f_0 fulfill $f_0 > 2B$ and $f_c \gg f_0$ [MANEIROCATOIRA 2014a]; and finally,
- the spectrum occupied by all multipath signal components at the output of the TMA is free of interferences from other signals, i.e., the carriers $f_c + mf_0$, with $m \in \Psi$ are occupied only with the received signals $y_m(t)$.

At the TMA output, the received signal $r_m(t)$ over the $F_m(\theta, t)$ radiation pattern is the superposition of all multipath signals plus the AWGN noise $\nu_m(t)$,

$$r_m(t) = \sum_{l=0}^{L-1} F_m^{\mathrm{TMA}}(\theta_l, t) y_l(t) + \nu_m(t). \tag{4.7}$$

Recall that the radiation pattern satisfies $|F_m(\theta_l, t) \approx 0, \forall m \neq l|$, and that the signal received over the TMA m-th pattern appears at the frequency $f_c + mf_0$. Hence Eq. (4.7) simplifies to

$$r_m(t) = \alpha_m \mathrm{e}^{-j\phi_m} F_m^{\mathrm{TMA}}(\theta_m, t) \sqrt{P} u(t) \mathrm{e}^{j2\pi(f_c + mf_0)t} + \nu_m(t), \tag{4.8}$$

where $y_l(t)$ was substituted by its definition in Eq. (4.5) for a carrier frequency $f_c + mf_0$.

A conventional TMA exhibits a nonlinear behavior due to the application of periodic (with fundamental frequency f_0) rectangular pulses to the array excitations. Taking Eq. (4.2) into

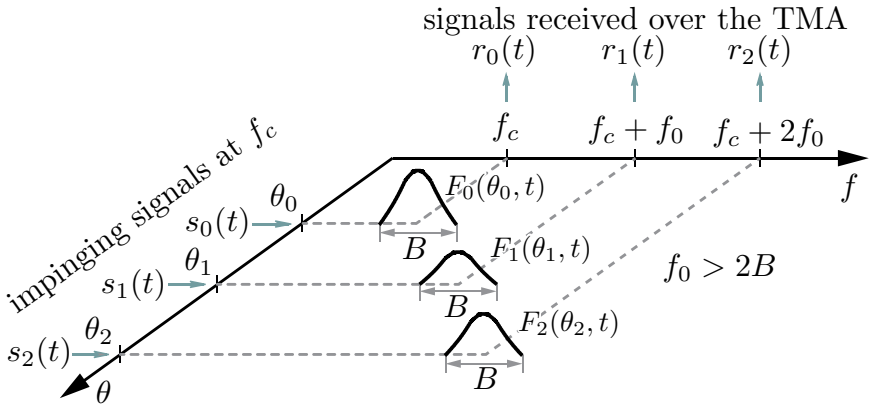

Figure 4.2: Behavior of the TMA. The signals received over the TMA harmonic patterns are translated into the corresponding harmonic frequencies.

account, the array factor of the TMA is

$$\begin{aligned} F^{\text{TMA}}(\theta, t) &= \sum_{q=-\infty}^{\infty} F_q^{\text{TMA}}(\theta, t) \\ &= \sum_{q=-\infty}^{\infty} \mathrm{e}^{j2\pi(f_c+qf_0)t} \sum_{n=0}^{N-1} G_{nq} I_n \mathrm{e}^{jkz_n \cos\theta}, \end{aligned} \tag{4.9}$$

where G_{nq} are the Fourier coefficients of the periodic rectangular pulses (see Eq. (4.1)), which depend on the pulse durations ξ_n and on the switch-on instants o_n. By properly choosing G_{nq} (that is, ξ_n and o_n), and under the conditions defined above in this section, it is possible to *window* the useful harmonics as much as possible. Then, Eq. (4.9) can be rewritten as

$$F^{\text{TMA}}(\theta, t) \approx \sum_{q=-(L-1)}^{L-1} \mathrm{e}^{j2\pi(f_c+qf_0)t} \sum_{n=0}^{N-1} G_{nq} I_n \mathrm{e}^{jkz_n \cos\theta} \tag{4.10}$$

to obtain orthogonal patterns that, jointly with the condition $f_0 > 2B$, allow for taking advantage of the aforementioned nonlinear behavior as shown in Fig. 4.2. Therefore, narrowband multipath signals whose carrier frequency is f_c can be received over the different TMA harmonic patterns, which are translated into the corresponding harmonic frequencies.

The received signal $r(t)$ at the TMA output is the superposition of all received signals $r_m(t)$ and occupies a total bandwidth $B^{\text{TMA}} = (L-1)f_0 + B/2$, with B being the bandwidth of $s(t)$. Therefore, the sampling frequency of the ADC must satisfy the Nyquist criterion, i.e.,

$$f_s^{\text{TMA}} > 2(f_I + (L-1)f_0 + B/2), \tag{4.11}$$

where f_I is the intermediate carrier frequency at the output of the down-converter.

On the other hand, the baseband equivalent of the m-th received signal $r_m(t)$ at each TMA element output can be written as

$$\tilde{r}_m(t) = \alpha_m \mathrm{e}^{-j\phi_m} F_m^{\text{TMA}}(\theta_m, t)\sqrt{P}u(t) + \tilde{\nu}_m(t), \tag{4.12}$$

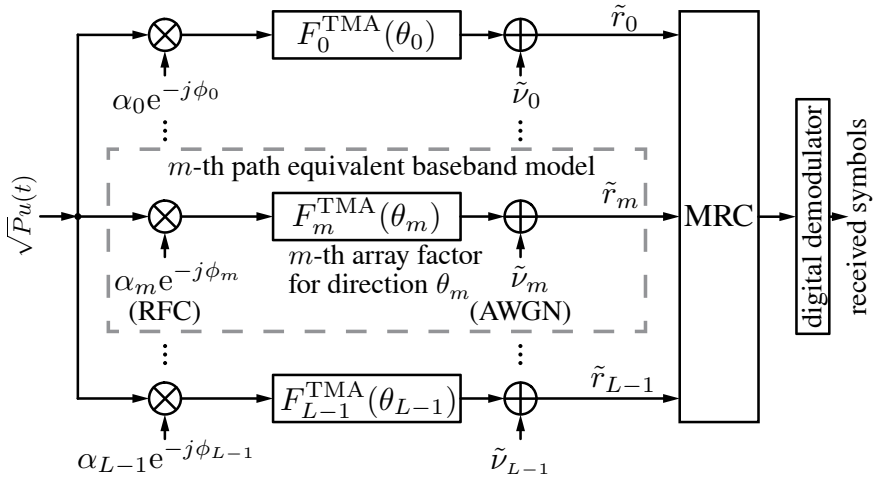

Figure 4.3: Equivalent baseband representation of the TMA-based wireless digital communication system shown in Fig. 4.1 that exploits the L multipath replicas from the transmitted signal $s(t)$ through an RFC.

with $\tilde{\nu}_m(t)$ being the baseband equivalent AWGN in $\tilde{r}_m(t)$.

In summary, the operations carried out by the TMA followed by the RF front-end and the L I/Q digital demodulators shown in Fig. 4.1 can be interpreted as a SIMO subsystem that produces L multipath replicas from the signal transmitted. The baseband equivalent representation of such a SIMO subsystem is shown in Fig. 4.3.

4.3 Average SNR per Symbol and Path

In a context where a wireless digital communication system is subject to fading impairments, the average SNR is an adequate metric of the overall system performance since it quantifies the received signal fidelity. Given that the instantaneous SNR per symbol at the m-th branch in Fig. 4.3 is a random variable and is expressed as

$$\gamma_m^{\text{TMA}} = \alpha_m^2 G_m^{\text{TMA}} E_s/N_0, \tag{4.13}$$

where E_s is the average energy per transmitted symbol, N_0 is the AWGN power spectral density, α_m^2 is the instantaneous power of the m-th multipath channel component, G_m^{TMA} is the antenna gain accounting for the power received in the direction of the peak radiation with respect to an isotropic source and is given by [YANG 2004]

$$G_m^{\text{TMA}} = \eta_{\text{TMA}} \frac{4\pi |F_m^{\text{TMA}}(\theta_m, t)|^2}{P_R^{\text{TMA}}}. \tag{4.14}$$

Let us study in detail the different variables in Eq. (4.14). A crucial parameter in this analysis is the total efficiency of the TMA expressed as

$$\eta_{\text{TMA}} = \eta_s \cdot \eta(L), \tag{4.15}$$

η_s being the efficiency of the network switch [ZHU 2012a] that accounts for the absorption of energy when the switches are off, and $\eta(L)$ being the TMA power efficiency when $L-1$ harmonics[1] are exploited in addition to the fundamental mode. Such power efficiency is defined as the ratio between the useful mean received power P_U^{TMA} and the total mean received power P_R^{TMA}, i.e.,

$$\eta(L) = \frac{P_U^{\text{TMA}}}{P_R^{\text{TMA}}} = \frac{\sum_{q=0}^{L-1} p_q}{\sum_{q=-\infty}^{\infty} p_q}, \tag{4.16}$$

where p_q is the total mean received power at the q-th harmonic when a carrier is received over a TMA, and is given by[MANEIROCATOIRA 2014a]

$$p_q = 4\pi \left[\sum_{n=0}^{N-1} |I_n|^2 |G_{nq}|^2 + 2 \sum_{n=0}^{N-1} \sum_{\substack{l=0 \\ l\neq n}}^{N-1} \text{Re}\{I_l I_n^* G_{lq} G_{nq}^*\} \text{sinc}(k(z_l - z_n)) \right]. \tag{4.17}$$

On the other hand, by considering Eqs. (4.1) and (4.2), we can easily quantify $|F_m^{\text{TMA}}(\theta_m, t)|^2$ as

$$\begin{aligned} |F_m^{\text{TMA}}(\theta_m, t)|^2 &= \sum_{n=0}^{N-1} \xi_n^2 \text{sinc}^2(m\pi\xi_n) + \\ &+ 2 \sum_{n=0}^{N-1} \sum_{\substack{l=0 \\ l\neq n}}^{N-1} |I_l||I_n| \xi_l \xi_n \text{sinc}(m\pi\xi_l) \text{sinc}(m\pi\xi_l) \cos\{m\pi[\Delta\xi_{nl} + 2\Delta o_{nl}] + k\Delta z_{nl} \cos\theta_m - \Delta\varphi_{nl}\}, \end{aligned} \tag{4.18}$$

with $\Delta\xi_{nl} = \xi_n - \xi_l$, $\Delta o_{nl} = o_n - o_l$, $\Delta z_{nl} = z_n - z_l$, and $\Delta\varphi_{nl} = \varphi_n - \varphi_l$.

Once analyzed in detail the different components of G_m^{TMA}, we can obtain, by virtue of Eq. (4.13), the average SNR per symbol[2] at the m-th branch in Fig. 4.3, arriving at

$$\overline{\gamma}_m^{\text{TMA}} = \text{E}[\alpha_m^2 G_m^{\text{TMA}} E_s/N_0] = \Omega_m G_m^{\text{TMA}} E_s/N_0, \tag{4.19}$$

where Ω_m is the mean square value of α_m^2 (recall Eq. (4.6)).

Therefore, by substituting, on the one hand, Eq. (4.17) into Eqs. (4.16) and (4.16) into Eq. (4.15) and, on the other, Eqs. (4.15) and (4.18) into Eq. (4.14), and finally, Eq. (4.14)

[1] As $g_n(t)$ is a real signal, its Fourier coefficients verify $G_{nq} = G_{n(-q)}^*$, and it is easy to prove (see Eq. (4.2)) that $|F_q^{\text{TMA}}(\theta, t)|^2 = |F_{-q}^{\text{TMA}}(\pi - \theta, t)|^2$, unavoidably synthesizing a couple of diagrams for q and $-q$, which are symmetric with respect to $\theta = \pi/2$. This lack of independence between couples of harmonic patterns of the same order does not match with the randomness nature of the DOAs. Therefore, we restrict the adaptive beamforming either to the positive or the negative harmonics to achieve an adequate level of flexibility. This fact limits the power efficiency of the system shown in Fig. 4.1. The feasibility of independence between harmonic patterns of the same order in a TMA needs to be overcome in future works.

[2] Note that $\overline{\gamma}_m = \text{E}[\gamma_m] = \int_0^\infty \gamma_m p(\gamma_m) d\gamma_m$ is the average SNR per symbol, where $p(\gamma_m)$ denotes the probability density function (PDF) of γ_m which, for the case of RFC, is $p(\gamma_m) = \frac{\gamma_m}{\overline{\gamma}_m} \text{e}^{-\frac{\gamma_m}{\overline{\gamma}_m}}, \gamma_m \geq 0$ [SKLAR 2001].

into Eq. (4.19), we obtain a closed-form expression (in Eq. (4.44) such an expression is shown for a particular case) for the average SNR $\overline{\gamma}_m^{\text{TMA}}$ in terms of the TMA parameters (ξ_n, o_n), the number of paths exploited (L), the average power of the fading path (Ω_m), and the ratio of the average energy per transmitted symbol to the AWGN power spectral density (E_s/N_0). Finally, the average SNR at the output of the MRC is the sum of the individual average SNR values at the L input branches, i.e.,

$$\overline{\gamma}^{\text{TMA}}(\xi_n, o_n, L, \Omega_m, E_s/N_0) = \sum_{m=0}^{L-1} \overline{\gamma}_m^{\text{TMA}}, \tag{4.20}$$

with $\overline{\gamma}_m^{\text{TMA}}$ defined in Eq. (4.19), in contrast to the average SNR at the input of the MRC, which is L times smaller than $\overline{\gamma}^{\text{TMA}}$.

4.4 Average SER Characterization

The average SER is another widely used figure of merit for the evaluation of digital communication systems (DCSs). The average SER for a digital receiver with an instantaneous input SNR γ is determined as

$$\text{SER} = \int_0^\infty P_S(e|\gamma) p(\gamma) d\gamma, \tag{4.21}$$

with $P_{\text{S}}(e|\gamma)$ the conditional SER for a given instantaneous SNR γ, and $p(\gamma)$ the PDF of γ. Recall that there exist closed-form expressions, in terms of the Gaussian Q-function, for the conditional SER of the majority of the most widely used LDM formats [GOLDSMITH 2005, Chapter 5, p. 140]. The average SER is obtained after solving the integral in Eq. (4.21).

According to Fig. 4.1, the input signal to the demodulator is the output signal from the MRC. The instantaneous SNR at the MRC output relates to the instantaneous SNR values at the MRC input branches as $\gamma = \sum_{m=0}^{L-1} \gamma_m$. Hence, in order to determine the average SER we must average the L dimensional conditional SER values $P_{\text{S}}(e|\gamma_0, \gamma_1, \ldots, \gamma_{L-1})$ over the joint PDF $p(\gamma_0, \gamma_1, \ldots, \gamma_{L-1})$ of the instantaneous SNR values $\gamma_0, \gamma_1, \ldots \gamma_{L-1}$. Since the random variables γ_m are assumed to be statistically independent, $p(\gamma_0, \gamma_1, \ldots, \gamma_{L-1}) = \prod_{m=0}^{L-1} p(\gamma_m)$, and the averaging procedure results in

$$\text{SER} = \underbrace{\int_0^\infty \cdots \int_0^\infty}_{L-\text{fold}} P_{\text{S}}(e|\gamma_o \ldots \gamma_{L-1}) \prod_{m=0}^{L-1} p(\gamma_m) d\gamma_0 \ldots \gamma_{L-1}. \tag{4.22}$$

For the case of LDM signals, $P_{\text{S}}(e|\gamma_0, \gamma_1, \ldots, \gamma_{L-1})$ is a Gaussian Q-function of the form [M K SIMON 2005, Chapter 9, p. 267]

$$P_{\text{S}}(e|\gamma_0, \gamma_1, \ldots, \gamma_{L-1}) = Q\left(\sqrt{2 g_{\text{MOD}} \sum_{m=0}^{L-1} \gamma_m}\right), \tag{4.23}$$

where g_{MOD} is a parameter depending on the LDM format and the constellation size M. For the most widely used LDMs the value of such a parameter is

$$g_{\text{ASK}} = 3/(M^2-1) \tag{4.24}$$

$$g_{\text{PSK}} = \sin^2(\pi/M) \tag{4.25}$$

$$g_{\text{QAM}} = 3/(2(M-1)), \tag{4.26}$$

Solving the integral Eq. (4.22) is difficult. However, by considering an alternative expression of $Q(\cdot)$, the conditional SER Eq. (4.23) can be expressed as [SIMON 1998b]

$$P_{\text{S}}(e|\gamma_0,\gamma_1,\ldots,\gamma_{L-1}) = \frac{1}{\pi}\int_0^{\frac{\pi}{2}} \mathrm{e}^{-\frac{g_{\text{MOD}}\sum_{m=0}^{L-1}\gamma_m}{\sin^2\varrho}} d\varrho. \tag{4.27}$$

Substituting Eq. (4.27) into Eq. (4.22) and having in mind that for the RFC model $p(\gamma_m)$ is an exponential PDF with mean $\overline{\gamma}_m$, the following expressions for the average SER corresponding to ASK, PSK and QAM modulation formats [SIMON 1998a] are obtained:

$$\text{SER}_{\text{ASK}} = \tfrac{2(M-1)}{M\pi}\int_0^{\frac{\pi}{2}} \prod_{m=0}^{L-1}\left(1+\frac{\overline{\gamma}_m g_{\text{ASK}}}{\sin^2\varrho}\right)^{-1} d\varrho, \tag{4.28}$$

$$\text{SER}_{\text{PSK}} = \frac{1}{\pi}\int_0^{\frac{(M-1)\pi}{M}} \prod_{m=0}^{L-1}\left(1+\frac{\overline{\gamma}_m g_{\text{PSK}}}{\sin^2\varrho}\right)^{-1} d\varrho, \tag{4.29}$$

$$\begin{aligned}\text{SER}_{\text{QAM}} = \frac{4}{\pi}\left(1-\tfrac{1}{\sqrt{M}}\right)\Bigg[&\int_0^{\frac{\pi}{2}} \prod_{m=0}^{L-1}\left(1+\frac{\overline{\gamma}_m g_{\text{QAM}}}{\sin^2\varrho}\right)^{-1} d\varrho - \\ &-\left(1-\tfrac{1}{\sqrt{M}}\right)\int_0^{\frac{\pi}{4}} \prod_{m=0}^{L-1}\left(1+\frac{\overline{\gamma}_m g_{\text{QAM}}}{\sin^2\varrho}\right)^{-1} d\varrho\Bigg],\end{aligned} \tag{4.30}$$

Recall also that when considering the receiver with TMA shown in Fig. 4.1, the average SNR $\overline{\gamma}_m$ is $\overline{\gamma}_m^{\text{TMA}}$ given by Eq. (4.19). Hence, under the assumptions established in Section 4.2.1, we can plot the average SER in terms of the SNR per symbol E_s/N_0 with a closed-form expression involving the TMA synthesis parameters.

4.5 Trade-off Between the TMA Efficiency and the Number of Multipath Components

In view of Eqs. (4.1) and (4.2), and assuming $|I_n| = 1$, the squared moduli of the dynamic excitations of the m-th harmonic pattern are given by

$$\left|I_{nm}^{\text{TMA}}\right|^2 = G_{nm}^2 = \xi_n^2 \text{sinc}^2(\pi m \xi_n), \qquad n \in \Upsilon. \tag{4.31}$$

On the other hand, and according to the Fourier series expansion theory, G_{nm}^2 are a set of N samples –at the fixed harmonic frequency $f = m/T_0$– taken from each $|G_n(f)|^2$, with $G_n(f)$

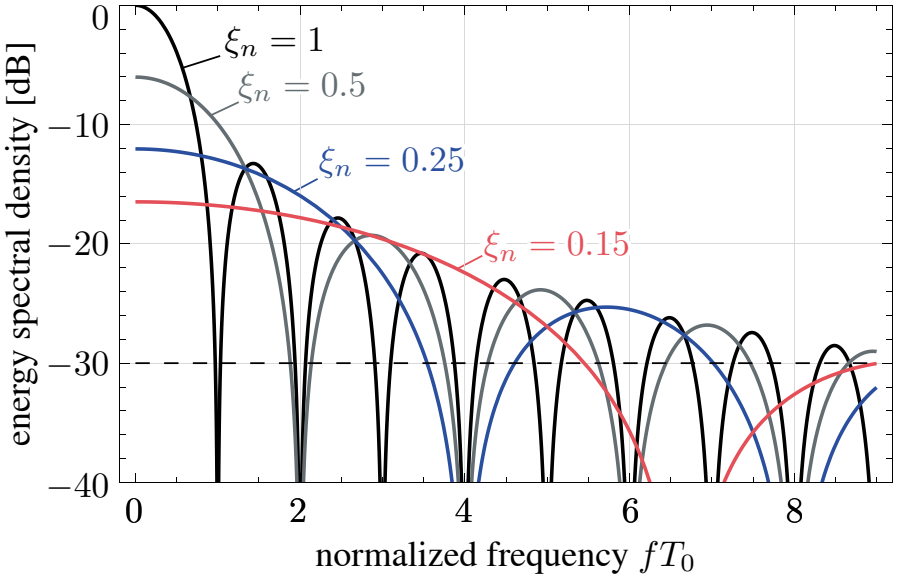

Figure 4.4: Frequency-normalized ESD of a rectangular pulse, $|G_n(f)|^2$, for different values of ξ_n. The squared amplitude of the n-th excitation corresponding to the m-th harmonic pattern can be graphically identified in the plot as $|I_{nm}^{\text{TMA}}|^2 = G_{nm}^2 = |G_n(m)|^2$.

being the Fourier transform of the basic rectangular pulse (with a width ξ_n) that constitutes the periodic train $g_n(t)$. By normalizing the frequency axis with respect to $f_0 = 1/T_0$ we have that

$$\left|I_{nm}^{\text{TMA}}\right|^2 = |G_n(m)|^2, \qquad n \in \Upsilon, \tag{4.32}$$

and therefore, to include successive harmonics ($fT_0 = 1, 2, 3, \dots$) below the main lobe of the energy spectral density (ESD) of each pulse, it is necessary to reduce ξ_n properly (see Fig. 4.4). However, note that ξ_n cannot be too close to zero because, in such a case, the efficiency of the TMA, $\eta_{\text{TMA}} = \eta_s \cdot \eta(L)$, would be significantly degraded, and consequently, the average SNR per path $\overline{\gamma}_m^{\text{TMA}}$ would also be reduced.

Hence, for a given L –determined by the number of harmonics to be exploited in the beamforming– it is necessary to synthesize a TMA, according to the efficiency requirements, with the largest possible ξ_n values, thus enabling the corresponding $\text{sinc}(\cdot)$ functions in Fig. 4.4 to incorporate such harmonics. At the same time, the values of ξ_n, together with o_n, must be able to shape the corresponding radiation patterns.

4.6 Linear Beamforming

In order to better understand the impact on the performance of a digital communication system when considering a TMA at reception, in this section we will analyze the performance of such a system when an array with linear beamforming is considered.

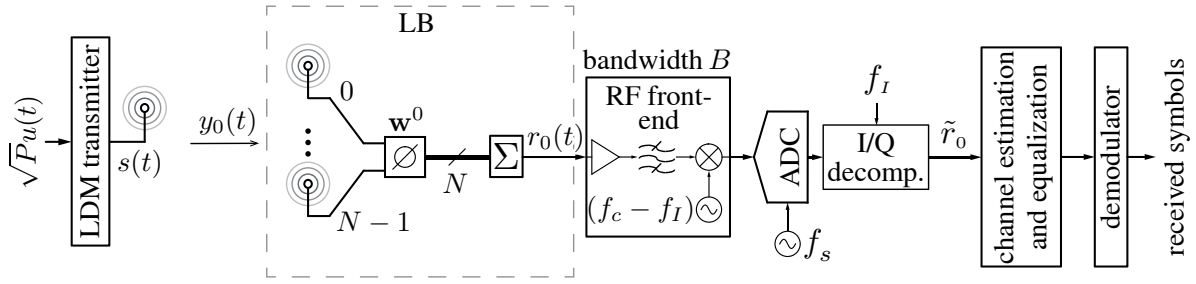

Figure 4.5: Block diagram of the system in Fig. 4.1 but using a receiver equipped with a single linear beamformer (LB) having a radiation pattern with the same spatial shape as the TMA fundamental one. This receiver only acquires a single replica $y_0(t)$ of the transmitted signal and cannot exploit channel diversity.

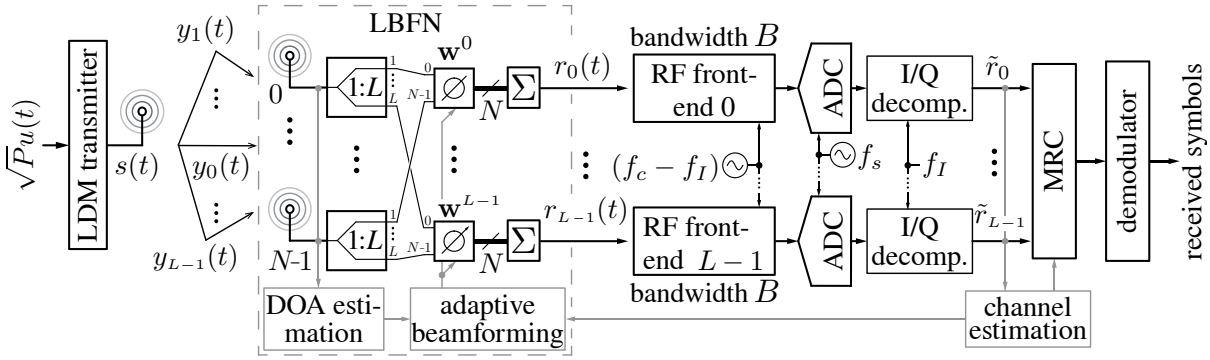

Figure 4.6: Block diagram of the system in Fig. 4.1 but now using a receiver equipped with an LBFN consisting of a conventional array (excitation weights $\mathbf{w}^0$) plus a set of adaptive LBs ($\mathbf{w}^m$, $m = 1, \ldots, L-1$). Such an LBFN simultaneously synthesizes a series of spatial radiation patterns with the same shapes as those generated by the TMA. There are N elements, each one connected to an L-way power splitter, while the power splitters are connected to L phase shifters (the first one is static).

4.6.1 Linear Beamforming without Angular Diversity

We start considering a conventional array with a linear beamformer (LB) capable of synthesizing the same radiation pattern as that of the fundamental beam of a TMA (see Fig. 4.5). Recall that this radiation pattern points the maximum towards the main multipath direction θ_0 while it cancels the remaining ones. Hence, the receiver in this case cannot exploit the angular diversity of the multipath channel. The baseband equivalent representation of the receiver shown in Fig. 4.3 reduces to a SISO system.

The radiation pattern of the fundamental mode of the TMA in Fig. 4.1 can be accomplished with an LB by choosing the array complex excitations as the elements of the column vector $\mathbf{w}_0$ given by $w^0_{n+1} = G_{n0} I_n \mathrm{e}^{-jkz_n \cos\theta_0} = I_n \xi_n \mathrm{e}^{-jkz_n \cos\theta_0}$, $n \in \Upsilon$. The array now provides a single signal whose baseband equivalent representation is

$$\tilde{r}_0(t) = \alpha_0 \mathrm{e}^{-j\phi_0} F^{\mathrm{LB}}(\theta_0, t) \sqrt{P} u(t) + \tilde{\nu}_0(t). \tag{4.33}$$

Recall that the equivalent channel response now depends on $F^{\text{LB}}(\theta_0, t)$, namely the array factor of the LB towards the main multipath direction θ_0.

We next determine the average SNR per symbol at the output of the LB. The expression is similar to Eq. (4.19):

$$\overline{\gamma}^{\text{LB}} = \text{E}[\alpha_0^2 G^{\text{LB}} \tfrac{E_s}{N_0}] = \Omega_0 G^{\text{LB}} E_s/N_0, \tag{4.34}$$

with

$$G^{\text{LB}} = 4\pi |F^{\text{LB}}(\theta_0, t)|^2 / P_{\text{R}_0}^{\text{LB}} > G_0^{\text{TMA}}. \tag{4.35}$$

Note that the parameter $\eta(L)$, inherent to the sideband radiation phenomenon, is not present in an LB. Recall that $|F^{\text{LB}}(\theta, t)|^2 = |F_0^{\text{TMA}}(\theta, t)|^2$ and hence it can be computed from Eq. (4.18). Finally, the power received by the LB, P_{R}^{LB}, can be calculated as the total mean received power over the array factor $F^{\text{LB}}(\theta, t)$, i.e.,

$$P_{\text{R}}^{\text{LB}} = \int_0^{2\pi} \int_0^{\pi} |F^{\text{LB}}(\theta, t)|^2 \sin(\theta) d\theta d\varphi. \tag{4.36}$$

On the other hand, remember that the average SER can be obtained for each LDM format by particularizing Eqs. (4.28) to (4.30) for $L = 1$ and $\overline{\gamma}_0 = \overline{\gamma}^{\text{LB}}$ as in Eq. (4.34).

4.6.2 Linear Beamforming with Angular Diversity

It is possible to consider an LBFN to exploit the angular diversity in a multipath radio channel. The idea is to design an LB to receive each of the L multipath signals. Then, the signals provided by the LBs are linearly combined with an MRC to obtain a signal with improved SNR. Fig. 4.6 plots the block diagram of a DCS receiver with an LBFN and an MRC.

We assume that the LBFN is able to synthesize L spatial radiation patterns with the same shapes as the ones generated by the TMA at its different harmonic frequencies. Since the beamforming network is linear, all the radiation patterns perform at the same frequency f_c. As mentioned above, such radiation patterns point to a different multipath direction while they cancel the other ones. In this manner the LBFN provides different replicas of the transmitted signal and allows the receiver to exploit the channel angular diversity. The baseband equivalent representation of the receiver now corresponds to the SIMO system shown in Fig. 4.6.

The LBFN weights for the m-th beam are $w_{n+1}^m = G_{nm} I_n \text{e}^{-jkz_n \cos\theta_m}$, with $m \in \Psi$ and $n \in \Upsilon$ as in Eq. (4.1). Such elements are collected into the column vector $\mathbf{w}_m$. The phase adjustment in each w_n^m is physically carried out by phase shifters having an insertion loss at f_c represented by $K_{\text{ps}} < 1$ (and expressed in natural units). In this case, the generic m-th path model is similar to that developed in Section 4.2, but modifying the gain terms. Instead of $F_m^{\text{TMA}}(\theta_m, t)$ we now have $K_{\text{ps}} F_m^{\text{LB}}(\theta_m)/L$ due to the existence of the phase shifters and the L-way power splitters necessary to implement the LBFN. Under these circumstances, the average SNR for the m-th path is given by Eq. (4.19):

$$\overline{\gamma_m}^{\text{LBFN}} = \text{E}\left[\alpha_m^2 \frac{K_{\text{ps}} G_m^{\text{LBFN}}}{L} \frac{E_s}{N_0}\right] = \Omega_m \frac{K_{\text{ps}} G_m^{\text{LBFN}}}{L} \frac{E_s}{N_0}, \tag{4.37}$$

Table 4.1: Complexity comparison between the proposed TMA system (see Fig. 4.1) and the two alternatives considered: LB and LBFN (see Figs. 4.5 and 4.6, respectively).

	RF front-ends	**ADCs**	**demodulators**	**MRC**
TMA	1^*	$1^\#$	L	yes
LB	1	1	1	no
LBFN	L	L	L	yes

*: requires a larger bandwidth ($B^{\text{TMA}} > B$).

$^\#$: requires a higher sampling frequency ($f_s^{\text{TMA}} > f_s$).

with

$$G_m^{\text{LBFN}} = 4\pi |F_m^{\text{LBFN}}(\theta_m, t)|^2 / P_{\text{R}_m}^{\text{LBFN}} > G_m^{\text{TMA}}, \tag{4.38}$$

Again, $|F_m^{\text{LBFN}}(\theta_m, t)|^2 = |F_m^{\text{TMA}}(\theta_m, t)|^2$ and thus $|F_m^{\text{LBFN}}(\theta_m, t)|^2$ can be obtained from Eq. (4.18). Correspondingly, $P_{\text{R}_m}^{\text{LBFN}}$ is calculated by plugging $F(\theta, t) = F_m^{\text{LBFN}}(\theta_m, t)$ into Eq. (4.36). Similarly to Eq. (4.20), the average SNR at the MRC output is

$$\overline{\gamma}^{\text{LBFN}} = \sum_{m=0}^{L-1} \overline{\gamma_m}^{\text{LBFN}}, \tag{4.39}$$

Finally, the average SER for the different M-ary LDM formats can be determined for a given E_s/N_0 by plugging $\overline{\gamma_m} = \overline{\gamma_m}^{\text{LBFN}}$ –as in Eq. (4.37)– into Eqs. (4.28) to (4.30).

4.6.3 Hardware Complexity Comparison

Table 4.1 shows the resources required by each of the three considered systems: TMA, LB, and LBFN[3]. Remarkably, the TMA solution is cheaper, in terms of hardware complexity, than the LBFN approach. Nevertheless, as described in Section 4.2.1, in the TMA-based approach the ADC sampling frequency and the RF front-end bandwidth grow linearly with the number of multipath components L. On the other hand, the MRC is needed in both TMA and LBFN, but the latter is considerably more complex in terms of hardware, requiring additional power splitters and phase shifters. Obviously, the LB solution, as it does not exploit the diversity of the channel, is the simplest and cheapest one.

[3] Notice that the sampling frequency corresponding to the ADCs in the LBFN shown in Fig. 4.5 must satisfy Eq. (4.11). Therefore, the minimum sampling frequencies of both systems satisfy $f_s^{\text{TMA}} - f_s^{\text{LBFN}} = 4(L-1)B$, whereas the percentage increase in the sampling frequency when the TMA is used with respect to the LBFN is given by $\Delta f_s[\%] = \left((f_s^{\text{TMA}} - f_s^{\text{LBFN}})/f_s^{\text{LBFN}}\right) \cdot 100 = 4(L-1)/(2(f_I/B)+1) \cdot 100$, and we observe that if $f_I \gg B$, then $\Delta f_s[\%]$ is very low (recall that L is upper bounded due to the trade-off with the TMA efficiency), and therefore, it is even possible to use the same ADC for both solutions.

4.7 Performance Comparison

4.7.1 TMA Assumptions: Simplified Expressions

Under the assumptions of uniform amplitude for the static currents, as well as an inter-element distance of half a wavelength, i.e.,

$$|I_n| = 1, \forall n \in \Upsilon, \text{ and } d = \Delta z_{nl} = \lambda/2, \tag{4.40}$$

the calculation of P_R^{TMA} in the denominator of Eq. (4.16) is reduced to

$$P_R^{\text{TMA}} = 4\pi \sum_{n=0}^{N-1} \sum_{q=-\infty}^{\infty} |G_{nq}|^2 = 4\pi \sum_{n=0}^{N-1} \xi_n^2 \sum_{q=-\infty}^{\infty} \text{sinc}^2(q\pi\xi_n). \tag{4.41}$$

Having now in mind that for all $\xi_n \in (0, 1)$ the sinc-square infinite series converges to

$$\sum_{q=-\infty}^{\infty} \text{sinc}^2(q\pi\xi_n) = 1/\xi_n, \tag{4.42}$$

we arrive at a simplified version of Eq. (4.41)

$$P_R^{\text{TMA}} = 4\pi \sum_{n=0}^{N-1} \xi_n. \tag{4.43}$$

Finally, by considering the assumptions Eq. (4.40) in Eq. (4.18), and substituting Eq. (4.18) together with Eq. (4.43) into Eq. (4.14), and finally Eq. (4.14) into Eq. (4.19), we arrive at the following closed-form expression

$$\begin{aligned} \overline{\gamma}_m^{\text{TMA}} = & \frac{\eta_s \Omega_m \sum_{q=0}^{L-1} \sum_{n=0}^{N-1} \xi_n^2 \text{sinc}^2(q\pi\xi_n)}{\left(\sum_{n=0}^{N-1} \xi_n\right)^2} \cdot \frac{E_s}{N_0} \cdot \\ & \cdot \left[\sum_{n=0}^{N-1} \xi_n^2 \text{sinc}^2(m\pi\xi_n) + 2 \sum_{n=0}^{N-1} \sum_{\substack{l=0 \\ l \neq n}}^{N-1} \xi_l \xi_n \text{sinc}(m\pi\xi_l) \text{sinc}(m\pi\xi_l) \cdot \right. \\ & \left. \cdot \cos\{m\pi[\Delta\xi_{nl} + 2\Delta o_{nl}] + \pi \cos\theta_m - \Delta\varphi_{nl}\} \right], \end{aligned} \tag{4.44}$$

which gives the average SNR per symbol at the m-th MRC input branch in terms of the network parameters.

4.7.2 Description of the TMA Synthesis Method

The method is based on the same optimization algorithm proposed in [ROCCA 2014, Section III.A], the particle swarm optimization (PSO), but some innovations have been introduced, both in the TMA architecture and at the algorithm level in order to optimize

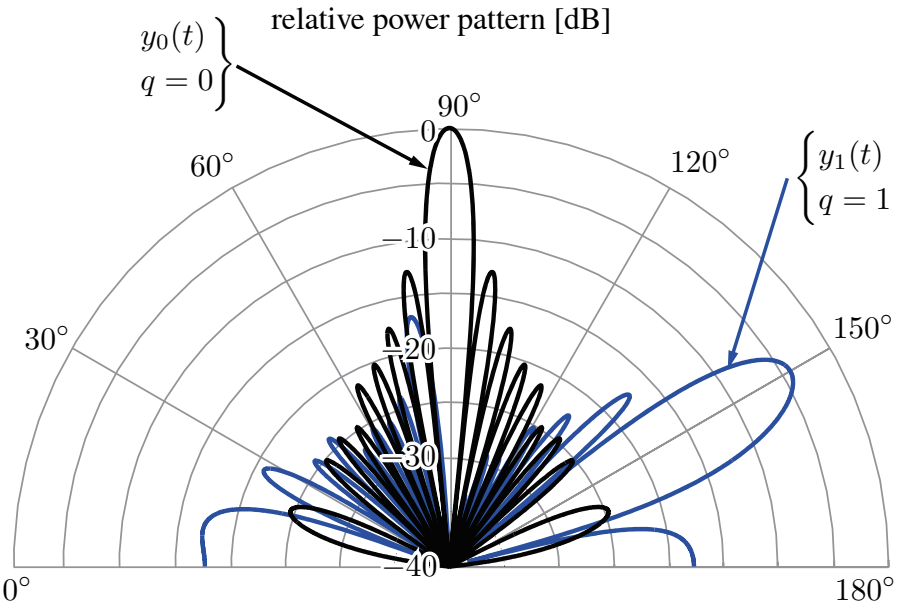

Figure 4.7: Optimized radiation receiving pattern implementing the simplest configuration for the system in Fig. 4.1. Only the first harmonic ($L = 2$) of the TMA is exploited for adaptive beamforming. Notice the high level of mutual spatial orthogonality of the diagrams in the respective DOAs ($\theta_0 = 90°$ and $\theta_1 = 150°$).

the metrics established in Eqs. (4.28) to (4.30) when the TMA beamforming is applied to digital communications in multipath scenarios. Such improvements on the technique of [ROCCA 2014] are:

- The use of multi-throw switches, (i.e. the use of a single RF switch for the control of two adjacent elements) in order to simultaneously maximize both factors of the TMA efficiency, namely η_s, and $\eta(L)$. The PSO has been properly customized to only generate pairs of complementary pulses, as requested for the control of this new employed type of switches. As compared to the previous solutions, the new obtained results have shown improved or even ideal η_s [ZHU 2012a]. In the subsequent examples, single-pole triple-throw (SP3T) switches are used to exploit up to an $L = 3$ multipath channel. For each switch, two throws are connected to a consecutive pair of elements of the array. For the case of $L = 2$ the third throw will not be programmed or used, and for the case $L = 3$ such a throw is used as the off state.
- The weighting coefficients used in the fitness function (see [ROCCA 2014, Eq. 10]) have been adapted to the particular features of a signal-performance oriented scenario, aimed to safeguard the TMA efficiency and the SNR at the receiver. Concerning this, the relative weight of the orthogonalization functional has been increased while the other weights on the side-lobe level (SLL) functional as well as on the "equalization among the patterns maximums" functional, were relatively relaxed.

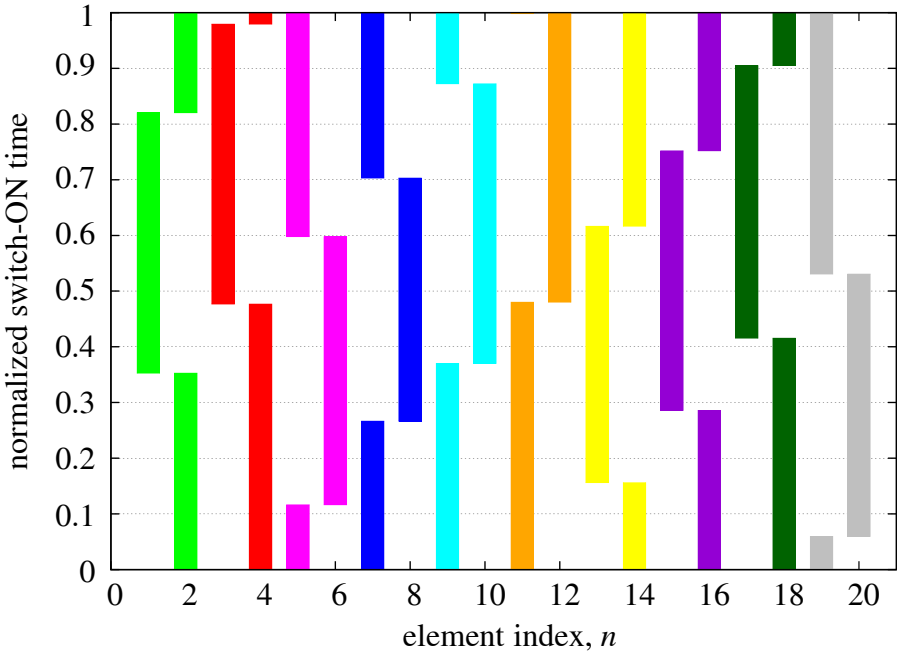

Figure 4.8: Plot of the normalized time sequences which synthesize the radiation receiving pattern in Fig. 4.7.

4.7.3 Multipath Channel with Two Multipath Components

The simplest scenario capable of exploiting the TMA angle diversity according to Fig. 4.1 involves only the first harmonic pattern to carry out the adaptive beamforming. For the numerical simulations we take into account the following considerations:

- The average gain of the channel paths are identical and normalized, i.e., $\Omega_0 = \Omega_1 = 1$;
- The LDM considered is the qauadrature amplitude modulation (QAM) with $M = 16$. The operational frequencies are: $f_c = 2.4\,\text{GHz}$, $f_0 = 500\,\text{kHz}$, $f_I = 10\,\text{MHz}$ and $B = 150\,\text{kHz}$. These numbers lead to ADC sampling frequencies satisfying $f_s^{\text{TMA}} > 21.15\,\text{MHz}$ and $f_s > 20.15\,\text{MHz}$; Fig. 4.7 shows the TMA optimized receiving radiation pattern considered for the analysis, which is synthesized with the normalized time sequences given in Fig. 4.8 whose ON and OFF instants for the TMA pulses are complementary. It is also remarkable the good level of orthogonalization between the patterns. Both characteristics, complementarity and orthogonality, are dictated by the algorithm described in Section 4.7.2.
- The resulting switches network efficiency is $\eta_s = 1$ (0 dB)[4] (as the switches never acquire the OFF state) and as the TMA power efficiency calculated through Eq. (4.16) is found to be $\eta(L) = 0.7$ ($-1.55\,\text{dB}$), and according to Eq. (4.15) we arrive at an $\eta_{\text{TMA}} = 0.7$ ($-1.55\,\text{dB}$);

[4]For any of the described TMA efficiencies (switches network, power or total efficiencies) —generally symbolized here as η– the corresponding values of $10\log_{10}(\eta)$ in decibels are also provided in brackets in the text, after the corresponding value in natural units. Such values expressed in decibels can be considered as losses inherent to the TMA technique, and are useful for an easier comparison with other techniques such as LBFN.

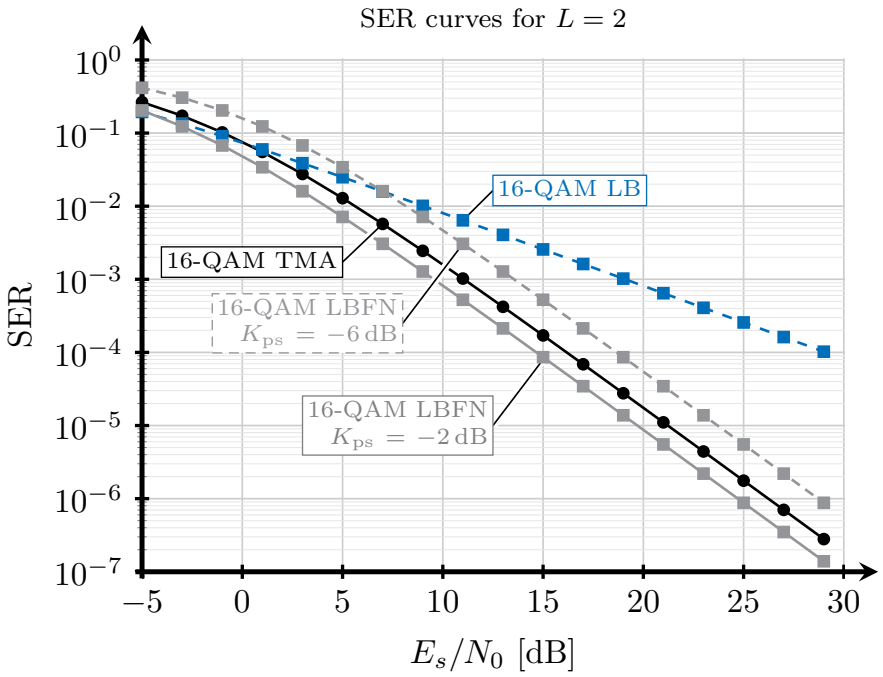

Figure 4.9: SER curves comparing the performance of the SIMO TMA system with other solutions based on conventional arrays for the case of $L = 2$ (a two-path channel).

- The LBFN described in Section 4.6.2 includes phase shifters. As the insertion loss K_{ps} of a phase shifter strongly depends on the carrier frequency (varying from -2 to $-13\,\text{dB}$), and we arbitrarily choose the S-band, we have considered two scenarios for the LBFN: an optimistic one with $K_{\text{ps}} = -2\,\text{dB}$, and a pessimistic with $K_{\text{ps}} = -6\,\text{dB}$ according to the typical values at the f_c considered (see, for example, [MINICIRCUITS 2017]);
- Finally, a set of SER[5] curves with respect to the E_s/N_0 is considered for the 16-QAM case. The SER curves are obtained by plugging the corresponding values for $\overline{\gamma}_m$ into Eq. (4.30).

Fig. 4.9 shows the aforementioned SER curves with respect to the E_s/N_0. From Fig. 4.9 it can be concluded that in this particular case the proposed TMA solution exhibits a significant performance improvement with respect to the LB-based approach and presents a competitive behavior with respect to the LBFN-based solution. This is because the TMA-based system can extract all the diversity ($L = 2$) offered by the channel, as the LBFN-based system does, while the LB-based solution only acquires a single replica of the received signal, thus not exploiting any channel diversity. This effect is clearly shown by the slope of the SER curves in Fig. 4.9: the higher the slope, the more diversity is extracted from the channel.

[5]For a given scenario of DOAs, improved efficiency at the expense of a worse "equalization among patterns maximums" is a trade-off present in the TMA design. Therefore, different radiation patterns (with a distinct set of $|F_m^{\text{TMA}}(\theta_m, t)|^2$ but also associated to a distinct η_{TMA}) may lead to the same behavior in terms of SER. Quantitatively, sets of different values of $|F_m^{\text{TMA}}(\theta_m, t)|^2$ and η_{TMA} in Eqs. (4.14) and (4.19) may conduct to identical SER values in Eqs. (4.28) to (4.30). Under these circumstances, the designer decides the best solution from a radiation pattern point of view.

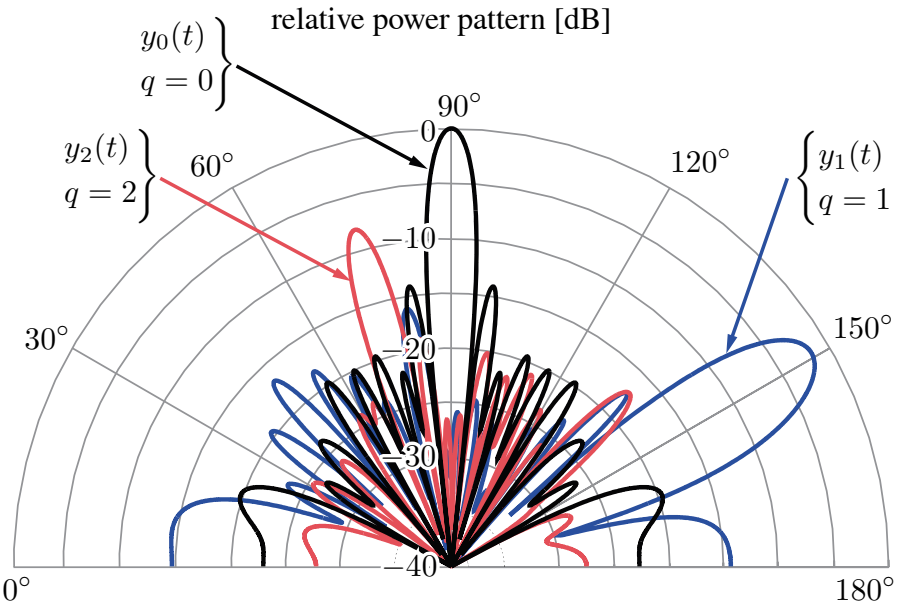

Figure 4.10: Optimized radiation receiving pattern implementing the configuration for the system in Fig. 4.1 exploiting two harmonics ($L = 3$) of the TMA for adaptive beamforming. Notice the level of mutual spatial orthogonality between the diagrams in the respective DOAs ($\theta_0 = 90°$, $\theta_1 = 150°$, and $\theta_2 = 74°$).

4.7.4 Multipath Channel with Three Multipath Components

We have also considered a scenario (see Fig. 4.10) with three impinging signals, where:

- The considerations about the gain of the channel paths, the LDM, the frequencies and the insertion losses K_{ps} in the LBFN are the same as those given in Section 4.7.3.
- The radiation pattern shown in Fig. 4.10 is synthesized with the pulse sequences given in Fig. 4.11. Note that due to the trade-off between L and the η_{TMA} –analyzed in Section 4.5– it is not possible a perfect complementarity between a sequence and the following, i.e. it is necessary to have an OFF interval.
- Now $\eta_s = 0.62$ ($-2.08\,\text{dB}$) (because the switches are OFF a fraction of the time) and since the TMA power efficiency is $\eta(L) = 0.61$ ($-2.15\,\text{dB}$), we arrive at an $\eta_{\text{TMA}} = 0.38$ ($-4.23\,\text{dB}$);
- The curves in Fig. 4.12 show the behavior of the TMA compared to those of both the LBFN and the LB. In spite of the efficiency penalization due to the smaller ξ_n, the TMA is comparable to the LBFN for its more pessimistic scenario. Recall that for $L = 3$, the benefits of the TMA with respect to the LBFN in terms of the system hardware complexity are really remarkable (see Table 4.1). Note also that if the carrier frequency were arbitrarily higher –for example $6\,\text{GHz}$– the behavior of both systems would converge because typical values of K_{ps} increase with the carrier frequency [MINICIRCUITS 2017].

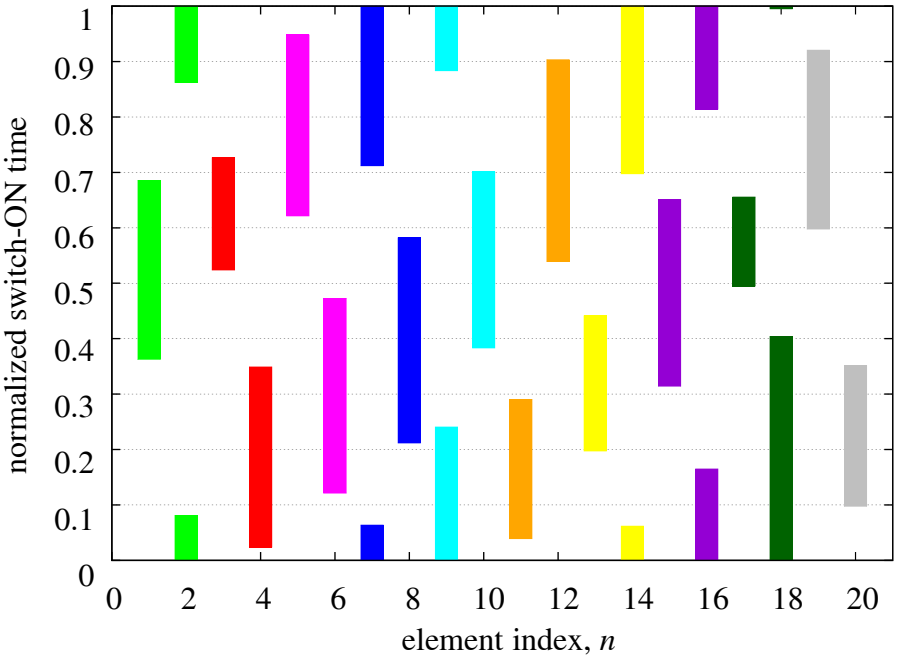

Figure 4.11: Plot of the normalized time sequences which synthesize the radiation receiving pattern in Fig. 4.10.

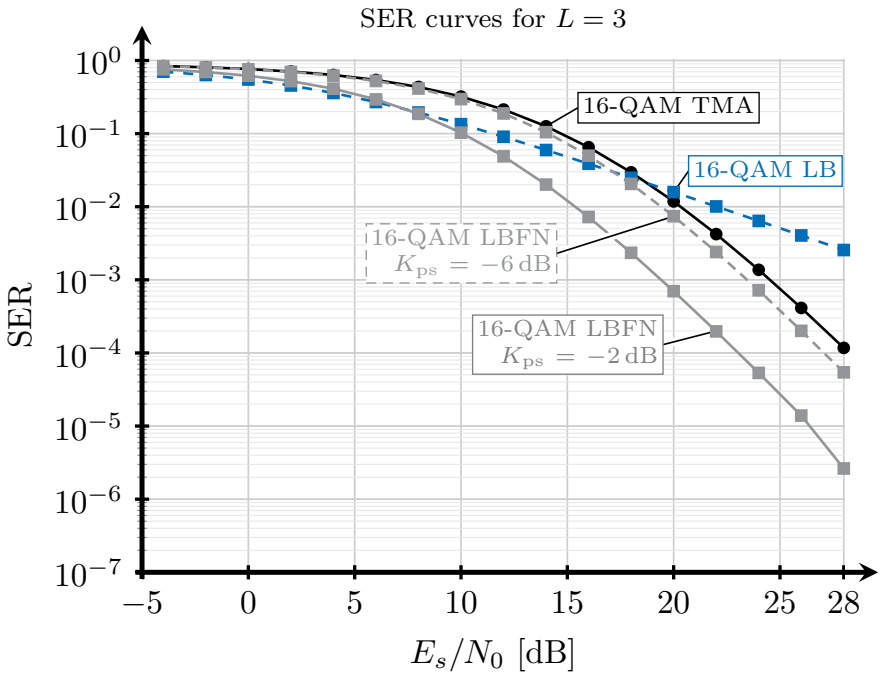

Figure 4.12: SER curves comparing the performance of the SIMO TMA system with other solutions based on conventional arrays for the case of $L = 3$ (a three-path channel).

4.8 Conclusions

We proposed a wireless communication receiver consisting of a TMA performing nonlinear beamforming followed by an MRC subsystem devoted to extract channel diversity in the form

of angular diversity captured by the sideband radiation exhibited by the TMA. We considered the transmission of LDM signals through an RFC exhibiting channel diversity. As a reference, we compared the performance of the TMA-based receiver to that exhibited by a single LB-based receiver (thus not exploiting channel diversity) and to that offered by an LBFN-based receiver (also equipped with an MRC). We derived closed-form expressions for the SER with respect to the SNR when LDM signals are transmitted and considering the three aforementioned receivers. Remarkably, the SER of the TMA-based receiver can be expressed directly in terms of the main parameters of the TMA itself, hence providing a fundamental tool for the designer. A new optimization algorithm to synthesize the radiation pattern conditioned to a specific architecture that allows for maximizing the TMA efficiency was implemented.

Finally, numerical simulations for the cases of two and three incoming signal replicas were also presented. The SER versus SNR results showed that both TMA-based and LBFN-based receivers were able to profitably exploit the channel diversity. Such SER versus SNR results also illustrated that the TMA exhibits the best trade-off between hardware and software complexity with respect to the performance obtained. Due to the compromise between L and the TMA power efficiency, inherent to the rectangular pulses, there is still room for improving the beamforming performance with TMAs by exploring more appropriate shapes for the basic pulses $g_n(t)$, as well as in the preprocessing of such pulses to achieve full independence between different harmonic patterns.

Chapter 5

Enhanced TMAs for Harmonic Beamforming

In Chapter 4 we have analyzed the performance of time-modulated arrays (TMAs) in multipath scenarios. This chapter of the thesis is devoted to investigate the performance improvement of TMAs in such scenarios by means of time-modulating the array excitations with periodic sum-of-weighted-cosine (SWC) pulses instead of periodic rectangular pulses.

This chapter is mainly based on the following co-authored publications:

- R. Maneiro-Catoira, J. Brégains, J. A. García-Naya, and L. Castedo. "**Enhanced time-modulated arrays for harmonic beamforming**". *IEEE Journal of Selected Topics in Signal Processing*, vol. 11, no. 2, 2017, pp. 259–270. ISSN: 1932-4553. DOI: 10.1109/jstsp.2016.2627178
- R. Maneiro-Catoira, J. Brégains, J. A. García-Naya, and L. Castedo. "**Time-modulated arrays with sum of weighted cosine pulses**". *Proc. of 2016 IEEE International Symposium on Antennas and Propagation and USNC-URSI Radio Science Meeting (2016 IEEE AP-S & USNC-URSI)*. Fajardo, Puerto Rico, 2016, pp. 697–698. DOI: 10.1109/APS.2016.7696057

The rest of this chapter is structured as follows. In Section 5.2, after quantifying the vulnerabilities of rectangular pulses for harmonic beamforming with TMAs, a new family of TMAs based on SWC pulses are proposed to override such limitations. These novel TMAs are termed as enhanced time-modulated arrays (ETMAs). Section 5.3 describes a synthesis method for harmonic beamforming with ETMAs and discusses some possible hardware structures for such antennas. The benefits of ETMAs, i.e., a more versatile and efficient beamforming, are shown in Section 5.4 by means of a comparative study with respect to conventional TMAs. Finally, Section 5.5 is devoted to the conclusions.

5.1 Introduction

The on-off switching of the antenna array excitations involved in the TMA beamforming process is mathematically modeled as the multiplication between the antenna array excitations and periodic rectangular pulses [POLI 2011b; TONG 2012b] (see right-hand side of Fig. 5.1). The frequency behavior of the rectangular pulses, however, is not the best one to efficiently distribute the spectral energy among the harmonic patterns to be exploited. Specifically, a minimum main-lobe width and a modest side-lobe level (SLL), together with a slow asymptotic side-lobe decay, are well-known characteristics of the rectangular pulses frequency response which will restrict not only the TMA efficiency but also the signal-to-noise ratio (SNR) level at the receiver. Hence, a pulse with a certain trade-off between its time and frequency responses is preferred for TMA beamforming. On the one hand, we seek for simplicity in the time domain in the sense that pulses would be easily generated. On the other hand, we look for pulses with some specific windowing features in the frequency domain.

As a first approach, and inspired by the so-called apodization procedures in signal processing[1], we look for suitable pulse functions which smoothly decay towards zero in the time domain with the aim of achieving a better performance in terms of SLL and asymptotic decay in the frequency domain. One possibility is the multiplication of a rectangular pulse by a sinusoidal function in the time domain. Such a multiplication causes a pulse shift in the frequency domain. Consequently, if a strategic linear combination of sinusoids (cosines) is used to multiply a rectangular pulse, a frequency response made up of a linear combination of weighted and frequency-shifted replicas of sinc functions will be obtained. This flexible way of smoothing the time response implies, of course, an increase of the pulse bandwidth (which is welcome when the objective consists in exploiting higher order harmonics) while providing room for shaping the frequency response.

With the previous ideas in mind, we have found that the so-called SWC pulses [NUTTALL 1981], [MANEIROCATOIRA 2016] are particularly adequate for our purposes, since they are precisely composed of frequency-shifted replicas of the sinc function, as illustrated in Fig. 5.2. Despite their simple form, such pulses allow for a flexible windowing of the harmonics involved. In addition to that, they provide an extra degree of freedom for the TMA harmonic patterns design. Hence, we have the following parameters to perform TMA beamforming:

- the usual TMA timing parameters, i.e, durations and shifts of the pulses, and
- a set of non-timing parameters corresponding to the weights of the SWC pulses.

Adaptive beamforming can be performed by changing dynamically the normalized time shifts and the SWC weights, while using statically the pulse time durations to design a quiescent (non-adapted) pencil beam pattern in the fundamental frequency, which can be replicated and

[1] In discrete-time signal processing the samples may be abruptly truncated causing unwanted frequency side-lobes when performing the discrete Fourier transform. Such an abrupt truncation can be smoothed by properly multiplying the corresponding sample region times a suitable time function. This procedure is known as apodization.

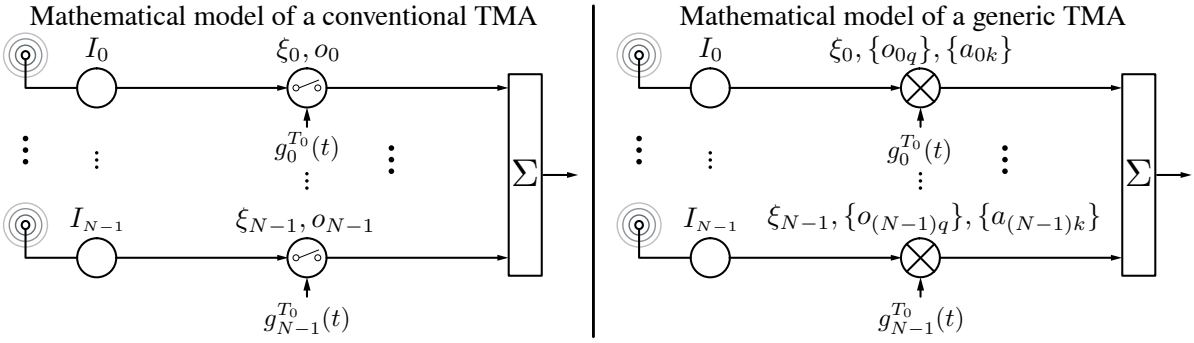

Figure 5.1: Block diagrams of the mathematical model of a conventional TMA (left-hand side) and a generic TMA (right-hand side). A conventional TMA is a TMA implemented with on-off switches. The parameters that can be adjusted to optimize the array depend on its type. In a generic TMA, the involved parameters are ξ_n (normalize pulse durations), o_{nq} (normalize pulse time shifts), and a_{nk} (pulse weights), $n \in \{0, 1, \ldots, N-1\}$, $q \in \{0, \pm 1, \ldots, \pm L\}$, and $k \in \{0, 1, \ldots, K\}$, where L is the order of the highest exploited harmonic, and K is the order of the pulse.

adapted in a chosen number of harmonic frequencies. That is the idea behind the so-called ETMA, which is proposed in this chapter and described in detail in Section 5.2.2. Notice that the mathematical model of ETMAs fits into the generic TMA graphical description shown in Fig. 5.1 (right-hand side) in contrast to conventional TMAs shown in Fig. 5.1 (left-hand side).

The main contributions of this chapter are the following:

1. The quantification of the vulnerabilities of rectangular pulses in conventional TMAs for beamforming purposes.
2. The introduction of a novel signal processing procedure to obtain fully-independent TMA harmonic patterns, leading to unprecedented levels of flexibility and efficiency.
3. The description of a method for synthesizing ETMAs together with a demonstration showing that such a method is compatible with both classical nulling methods –based on exclusively perturbing the excitation phases– and pattern nulling algorithms –specifically designed for conventional TMAs.
4. The specification of the hardware required to implement ETMAs and a comparison to that employed by conventional TMAs.
5. A comparison in terms of power efficiency between the proposed ETMAs and existing conventional TMAs.

5.2 Impact of TMA Pulses on Harmonic Beamforming

Let us consider a linear TMA with N isotropic elements, each one modulated by a periodic (with fundamental period T_0) pulse $g_n^{T_0}(t)$ where $n \in \{0, 1, \ldots, N-1\}$. We assume that the beamforming is performed over the harmonic frequencies qf_0, with $q \neq 0$, $f_0 = 1/T_0$ being the

TMA periodic pulse train fundamental frequency, and $q \in \{0, \pm 1, \pm 2, ..., \pm L\}$, where L is the order corresponding to the highest exploited harmonic. The array factor corresponding to the harmonic frequency qf_0 (with $q \neq 0$) is given by [MANEIROCATOIRA 2014a]

$$F_q(\theta, t) = \sum_{n=0}^{N-1} I_n G_{nq} \mathrm{e}^{jkz_n \cos\theta} \mathrm{e}^{j2\pi(f_c + qf_0)t}, \tag{5.1}$$

where z_n represents the n-th array element position on the z axis, $I_n = |I_n|\mathrm{e}^{j\varphi_n}$ is the complex representation of the per-antenna current static excitation, θ is the angle with respect to the main axis of the array, k is the wavenumber, and f_c is the carrier frequency.

5.2.1 Vulnerabilities of Rectangular Pulses

Given a rectangular pulse defined as

$$g_n(t) = \mathrm{rect}(t/\tau_n) = \begin{cases} 1 & t \in (-\tau_n/2, \tau_n/2) \\ 0 & \text{otherwise,} \end{cases} \tag{5.2}$$

the periodic (T_0) extension of such a pulse admits the following exponential Fourier series representation

$$g_n^{T_0}(t) = \sum_{q=-\infty}^{\infty} G_{nq} \mathrm{e}^{jq\frac{2\pi}{T_0}t}, \tag{5.3}$$

where G_{nq} are the exponential Fourier series coefficients. Since the Fourier transform of $g_n(t) = \mathrm{rect}(t/\tau_n)$ is $G_n(f) = \tau_n \mathrm{sinc}(\pi\tau_n f)$, the coefficients G_{nq} are given by

$$G_{nq} = \frac{1}{T_0} G_n(q/T_0) = \xi_n \mathrm{sinc}(\pi q \xi_n), \tag{5.4}$$

with $\xi_n = \tau_n/T_0$ being the normalized pulse durations. In view of Eq. (5.1) and Eq. (5.4), it is found that

$$I_{nq}^{\mathrm{TMA}} = I_n G_{nq} = I_n \xi_n \mathrm{sinc}(\pi q \xi_n) \tag{5.5}$$

are the dynamic excitations of the q-th harmonic pattern of the TMA. Therefore, the design and optimization of TMAs for harmonic beamforming purposes using rectangular pulses unavoidably encounters the limitations imposed by the features of the sinc function, whose energy spectral density (ESD) exhibits the following properties (see Fig. 4.4, page 51, for $\xi_n = 1$): (a) a normalized main-lobe width (NMLW)[2] equal to 1, which is the minimum possible value; (b) a maximum side-lobe level (MSLL) of -13 dB; and (c) a first order ($1/f$) spectrum roll-off or asymptotic decay.

In order to include successive harmonics (with normalized frequencies corresponding to the values $1, 2, 3 \ldots$) under the main lobe through time-modulation techniques, it is necessary to

[2]Note that the frequency axis is normalized with respect to the minimum pulse width $f_0 = 1/T_0$, which is the time-modulation frequency.

reduce the width of the pulses in the time domain by virtue of (a), but the desired windowing effect with the working harmonics –to avoid an efficiency loss– is not achieved unless those pulse widths are close to zero due to (b) and (c). Under these circumstances, the power efficiency levels are safeguarded but, unfortunately, with pulse widths too close to zero, the TMA gain (and hence the SNR at the receiver) is reduced when compared to conventional linear beamforming solutions that synthesize the same pattern. Indeed, the average SNR of a signal received over the TMA q-th harmonic is proportional to the antenna gain in the direction of the radiation peak of such a pattern, G_q^{TMA} [ZHU 2012a], i.e.,

$$\text{SNR}_q^{\text{TMA}} \propto \mathbf{G}_q^{\text{TMA}} = \eta_{\text{TMA}}^{\text{Rect}} \frac{4\pi |F_q(\theta_q, t)|^2}{P_{\text{R}}^{\text{TMA}}}, \tag{5.6}$$

where $\eta_{\text{TMA}}^{\text{Rect}}$ is the total efficiency of the TMA given by

$$\eta_{\text{TMA}}^{\text{Rect}} = \eta_s \eta(L), \tag{5.7}$$

with η_s being the efficiency of the switching network accounting for the energy absorption when the switches are off, and $\eta(L)$ the TMA power efficiency when $L-1$ harmonics are exploited in addition to the fundamental mode. Such a power efficiency is defined as the ratio between the useful mean received power P_U^{TMA} and the total mean received power P_R^{TMA}, i.e.,

$$\eta(L) = \frac{P_{\text{U}}^{\text{TMA}}}{P_{\text{R}}^{\text{TMA}}} = \frac{\sum_{q=-L}^{L} p_q}{\sum_{q=-\infty}^{\infty} p_q}, \tag{5.8}$$

where $P_{\text{U}}^{\text{TMA}}$ and $P_{\text{R}}^{\text{TMA}}$ are the useful and total mean received power values, respectively, which can be expressed in terms of p_q, the total mean received power at the q-th harmonic when a carrier is received over the TMA [BRÉGAINS 2008]. In view of Eq. (5.8), the level of non-exploited harmonics must be kept below a certain level in order to efficiently achieve the appropriate values, which are close to 1. On the other hand, we can compare G_q^{TMA} to the gain of a static array (STA), G_q^{STA}, which accomplishes linear beamforming generating the same spatial radiation patterns $|F_q(\theta_q, t)|^2$ as the TMA, and thus having the same static excitations $I_{nq}^{\text{STA}} = I_{nq}^{\text{TMA}}$. We can express such a gain as

$$G_q^{\text{STA}} = \alpha_{\text{BFN}} \frac{4\pi |F_q(\theta_q, t)|^2}{P_{\text{R}}^{\text{STA}}}, \tag{5.9}$$

with α_{BFN} being the attenuation of the STA beamforming network (BFN) and $P_{\text{R}}^{\text{STA}}$ the total mean received power for the STA. By considering an inter-element distance of $\lambda/2$, $|I_n|$=1, and according to [MANEIROCATOIRA 2014a, Eq. (42)]:

$$p_q = 4\pi \sum_{n=0}^{N-1} |G_{nq}|^2 = 4\pi \sum_{n=0}^{N-1} \xi_n^2 \text{sinc}^2(\pi q \xi_n), \tag{5.10}$$

and the following expression is easily obtained [BRÉGAINS 2008]

$$\frac{G_q^{\text{TMA}}}{G_q^{\text{STA}}} = \frac{\eta_{\text{TMA}}}{\alpha_{\text{BFN}}} \cdot \frac{\sum_{n=0}^{N-1} \xi_n^2 \text{sinc}^2(\pi q \xi_n)}{\sum_{n=0}^{N-1} \xi_n}. \tag{5.11}$$

Table 5.1: TMA modes for harmonic beamforming depending on the character of the variables of the SWC pulses. Pattern synthesis requirements are also illustrated.

TMA mode	type of parameter			optimization	
	ξ_n	o_{nq}	a_{nk}	**type**	**complexity**
conventional TMA	adaptive	adaptive	nonadaptive	systematic	high$^{(*)}$
enhanced TMA (ETMA)	nonadaptive	adaptive	adaptive	heuristic	low
advanced TMA	adaptive	adaptive	adaptive	systematic	high

(*): The terms "high" or "low" are qualitative more than quantitative. Therefore, in relative terms, the systematic optimization complexity is "high" compared to the heuristic optimization. The main reason is that the optimization level required in ETMAs is minimum as the initial pattern synthesized (two simple steps) already has an excellent efficiency.

This ratio shows –by simply analyzing any of the two ratios of the expression– that, with pulse durations ξ_n too close to zero, $G_q^{\text{TMA}} \ll G_q^{\text{STA}}$, hence yielding $\text{SNR}_q^{\text{TMA}} \ll \text{SNR}_q^{\text{STA}}$ after applying Eq. (5.6).

Regarding the excitation phases of the harmonic patterns, we easily arrive at a more generalized version of Eq. (5.4) when a non-even rectangular pulse $g_n(t)$ is considered and a normalized time-shift o_n is applied to $g_n^{T_0}(t)$ [ROCCA 2014]

$$G_{nq} = \xi_n \text{sinc}(q\pi\xi_n) \text{e}^{-jq\pi(\xi_n+2o_n)}. \tag{5.12}$$

Therefore, by substituting Eq. (5.12) into Eq. (5.5), we obtain the excitations for the successive harmonic patterns ($q \geq 1$) and we notice that the switching architecture imposes that harmonic patterns with different order exhibit a dependency between their phases. This property seriously limits the performance of a TMA in a realistic scenario where the direction of arrivals (DOAs) are random. In this sense, and more specifically, sophisticated multi-objective optimization methods [ROCCA 2014, Section III-A] are used to shape the required beams under such a restriction, but the price to be paid is a serious degradation of the TMA power efficiency as it is shown in Section 5.4.2, which is devoted to calculate the TMA power efficiency in some of the designs existing in the recent literature.

In summary, the designer lacks of full freedom –due to the trade-off between flexibility and power efficiency– to assign the corresponding phases and synthesize a series of independent harmonic diagrams according to the adaptive beamforming.

5.2.2 SWC Pulses: The Enhanced TMA (ETMA) Concept

Due to the harmonic beamforming limitations of rectangular pulses described in the subsection above, our aim is to identify a pulse with the following properties:

1. Easy generation in the time domain.

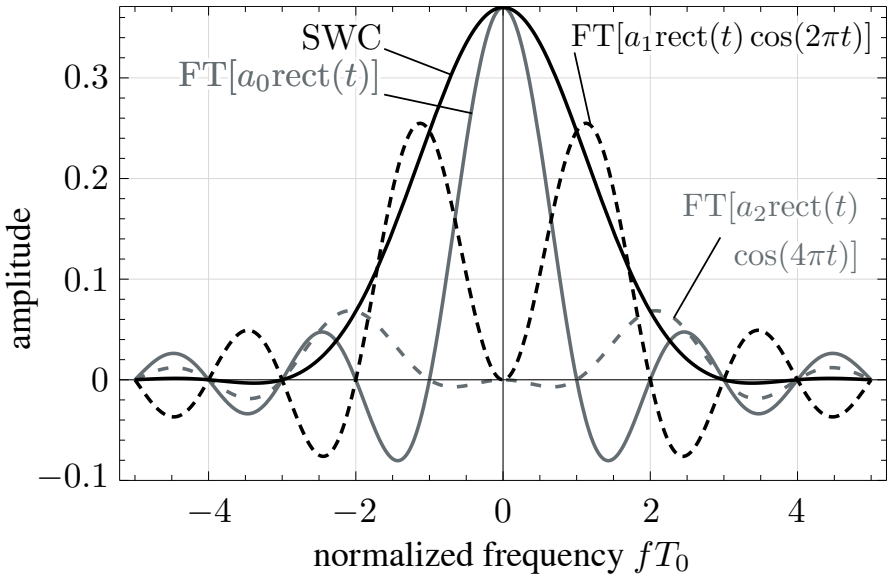

Figure 5.2: Synthesis of a 3-term SWC pulse as a superposition of frequency-shifted rectangular pulses. The pulse is appropriate for efficiently exploiting the first and the second harmonics with a TMA. The weighting coefficients are $a_0 = 0.37$, $a_1 = 0.49$, and $a_2 = 0.14$.

2. Good windowing features, i.e., a frequency response with a main lobe containing a large part of the total energy, an MSLL as small as possible relative to the main-lobe peak, and side-lobes decaying asymptotically at an appropriate rate.
3. Flexibility to shape dynamically and independently the harmonic patterns.

Such a versatility would give us the possibility of obtaining high values for the TMA power efficiency while working with pulse widths close to 1, thus overcoming the aforementioned SNR deterioration. The superposition of frequency-shifted rectangular pulses, presented in the introduction and shown in Fig. 5.2 –the so called SWC pulses– seems to fit very well into the pulse idea we are seeking. Let us now proceed to present a generalized analysis about the use of SWC pulses in a TMA to exploit its harmonic patterns. In order to construct such periodic pulse trains, $g_n^{T_0}(t)$, we first define a basic pulse given by an SWC over a finite duration $\tau_n \leq T_0$

$$b_n(t) = \sum_{k=0}^{K} a_{nk} \cos(2\pi k t/\tau_n)\, \mathrm{rect}(t/\tau_n), \tag{5.13}$$

where a_{nk} are real-valued constants with $k \in \{0, 1, \ldots, K\}$. K is the order of the basic pulse $b_n(t)$, and the constants a_{nk} satisfy the normalization condition

$$\sum_{k=0}^{K} a_{nk} = 1. \tag{5.14}$$

Recall that the pulses given by Eq. (5.13) have been used to design a widely known family of window functions with controllable side-lobe behavior [NUTTALL 1981].

Recall now that the exponential Fourier series representation of the periodic extension of

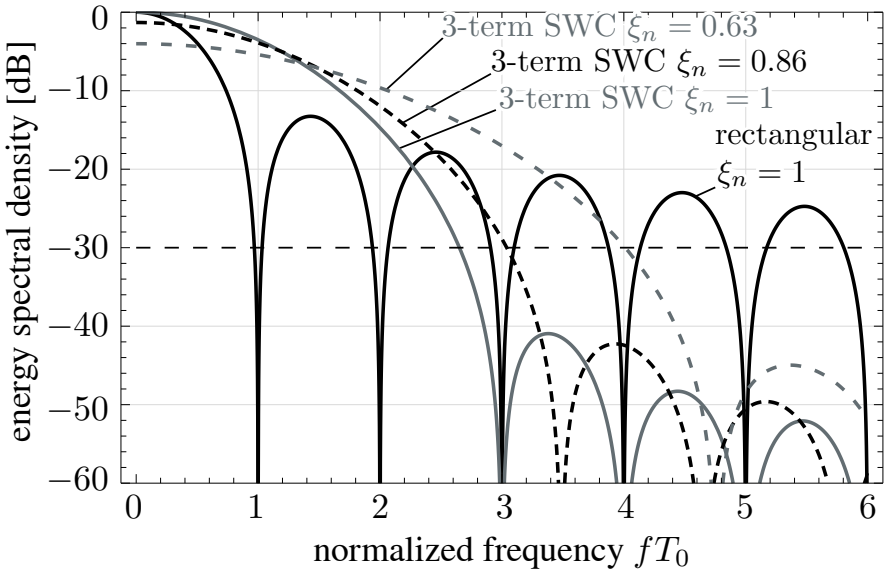

Figure 5.3: Examples of ESD vs. normalized frequency curves for the 3-term SWC pulse of Fig. 5.2, $|G_n(f)|^2$, for different values of the normalized pulse durations ξ_n and comparison with the rectangular pulse (corresponding to the minimum width, $\xi_n = 1$). Analogously to Fig. 5.2, $|I_{nq}^{\text{TMA}}|^2 = |G_n(q)|^2$. As a result of the pulse windowing behavior, a selection of $0.86 \leq \xi_n \leq 1$ allows for working selectively with the fundamental mode, the first and the second harmonics, i.e., exploiting $|q| \leq 2$ while keeping below -30 dB the higher order harmonics. For $0.63 \leq \xi_n \leq 0.86$, the order of the harmonics selectively exploited are those with $|q| \leq 3$. Hence, in view of the pulse response, it is guaranteed a selective exploitation of the harmonics for certain intervals of ξ_n and fixed pulse weights a_{nk}. Additionally, for a given interval of ξ_n, it is possible to adjust both the harmonic selectivity (since the pulse bandwidth can be modified) and the levels of the selected harmonics by varying the pulse weights a_{nk}. An example of this adjustment is shown in Section 5.4.

the basic pulse in Eq. (5.13) is given by

$$b_n^{T_0}(t) = \sum_{q=-\infty}^{\infty} B_{nq} \mathrm{e}^{jq(2\pi/T_0)t}, \tag{5.15}$$

where

$$B_{nq} = \frac{1}{T_0} B_n\left(\frac{q}{T_0}\right) = \frac{\xi_n^2 q}{\pi} \sin(\pi \xi_n q) \sum_{k=0}^{K} \frac{(-1)^k a_{nk}}{\xi_n^2 q^2 - k^2} \tag{5.16}$$

are the Fourier series coefficients. This result is obtained from

$$B_n(f) = \frac{\tau_n^2 f}{\pi} \sin(\pi \tau_n f) \sum_{k=0}^{K} \frac{(-1)^k a_{nk}}{(\tau_n^2 f^2 - k^2)}, \tag{5.17}$$

which is the Fourier transform of $b_n(t)$ [NUTTALL 1981]. On the other hand, let us introduce an additional periodic (T_0) signal, $v_n^{T_0}(t)$, which accounts for the phases of the excitations of the

harmonic patterns given by

$$v_n^{T_0}(t) = 1 + \sum_{q=1}^{L} \cos\left(\frac{2\pi q}{T_0}\left(t - \delta_{nq}\right)\right), \tag{5.18}$$

where each δ_{nq} is a time-delay used as a design parameter to properly control the phase of the excitation of the n-th element of the q-th order harmonic pattern. Since $v_n^{T_0}(t)$ is a real-valued signal, its Fourier series coefficients satisfy the Hermitian symmetry property and are given by

$$V_{nq} = V_{n(-q)}^{*} = \mathrm{e}^{-j2\pi q(\delta_{nq}/T_0)} = \mathrm{e}^{-j2\pi q o_{nq}}, \tag{5.19}$$

with $o_{nq} = \delta_{nq}/T_0$ being the normalized time-delays. Finally, we construct $g_n^{T_0}(t)$ from the periodic convolution

$$g_n^{T_0}(t) = v_n^{T_0}(t) \circledast b_n^{T_0}(t), \tag{5.20}$$

whose Fourier series coefficients satisfy[3]

$$G_{nq} = V_{nq} B_{nq}. \tag{5.21}$$

By considering Eq. (5.16) and Eq. (5.21), we can identify in Eq. (5.1)

$$I_{nq}^{\mathrm{TMA}} = I_n \frac{\xi_n^2 q}{\pi} \sin(\pi \xi_n q) \sum_{k=0}^{K} \frac{(-1)^k a_{nk}}{\xi_n^2 q^2 - k^2} \mathrm{e}^{-jq2\pi o_{nq}} \tag{5.22}$$

as the dynamic excitations of the q-th harmonic pattern of the TMA.

Fig. 5.3 shows the ESD of the pulse synthesized in Fig. 5.2 for different values of ξ_n, as well as the comparison with the rectangular pulse (case of minimum width $\xi_n = 1$). Note that by considering $|I_n| = 1$, then $|I_{nq}^{\mathrm{TMA}}|^2 = |G_n(q)|^2 = |B_n(q)|^2$ (see Eq. (5.16), Eq. (5.21), and Eq. (5.22)). Fig. 5.3 shows the suitability of such an SWC pulse for an efficient exploitation of the first and the second order harmonics.

In view of Eq. (5.22), we have different degrees of freedom in the harmonic beamforming design depending on the static (nonadaptive) or dynamic (adaptive) nature of the variables involved. Therefore, and according to Table 5.1, if a_{nk} are fixed while ξ_n and o_{nq} are adjusted dynamically, we have a so-called pure or conventional TMA. The radiation pattern optimization in this case is a sophisticated task based on multi-objective optimization methods (such as genetic algorithms, simulated annealing, or particle swarm) similar to those applied to the case of rectangular pulses. If, additionally, a_{nk} are dynamically adjusted –this is the case which we will henceforth refer to as advanced TMA– the problem has to be solved employing similar methods but with a larger number of parameters.

In order to have a more clear idea about the complexity of the systematic optimization methods to be applied for the synthesis of both conventional TMAs and advanced TMAs based

[3]If $x(t)$ and $y(t)$ are periodic (T) signals, its periodic convolution $z(t)$ is defined as: $z(t) = x(t) \circledast y(t) = 1/T \int_{<T>} x(\tau) y(t-\tau) d\tau$ and if a_k, b_k are the Fourier series expansion coefficients of $x(t)$ and $y(t)$, respectively, then $c_k = a_k b_k$ are the corresponding coefficients of $z(t)$.

on SWC pulses, we briefly describe a reference example with a specific method. Although such a method can be applied to conventional TMAs with rectangular pulses [ROCCA 2014, Section III-A], it can be also adapted to TMAs based on SWC pulses by using the Fourier coefficients G_{nq} (see Eqs. (5.1) and (5.21)) for the SWC pulses. As already pointed out, such coefficients provide an additional degree of freedom by means of the a_{nk}. In the systematic method in [ROCCA 2014, Section III-A] it is defined a fitness function [ROCCA 2014, Eq. (10)] consisting of three weighted functionals accounting, respectively, for the following features of the radiation pattern: 1) the SLL of the beams, 2) the level of equalization between the maxima of the beams, and 3) the position of the nulls. Such a fitness function is optimized, in this case, through a particle swarm optimization (PSO) algorithm. We have classified the complexity of this technique (see Table 5.1) as "high" in relative terms, i.e., when compared to the one described below and applied to a third type of TMAs with SWC pulses. Such a third alternative offers another possibility to perform adaptive beamforming by updating dynamically o_{nq} and a_{nk} while using the pulse time durations corresponding to the design of a quiescent (non-adaptive) pencil beam pattern in the fundamental frequency, which can be replicated and adapted in a chosen number of harmonic frequencies. That is the idea behind the ETMA, and its greatest advantage is the simplicity in the synthesis of the radiation diagrams, which is given by the following procedure consisting of four steps:

1. Assign to ξ_n the values synthesizing a particular pattern for the fundamental mode (which, according to the particular SWC pulse response, will be properly replicated at the harmonic frequencies).
2. Compute the initial values for a_{nk} by means of the equations given in Section 5.3.1, where K (the order of the pulses) depends on the number of harmonics L to be exploited.
   After these two steps, the achieved efficiency level is excellent (above 95 % in the examples in Section 5.4, summarized in the captions of Figs. 5.5 to 5.11). This is due to the adequate windowing features of SWC pulses in contrast to those exhibited by the rectangular pulses. The third and the fourth steps account for two extra features:
3. The possibility of using either classical nulling methods based on exclusively perturbing the excitation phases e.g. [STEYSKAL 1983], or more recent and sophisticated ones [POLI 2011a; ROCCA 2012b].
4. The optimization of the efficiency (becoming quasi-ideal) by strategically forcing to zero some a_{nk} of the array (see an example in Section 5.4, Fig. 5.6). In this regard, this is a heuristic mechanism that allows for looking for a sufficiently good –albeit not necessarily optimal– solution with a low computational complexity.
   Compared to systematic methods, we have described this last method as a "low" complexity one in Table 5.1.

Once the three modes of exploitation have been described, and since the goal of this work is to introduce the advantages of ETMAs based on SWC pulses, we will focus the forthcoming sections on ETMAs, leaving the case of advanced TMAs for future investigations.

5.3 Harmonic Beamforming with ETMAs

5.3.1 TMA Synthesis Method

The idea behind an ETMA is the possibility of carrying out an efficient harmonic beamforming without needing the pulse durations ξ_n to be too close to zero, which would cause unavoidably a degradation in terms of power efficiency and, consequently, a loss in the SNR at the receiver. Additionally, ETMAs provide flexibility in the radiation pattern synthesis by governing the amplitude variable a_{nk}, together with the time variables ξ_n and o_{nq} according to Eq. (5.22).

The operational mode proposed for the ETMAs is based on the design of a quiescent pencil beam pattern in the carrier frequency by means of properly setting the $I_n\xi_n$ products according to [KUMMER 1963]. The difference now is that, by means of the SWC pulses, it is possible to create replicas of such a pencil beam pattern at a given number of harmonic frequencies, with the novelty of using a_{nk} and o_{nq} to reconfigure these new diagrams adaptively according to Eq. (5.22). Under this assumption, ξ_n are time parameters involved in the design to improve the SLL in the quiescent pattern, but having a non adaptive character. On the other hand, note that since the phases of the excitations (caused by the time delays o_{nq}) of each harmonic pattern are independent, it is possible an autonomous application of pattern nulling methods to each harmonic diagram (see, for example, [STEYSKAL 1983]). Another possibility is to use the existing methods for TMA nulling [POLI 2011a; ROCCA 2012b], taking into account the new degrees of freedom introduced by the ETMA.

The radiation pattern synthesis procedure may exploit the following property of the Fourier Transform of an SWC pulse Eq. (5.16), Eq. (5.17) when $\xi_n = 1$

$$B_{nq}\Big|_{\xi_n=1} = \frac{1}{T_0} B_n\left(\frac{q}{T_0}\right)\Bigg|_{\xi_n=1} = \begin{cases} a_{n0} & q = 0 \\ a_{n|q|}/2 & q \neq 0; |q| \leq K \\ 0 & \text{otherwise,} \end{cases} \tag{5.23}$$

where K is the order of the basic SWC pulse in Eq. (5.13) and coincides with the highest order of the exploited harmonics, i.e., $K = L$. As mentioned before, the working interval for the TMA pulse durations ξ_n should be as close to 1 as possible for an efficient beamforming. On the other hand, it was analyzed in Section 5.2.2, and also shown in Fig. 5.3, that the SWC pulses allow for windowing, with a good level of equalization, the corresponding working harmonics for certain intervals of ξ_n in the proximity of 1. Then, we can expect a behavior of B_{nq} –and therefore of $|I_{nq}^{\text{TMA}}| = |I_n||B_{nq}|$ (see Eq. (5.22))– according to Eq. (5.23) for a certain interval of ξ_n relatively close to 1, i.e., the excitation amplitudes of the q-th harmonic pattern of the TMA (with excitations $|I_{nq}^{\text{TMA}}|$) can be governed reliably by the set of coefficients $\{a_{0|q|}, a_{1|q|}, \ldots, a_{(N-1)|q|}\}$ corresponding to each of the N pulses. Under those circumstances, it is possible to design harmonic beams with similar amplitude patterns by properly choosing the coefficients a_{nk} in Eq. (5.23) as a starting point in the design. Hence, in order to obtain identical

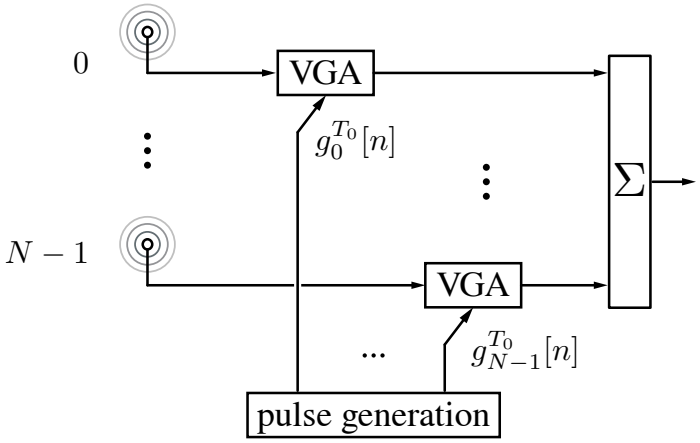

Figure 5.4: Diagram of an ETMA for adaptive beamforming. Note that the hardware is the same as the one of a conventional TMA but replacing the RF switches with RF VGAs equipped with digital control.

amplitude harmonic patterns, we should consider:

$$a_{n|q|} = 2a_{n0};\ |q| \leq K; q \neq 0 \text{ and } \forall n, \tag{5.24}$$

and if we apply the normalization condition Eq. (5.14), we easily express Eq. (5.24) as

$$a_{n|q|} = 2a_{n0} = \frac{2}{2K+1}, \tag{5.25}$$

which is an initial condition to obtain equal excitation amplitudes $|I_{nq}^{\text{TMA}}|$, $\forall\ |q| \leq K$, and consequently, replicated harmonic patterns. Since the windowing level is not ideal, due to the presence of the $\xi_n \leq 1$ (see Fig. 5.3), the attenuation of the first unexploited harmonics must be improved. A great advantage of this technique is that it is easy to control the level of such unwanted harmonics by a certain adjustment of a_{nk} with respect to the values given by Eq. (5.25), as we illustrate in one of the examples presented in Section 5.4. Recall that the remaining unwanted harmonics are already properly attenuated due to the SWC pulses spectral shape (see Fig. 5.3).

5.3.2 TMA Hardware Structures

In this section we analyze possible hardware structures for the ETMA based on SWC pulses. Additionally, they are compared to the corresponding architecture of conventional TMAs based on radio frequency (RF) switches. The available solutions are:

1) **RF variable gain amplifiers (VGAs) with digital control**. An initial potential implementation for the ETMA is the one proposed in [HE 2013] and illustrated in Fig. 5.4. Such a structure was originally proposed to implement a beamforming method using pure sinusoids [HE 2013] and presented as an alternative to beamforming with TMA. Notice that it has the same structure as a conventional TMA but replacing the

RF switches with RF VGAs with digital control. Recall that, as the pulses must be generated in the digital domain in any implementation of a TMA, we consider the same control unit or digital signal processor (DSP) for all the implementations presented here (including the TMA with RF switches). This very simple architecture is a reasonable choice for beamforming because it provides much better features –albeit increased power consumption– than the implementation based on RF switches.

2) **RF VGAs with analog control and digital-to-analog converters (DACs)**. According to the scheme shown in Fig. 5.4, it is possible to use VGAs with analog control, but additional DACs are required. This solution is more expensive than the previous one, being the cost inversely related to the power consumption of the VGAs. The DACs imply an extra cost but at least exhibiting a low power consumption. The architecture is more complex than the one in Fig. 5.4 yet still quite simple.
3) **RF multipliers with DACs**. The multipliers have a power consumption slightly higher than that of the VGAs with digital control for the same frequency, but with twice the cost. However, they are a competitive solution with respect to the VGA with analog control.

On the other hand, let us consider an adequate structure for the TMA based on RF switches envisaged for beamforming purposes:

4) **Conventional TMAs**. The appropriate type of switches to be considered, in order to carry out a fair comparison in terms of hardware, are the so-called single-pole triple-throw (SP3T) switches. A common denominator in this part of our research work is that the harmonic beamforming must be capable of safeguard the TMA power efficiency. In this sense, the use of a single RF switch for the control of two adjacent elements allows for improving the switching network efficiency whenever pairs of complementary pulses are synthesized [ZHU 2012a]. Therefore, in order to exploit up to three beams, it is only possible to achieve an adequate power efficiency level in the switching network (related to the fraction of the time that the switches are off), by using SP3T switches. For each switch, two throws are connected to a consecutive pair of array elements. For the case $L = 2$, the third throw will not be programmed or used, whereas for the case $L = 3$, such a throw is used as the off state.

Table 5.2: Hardware comparison of the beamforming networks implemented with TMAs.

		simple structure	cost	power consumption	size
conventional TMA	**RF switches**	excellent	excellent	excellent	excellent
enhanced TMA (ETMA)	**RF VGAs with digital control**	excellent	excellent	good	excellent
	RF VGAs with analog control	good	fair	good(*)	good
	multipliers	good	good	good	good

(*): Power and cost are inversely related.

Table 5.2 shows a comparison of the systems described above for TMA beamforming. Such a comparison is based, apart from the complexity of the hardware architecture, on key hardware

parameters like power consumption, cost, and size.

Notice that, from a signal processing point of view, the TMA technique carries out a nonlinear transformation (contrarily to a linear beamforming network (LBFN)) in the analog domain independently from the devices employed: switches, VGAs, multipliers, etc. Such a nonlinear transformation in the analog domain is determined by the application of periodic pulses at the antenna level and its effects (conversion of space diversity into frequency diversity) can be profitably exploited by using a single RF front end. With this in mind, we can briefly compare the ETMA (as a representative example of the TMA technique, because the comparison is valid for any of the aforementioned implementations) with conventional analog and digital beamforming schemes. Accordingly, we first consider a conventional array with N elements provided with an analog LBFN prepared to exploit up to L beams. Such an LBFN will have $L \times N$ phase shifters and $L \times N$ VGAs. Additionally, the receiver must be provided with L independent RF chains and L analog-to-digital converters (ADCs). In this sense, any TMA solution consisting of a single RF chain and a single ADC avoids practical problems related to synchronization and phase coherence. The same reasoning applies to the problem of coupling between RF chains. On the other hand, in a fully digital implementation of an LBFN, the number of required RF chains, L, is equal to the number of antenna elements N. When N is large, however, having an RF chain per antenna is unfeasible due to a number of reasons, being the power consumption per element in the RF front-end one of the most important ones as shown in [HEATH 2016, Table I]. In fact, beamforming with hybrid analog-digital architectures is currently becoming an increased trend.

In order to clarify the feasibility of ETMA synthesis with VGAs based on SWC pulses instead of pure sinusoids as in [HE 2013], let us analyze more in detail –also in the frequency domain– the parallelism between both beamforming techniques based on VGAs: ETMAs and periodical amplitude modulation [HE 2013].

The sinusoidal function $U_n(t) = A_n\,(1 + \cos(f_0 t + \varphi_n))$ in [HE 2013, Eq. (2)] governing the n-th VGA becomes, in the ETMA version, the function $g_n^{T_0}(t)$ (see (20)), also periodic but with its spectrum being a train of Dirac deltas not only consisting of "lines" at frequencies $-f_0$, 0, and f_0 as U_n of [HE 2013], but also at frequencies $-2f_0$, $2f_0$, $-3f_0$, $3f_0$, ..., for which the level of windowing of the SWC was designed by means of the a_{nk} values. The amplitude A_n in [HE 2013, Eq. (2)] determines the level of the spectral lines in $-f_0$, 0, and f_0, whereas for the ETMAs such a level is given by the Fourier coefficients G_{nq} (see (21)), which depend on ξ_n, a_{nk}, and o_{nq}, hence providing a powerful flexibility to the beamforming method.

Therefore, the applicability of the technique does not depend on the pure sinusoid character of the signals governing the VGAs. However, for both, pure sinusoids $U_n(t)$ and more complex periodic signals as $g_n^{T_0}(t)$, VGAs must satisfy the following conditions in the time domain:

- Their response time must be fast enough to follow $U_n(t)$ or $g_n^{T_0}(t)$. Therefore, the data acquisition frequency of the VGAs digital control signal must be high enough when compared to f_0. More specifically, greater than or equal to $N_s f_0$, being N_s the number

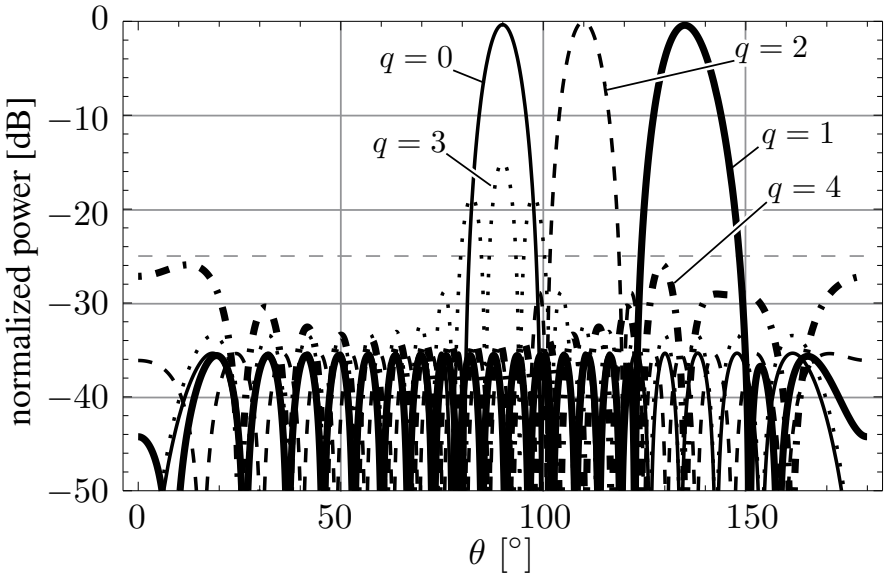

Figure 5.5: Radiation Pattern of an ETMA without adjusting a_{nk}. Array with $N = 20$ achieving beamforming ($\theta_0 = 90°$, $\theta_1 = 135°$, and $\theta_2 = 110°$) over the first and the second harmonics. The TMA uses 3-term SWC pulses ($K = 2$) with weights (see Eq. (5.25)): $a_{n1} = a_{n2} = 2a_{n0} = 2/5$. Hence $\mathrm{SLL}_0 = -35\,\mathrm{dB}$, $\mathrm{SLL}_1 = -35\,\mathrm{dB}$, and $\mathrm{SLL}_2 = -28\,\mathrm{dB}$. The maximum unwanted harmonic peak is $-15\,\mathrm{dB}$, with $P_0 = 19.24\,\%$, $P_{|1|} = 38.09\,\%$, and $P_{|2|} = 40.82\,\%$, yielding $\eta(L) = 98.15\,\%$, $E[\xi_n] = 0.88$, and $S[\xi_n] = 0.12$.

of samples per period of $U_n(t)$ or $g_n^{T_0}(t)$. For the case of VGAs with analog control the response time is specified in terms of a full scale step or a 3 dB gain step, which is the delay or time response corresponding to such abrupt variations. SWC pulses are windowing functions characterized, precisely, by smooth variations (and also its periodic convolution with a cosine), avoiding the introduction of important issues in this technique. In any case, the time response must be chosen relatively low enough when compared to T_0 to guarantee a correct behavior.

- They must faithfully replicate the amplitude levels of the control input signal ($U_n(t)$ or $g_n^{T_0}$). For the case of VGAs with digital control the so-called gain step must be low enough to avoid quantification and distortion errors, whereas for the case of analog VGA control the linear gain specifications must be adequate.

5.4 Results

We now present results that illustrate how the ETMA allows for achieving a twofold objective: (a) to exploit dynamically the first and the second order harmonic patterns with an adequate SLL, and (b) to achieve higher power efficiency levels, and thus higher average SNR at the receiver, than those obtained with rectangular pulses.

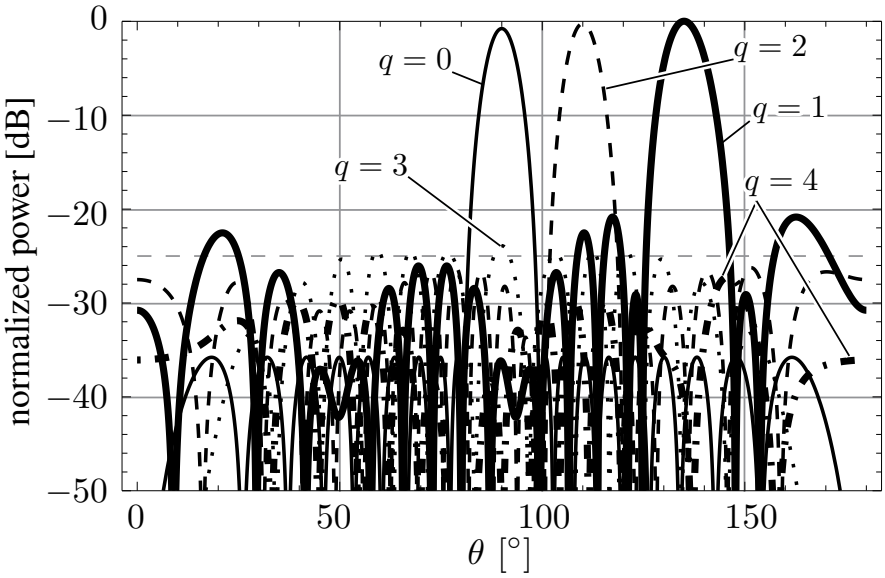

Figure 5.6: Adjusted radiation pattern of an ETMA ($N = 20$) achieving beamforming ($\theta_0 = 90°$, $\theta_1 = 135°$, and $\theta_2 = 110°$) over the first and the second order harmonics. The TMA uses 3-term SWC pulses ($K = 2$) with weights (see Eq. (5.25)): $a_{n1} = a_{n2} = 2a_{n0} = 2/5$ for $n \in [3, 16]$ and $a_{n0} = 1/5$, $a_{n1} = 4/5$, and $a_{n2} = 0$ for the rest of the elements. Hence $\mathrm{SLL}_0 = -35\,\mathrm{dB}$, $\mathrm{SLL}_1 = -22\,\mathrm{dB}$ and $\mathrm{SLL}_2 = -27\,\mathrm{dB}$. The maximum harmonic peak is $-25\,\mathrm{dB}$, with $P_0 = 22.34\,\%$, $P_{|1|} = 41.42\,\%$, and $P_{|2|} = 35.15\,\%$, yielding $\eta(L) = 98.91\,\%$, $E[\xi_n] = 0.88$, and $S[\xi_n] = 0.12$.

5.4.1 Beamforming Design for Time-Varying Scenarios

Let us consider a linear array with $N = 20$ antennas and an inter-element separation $d = \lambda/2$. The antenna excitations I_n are chosen to synthesize a Dolph-Chebyshev (DC) pattern with an $\mathrm{SLL} = -30$ dB. The beamforming design is organized in three steps:

- **Selection of** ξ_n. Since $I_{n0}^{\mathrm{TMA}} = I_n \xi_n$ (see Eq. (5.22)), the elements of the array are time-modulated by the periodical pulses in Eq. (5.20) to improve the SLL of the fundamental mode [KUMMER 1963]. We seek for an additional improvement of the SLL that, thanks to the SWC pulses, will be translated to all the harmonic patterns. In this example, a set of $\xi_n \in [0.59, 1]$, with a mean value $E[\xi_n] = 0.88$ and a standard deviation $S[\xi_n] = 0.12$, allows for an initial 5 dB SLL improvement of the working patterns, i.e., I_{n0}^{TMA} corresponds to the excitations of a DC pattern with $\mathrm{SLL} = -35\,\mathrm{dB}$.
- **Initial** a_{nk}. In this example the first and the second order harmonics are exploited, and hence $K = 2$ is considered together with 3-term SWC pulses. As a first approach, and according to Eq. (5.25), we take the following weights for such pulses and for all n: $a_{n1} = a_{n2} = 2a_{n0} = 2/5$. Fig. 5.5 illustrates the beamforming results for the fundamental mode and the first four harmonics[4]. Recall that we have the possibility of pointing the

[4]As $g_n^{T_0}(t)$ is a real-valued signal, its Fourier coefficients verify $G_{nq} = G_{n(-q)}^*$, and it is easy to prove (see Eq. (5.1)) that $|F_q^{\mathrm{TMA}}(\theta, t)|^2 = |F_{-q}^{\mathrm{TMA}}(180° - \theta, t)|^2$, synthesizing a couple of diagrams for q and $-q$, which are

maximum of each harmonic diagram independently through o_{nq}. In this case, we consider a scenario where $\theta_1 = 135°$ and $\theta_2 = 110°$.

It is apparent from Fig. 5.5 the excellent SLL behavior exhibited by all patterns. Nevertheless, although the power efficiency is high ($\eta(L) = 98.15\,\%$), the peak level of the third harmonic ($-15\,\text{dB}$) is too high and has to be improved.

- **Adjustment of** a_{nk}. As stated in Section 5.3, and by virtue of Eq. (5.23), the amplitude of each excitation of the radiation pattern of the q-th harmonic ($|I_{nq}^{\text{TMA}}|$) is proportional to the corresponding SWC pulse coefficient a_{nq}. In particular, $|I_{nK}^{\text{TMA}}|$, which governs the highest order harmonic pattern, is proportional to a_{nK}. Hence, by forcing a_{nK} to zero in the n-th SWC pulse (thus reducing its order to $K-1$), its shape will ensure a null contribution of the K-th harmonic and, additionally, a properly attenuated level of the $(K+1)$-th harmonic –due to the features of the SWC windowing function– once applied to the corresponding n-th element of the array. It is observed that by forcing a_{nK} to zero only in those pulses applied to the most distant elements of the center of the linear array, it is possible to reduce the peak level of the third harmonic to $-25\,\text{dB}$ (see Fig. 5.6). In this case, such a simple adjustment leads to $a_{n0} = 1/5$, $a_{n1} = 4/5$, and $a_{n2} = 0$ for the last three elements placed at both ends of the linear array. It is also observed that the adjustment slightly modifies the total power distribution among the different harmonics, transferring approximately $5\,\%$ of the power from the third ($|q| = 2$) to the other patterns ($|q| = 1$ and $q = 0$). The consequent improvement in the efficiency ($\eta(L) = 98.91\,\%$) is at the expense of a certain SLL degradation of the harmonic patterns: $\text{SLL}_1 = -22\,\text{dB}$, $\text{SLL}_2 = -27\,\text{dB}$, whereas such a parameter remains intact for the fundamental mode: $\text{SLL}_0 = -35\,\text{dB}$.

Once the patterns are synthesized, it is possible to dynamically exploit them in time-varying scenarios where adaptive beamforming is needed. The adaptive beamforming can be performed basically in terms of adaptive nulling because the harmonics are capable of pointing their maximums independently. The pattern nulling can be performed according to the method proposed in [POLI 2011a; ROCCA 2012b] but properly adapted to the ETMA. The method jointly optimizes the TMA parameters to synthesize a given pattern with predefined nulls.

In Fig. 5.7 we show the same pattern as the one in Fig. 5.6 but without plotting the harmonics with order $q = 3$ and $q = 4$ for the sake of clarity. Fig. 5.8 illustrates that it is possible to obtain mutual orthogonalization in a given radiation pattern by placing nulls at the angles corresponding to the maxima of the other diagrams, e.g. to exploit the TMA in a multipath communication. Notice that, for a given pattern, the directions of the corresponding maxima of the other ones are treated (in terms of nulling) as interference directions for this particular application, although we could have chosen any other spatial position for the nulls.

Because harmonic patterns with different order are independent between their phases (see Eq. (5.22)), in practice it is possible to introduce the nulls as in [POLI 2011a; ROCCA 2012b]

symmetric with respect to $\theta_0 = 90°$. For the sake of simplicity, we do not represent the "$-q$" harmonic versions.

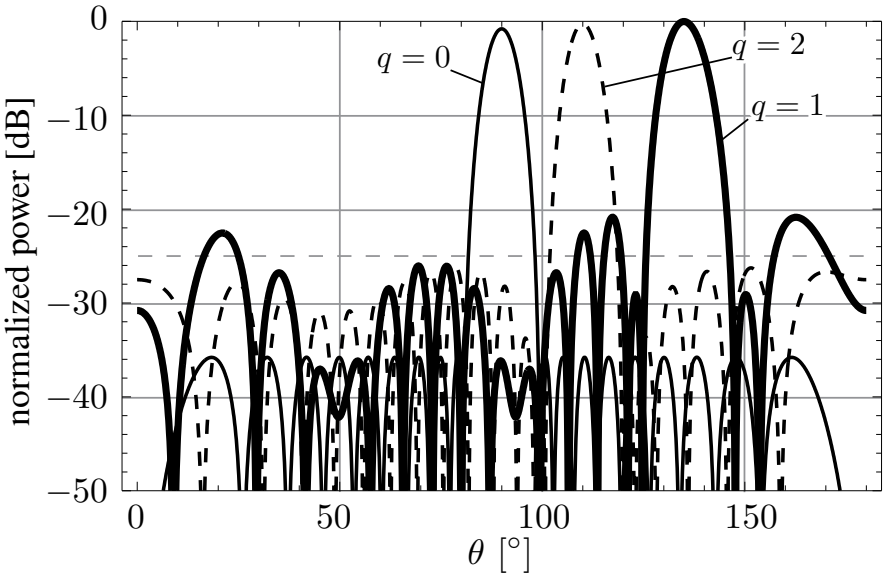

Figure 5.7: Radiation pattern shown in Fig. 5.6 but without plotting the harmonics with orders $q = 3$ and $q = 4$ for a major clarity of the previous situation before applying the adaptive nulling.

by changing only the phases of the excitations (in this case the average fluctuation of coefficients a_{nk} are below $1.77\,\%$). Therefore, when $d = \lambda/2$, as the excitation phases are not present in p_q Eq. (5.10) and, consequently, also not in Eq. (5.8), the nulling method does not impact on the power efficiency.

5.4.2 Power Efficiency of SWC and Rectangular Pulses

We have shown the high levels of power efficiency achieved by ETMAs based on SWC pulses. However, to complete the study, a comparison –in terms of power efficiency– between ETMAs based on SWC pulses and conventional TMAs based on rectangular pulses is included, provided that the same harmonic beamforming patterns are synthesized with both approaches.

The TMA power efficiency, when SWC pulses are used, is given by $\eta_{\mathrm{TMA}}^{\mathrm{SWC}} = \eta_{\mathrm{HW}} \cdot \eta(L)$, being η_{HW} the losses or the internal power dissipation in the hardware devices given in Table 5.2, and $\eta(L)$ the power efficiency, described in Section 5.2.1 and calculated by means of Eq. (5.8). For $d = \lambda/2$, we compute the total mean received power at the q-th harmonic when a carrier is received over the TMA, denoted as p_q, in Eq. (5.8) as it is done in [MANEIROCATOIRA 2014a, Eq. 42],

$$p_q = 4\pi \sum_{0}^{N-1} |I_n|^2 |G_{nq}|^2 = 4\pi \sum_{0}^{N-1} \left|I_{nq}^{\mathrm{TMA}}\right|^2, \tag{5.26}$$

with I_{nq}^{TMA} given in Eq. (5.22). We focus the study on the maximum efficiency of the TMA dictated by $\eta(L)$. The reason is that η_{HW} takes an arbitrary value depending on the specific properties of the hardware employed. Analogously, the analysis of the efficiency of a conventional TMA with switches is also addressed in terms of the power efficiency

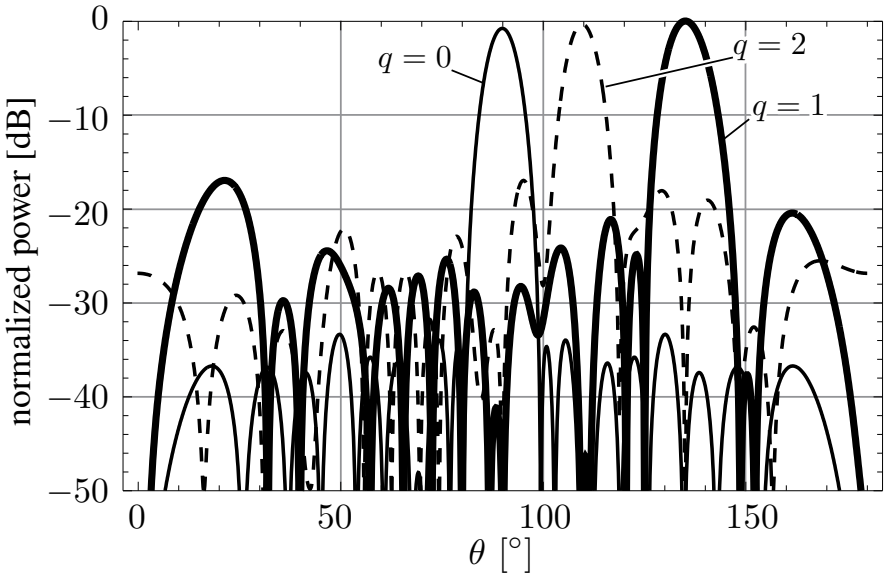

Figure 5.8: Radiation pattern shown in Fig. 5.7 after the application of the adaptive nulling algorithm given in [POLI 2011a; ROCCA 2012b].

$\eta(L)$ also due to the arbitrary switching network efficiency, which depends on the specific structure chosen, and may be based on single-pole single-throw (SPST) or single-pole multiple-throw (SPMT) switches or even on a Reconfigurable Power Divider/Combiner (RPDC) [CHEN 2016b].

From now on we consider three examples of harmonic beamforming pattern synthesis that can be found in the recent literature. Particularly, such patterns have been synthesized through TMAs with rectangular pulses [ROCCA 2014, Figs. 6, 10, and 11]. Our aim is twofold. Firstly, we synthesize the patterns through ETMAs based on SWC pulses, satisfying the same requirements in terms of DOAs, relative levels of maxima, and SLL. Secondly, the power efficiency exhibited by ETMAs based on SWC pulses is compared to that offered by the TMAs with rectangular pulses.

- **Example 1: ETMA versus optimized[5] TMA with two beams.** The TMA synthesized in [ROCCA 2014, Fig. 6] performs harmonic beamforming by exploiting the fundamental and the first order harmonics ($L = 1$), whereas its pulse sequences are the result of a PSO optimization procedure –in terms of the radiation diagram shape– which is specifically defined in [ROCCA 2014, Section II-2]. The multiobjective fitness function for such a PSO contemplates the SLL of the diagrams, the "equalization among the pattern maxima," and the mutual orthogonalization between patterns. In other words, the location of nulls of one pattern right in the direction of the maxima of the others[6].

[5]In this case the optimization is referred to the shape of the radiation diagram, without taking the power efficiency of the array into account.

[6]Notice that the efficiency of an ETMA, with $d = \lambda/2$, does not change when applied to the adaptive nulling algorithm presented in [POLI 2011a; ROCCA 2012b]. As explained at the end of Section 5.4.1, such an algorithm particularized for ETMAs is focused on the optimization of the independent (advantage of ETMAs with respect to

In the scenario considered, the maxima of the fundamental and first harmonic patterns, pointing to the corresponding DOAs, are respectively pointed towards the directions $\theta_0 = 90^\circ$ and $\theta_1 = 61^\circ$. In this example, a handicap for the time-modulation technique is the presence of uniform static excitations (which lacks of amplifiers and phase shifters) with $|I_n| = 1$ and zero-phase. Hence, the transformation of a simple static uniform pattern (with a modest $-13\,$dB SLL pattern) into the one shown in [ROCCA 2014, Fig. 6(b)] is done, exclusively, by applying the time-modulation with rectangular pulses (whose features –see [ROCCA 2014, Fig. 6(a)]– are the result of the PSO). The mean and the variance of the set of ξ_n necessary for this synthesis are equal to $E[\xi_n] = 0.1344$ (relatively close to 0) and $S[\xi_n] = 0.0074$, respectively. By substituting ξ_n into Eq. (5.10), we can compute p_q as well as the power efficiency by means of Eq. (5.8), arriving at $\eta(L) = 51.36\,\%$.

Now, and for comparison purposes, we synthesize a pattern with the same characteristics as in [ROCCA 2014, Fig. 6] by employing an ETMA. Firstly, we must obtain, through the application of time modulation, a pencil beam pattern in the fundamental frequency – which will be replicated in the first harmonic frequency– with an SLL about $-22\,$dB. We have chosen a DC pattern with an SLL of $-23\,$dB (other alternatives for pencil beam patterns are also valid, e.g., a normalized Gaussian pattern with a standard deviation of $2/3$). The set of ξ_n that synthesizes such a DC pattern has the following statistic properties: $E[\xi_n] = 0.7540$ (relatively closed to 1) and $S[\xi_n] = 0.0380$. According to the procedure described in Section 5.4.1 to exploit $L = 1$ harmonic beams, we use $N = 20$ identical SWC pulses with order $K = L = 1$ and, as indicated in Eq. (5.25), $a_{n1} = 2a_{n0} = 1/3$.

Fig. 5.9 illustrates the radiation pattern of this ETMA with the same characteristics as the one in [ROCCA 2014, Fig. 6]. The power efficiency, calculated by means of Eq. (5.26) and Eq. (5.8), is now $\eta(L) = 95.41\,\%$, which significantly improves the efficiency achieved with rectangular pulses ($\eta(L) = 51.36\,\%$). Notice that there is still room for a heuristic optimization of the power efficiency adjusting the appropriate trade-off between the SLL of the DC pattern (modifying ξ_n) and certain slight variations of a_{nk}, as shown in Section 5.4.1.

- **Example 2: ETMA versus non-optimized TMA with three beams.** The TMA synthesized in [ROCCA 2014, Fig. 10] exploits the fundamental, the first, and the second order harmonics ($L = 2$) in a scenario where the maxima of the fundamental, the first, and the second harmonic patterns point to the corresponding DOAs, which are respectively pointed towards the directions $\theta_0 = 90^\circ$, $\theta_1 = 116^\circ$, and $\theta_2 = 150^\circ$.

conventional TMAs) excitation phases of the harmonic patterns. Due to the fact that such phases are not included in the efficiency (see Eq. (5.8) whenever $d = \lambda/2$ (case of the three examples below), the nulling method has no impact on the efficiency. As the aim of this section consists in showing the efficiency of ETMAs, it is not necessary to locate the nulls at the end of the synthesis, like it was properly done in the example in Section 5.4.1.

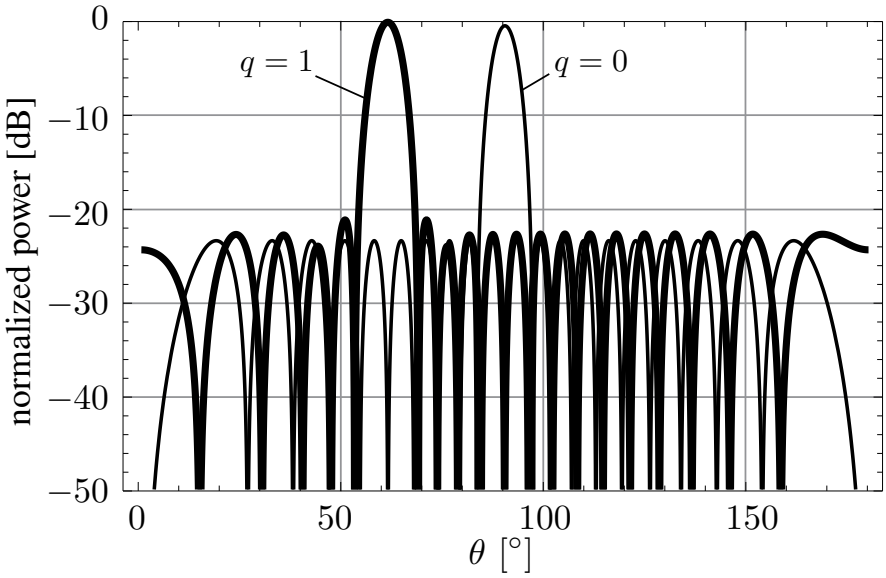

Figure 5.9: Radiation pattern of an ETMA synthesized by applying identical 2-term SWC pulses with $a_{n0} = 2/3$, $a_{n1} = 2$ and normalized time durations ξ_n capable of synthesizing a DC pencil beam pattern with $\mathrm{SLL} = -23\,\mathrm{dB}$. Such a pattern is equivalent to the one in [ROCCA 2014, Fig. 6], synthesized with rectangular pulses and optimized by means of PSO. The power efficiency of the TMA is $\eta(L) = 51.36\,\%$, whereas that of the ETMA (even without optimization) improves noticeably up to $\eta(L) = 95.41\,\%$, yielding a relative improvement of $85.77\,\%$.

The corresponding pulse sequences have a fixed duration $\xi_n = 0.25$ and the switch-on time-instants are sequentially chosen as shown in [ROCCA 2014, Fig. 10(b)]. The power efficiency, calculated analogously to the previous example for rectangular pulses, is $\eta(L) = 85.79\,\%$.

It is observed in [ROCCA 2014, Fig. 10] that the fundamental pattern corresponds to a uniform distribution (with an $\mathrm{SLL} = -13\,\mathrm{dB}$), and the harmonic patterns are attenuated replicas of such a pattern. Hence, it is possible to synthesize this pattern through an SWC-based infrastructure by simply choosing $\xi_n = 1$ and varying exclusively o_{nq}. In this sense, it is remarkable that when the beams correspond to uniform patterns, the synthesis can be carried out by using a degenerated mode of the ETMA, i.e., a mode of operation in which the time modulation is performed exclusively through the time shifts defined in Eq. (5.19) and fixing $\xi_n = 1$. Under this circumstances, the relationship given in Eq. (5.23) is perfectly satisfied, with B_{nq}^2 the level of the maximum of the q-th harmonic radiation pattern, whenever the N pulses are identical.

We use $N = 20$ identical SWC pulses with order $K = L = 2$, and therefore, the coefficients a_{nk} can be calculated by considering the attenuations –expressed in decibels– of the maximum of each harmonic pattern with respect to the maximum of the fundamental pattern [ROCCA 2014, Fig. 10] ($-1\,\mathrm{dB}$ and $-4\,\mathrm{dB}$, respectively)

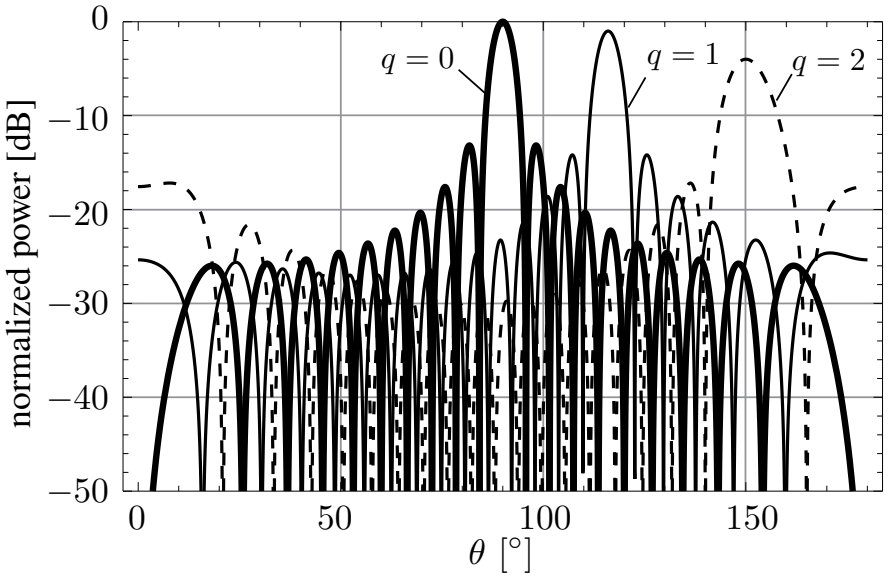

Figure 5.10: Radiation pattern of an ETMA synthesized by applying identical 3-term SWC pulses with $a_{n0} = 0.2473$, $a_{n1} = 0.4407$, $a_{n2} = 0.3120$, and normalized time durations $\xi_n = 1$, hence the ETMA works under a degenerated mode where only the time shifts take part in the technique. The pattern of the figure is equivalent to the one in [ROCCA 2014, Fig. 10], synthesized with rectangular pulses and showing an efficiency $\eta(L) = 85.79\,\%$. The ETMA, operating under this degenerated mode, exhibits its theoretical maximum efficiency, i.e., $\eta(L) = 100.00\,\%$, yielding a relative improvement of $16.56\,\%$.

by using the immediate equations: $20\log(B_{n1}/B_{n0}) = 20\log(a_{n1}/2a_{n0}) = -1$, $20\log(B_{n2}/B_{n0}) = 20\log(a_{n2}/2a_{n0}) = -4$, and the normalization condition in Eq. (5.14). Once solved this simple system of equations we obtain $a_{n0} = 0.2473$, $a_{n1} = 0.4407$, and $a_{n2} = 0.3120$. The theoretical power efficiency in an ETMA operating under the degenerated mode is $\eta(L) = 100.00\,\%$ because Eq. (5.23) is fully satisfied and the harmonic levels are zero for $|q| > K$. This fact can be proved by calculating the efficiency by means of Eq. (5.26) and Eq. (5.8).

Fig. 5.10 illustrates the radiation pattern of this ETMA with the same characteristics as that in [ROCCA 2014, Fig. 10].

- **Example 3: ETMA versus optimized TMA with three beams.** The TMA synthesized in [ROCCA 2014, Fig. 11] performs harmonic beamforming by exploiting the fundamental, the first, and the second order harmonics ($L = 2$), being the rectangular pulse sequences the result of the same PSO optimization procedure as in the first example. The DOAs scenario is the same as the one in the second example: $\theta_0 = 90°$, $\theta_1 = 116°$, and $\theta_2 = 150°$. The features of the pulse sequences applied to the static uniform excitations in order to obtain the diagram in [ROCCA 2014, Fig. 11(a)] are shown in [ROCCA 2014, Fig. 11(c)] and they are the result of the PSO. The mean and the variance of the set of ξ_n necessary for this synthesis are $E[\xi_n] = 0.0996$ (very close to 0) and

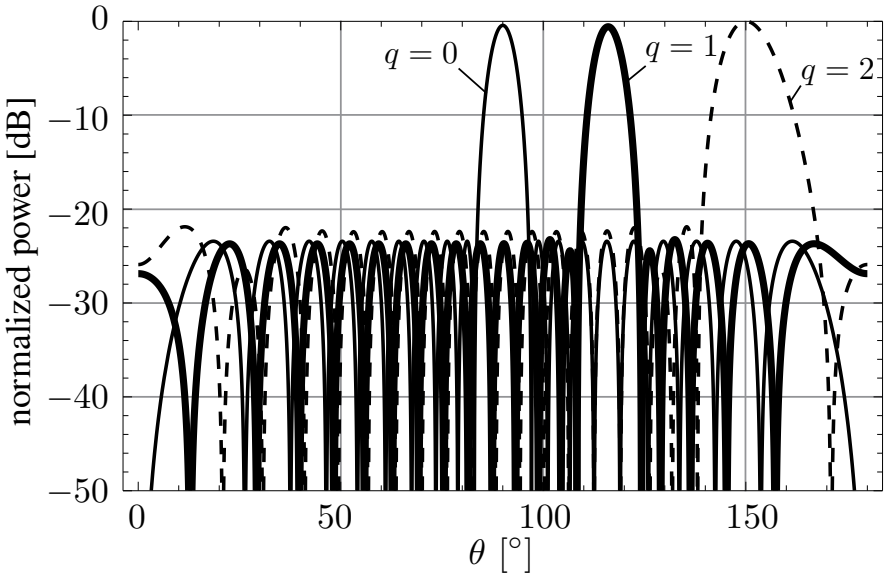

Figure 5.11: Radiation pattern of an ETMA synthesized by applying identical 3-term SWC pulses with $a_{n2} = a_{n1} = 2a_{n0} = 1/5$ and normalized time durations ξ_n capable of synthesizing a DC pencil beam pattern with $\mathrm{SLL} = -23\,\mathrm{dB}$. Such a pattern is equivalent to the one in [ROCCA 2014, Fig. 11], synthesized with rectangular pulses and optimized by means of the PSO. The power efficiency of the TMA is $\eta(L) = 50.41\,\%$, whereas that of the ETMA (even without optimization) improves noticeably up to $\eta(L) = 97.16\,\%$, yielding a relative improvement of $92.74\,\%$.

$S[\xi_n] = 0.0013$, respectively. Following the same procedure as in previous examples to calculate the power efficiency we arrive at $\eta(L) = 50.41\,\%$.

An ETMA with the same pattern characteristics as in [ROCCA 2014, Fig. 11(a)] can be synthesized by means of time-modulation with SWC pulses. The first step in the design consists in obtaining a pencil beam pattern in the fundamental frequency –which will be replicated or quasi-replicated in the first and in the second harmonic frequencies– with an SLL closed to $-22\,\mathrm{dB}$ as in the first example. We have also chosen a DC pattern with $\mathrm{SLL} = -23\,\mathrm{dB}$. Therefore, the set of ξ_n that synthesizes such a DC pattern are the same as those considered in the first example. To exploit $L = 2$ harmonic beams we employ $N = 20$ identical SWC pulses with order $K = L = 2$ and, as indicated in Eq. (5.25), $a_{n2} = a_{n1} = 2a_{n0} = 1/5$. Fig. 5.11 illustrates the radiation pattern of this ETMA with the same characteristics as the one in [ROCCA 2014, Fig. 11] regardless of the location of the nulls, which, as it was properly explained, does not impact on the power efficiency in this example. The power efficiency, calculated as in previous examples, is now $\eta(L) = 97.16\,\%$ which, again, significantly improves the efficiency achieved by means of rectangular pulses ($\eta(L) = 50.41\,\%$).

5.5 Conclusions

We have proposed a novel family of TMAs, termed enhanced TMAs (ETMAs), whose excitations are time modulated by SWC pulses rather than by rectangular pulses corresponding to the on-off switches of conventional TMAs. We have presented the relationship between the harmonic radiation patterns and the SWC pulse parameters, as well as the TMA synthesis method. We have discussed some possible hardware structures for the implementation of ETMAs which have been properly compared to both conventional TMAs and LBFNs. We have shown that time modulation with periodic SWC pulses provides a larger flexibility to control the harmonic radiation patterns and, consequently, improves both the TMA power efficiency and the SNR at the receiver when compared to conventional TMAs based on rectangular pulses.

Chapter 6

Conclusions and Future Work

6.1 Conclusions

The conclusions of this thesis are organized according to the corresponding possible modes of exploitation of the time-modulated arrays (TMAs).

Exploitation Concerning TMA Fundamental Pattern

- The constraints that allow for overriding the possible impact on the information content caused by TMAs when used for transmission of linearly modulated digital signals have been identified.
- Under those conditions, and together with the assumption of a fast decaying rate of the harmonics level as a function of their order, a generalized TMA power response has been accurately derived and simplified, with a final expression comprising the product of its power transfer function and the equivalent baseband signal power. The TMA power transfer function is defined as its canonical response, is inherent to both the antenna geometry and the time modulation parameters, and coincides with the TMA radiated power when a single carrier at its center-frequency is transmitted.
- Both time- and frequency-domain analyses have been carried out in order to quantify the power-radiated efficiency of the TMA when it is combined with digital linear modulation schemes.
- The BER of a linearly modulated digital communication system that incorporates a receive-TMA (synthesizing a pencil beam radiation pattern) has been theoretically characterized. The subsequent analysis using the derived forms shows the benefits provided by the TMA technique, namely the reconfigurability of the power pattern, while achieving ultra-low levels of SLL with a simplified feeding network, and obtained with a minimal impact on the BER.

Exploitation Concerning TMA Harmonic Patterns

- A wireless communication receiver has been modeled and analyzed. Such a model consists of a TMA performing nonlinear beamforming, followed by a maximum ratio combining (MRC) subsystem devoted to extract channel diversity in the form of angular diversity captured by the sideband radiation (SR) exhibited by the TMA.
- Closed-form expressions for the symbol error ratio (SER) with respect to the signal-to-noise ratio (SNR) when linear digital modulation (LDM) signals are transmitted over a Rayleigh-fading channel exhibiting channel diversity have been derived. Therefore and remarkably, the SER of the previous TMA-receiver can now be expressed directly in terms of the main parameters of the TMA itself, providing a fundamental analytical tool for the designer.
- A new optimization algorithm to synthesize the radiation pattern conditioned to a specific architecture that allows for maximizing the total TMA efficiency has been implemented. This turned out to be a pioneer work by optimizing a TMA in terms of its total efficiency.
- As a reference, it was compared the performance of this TMA-based receiver to that exhibited by a receiver equipped with a single linear beamformer (LB) (thus not exploiting channel diversity) and to that offered by a receiver based on a linear beamforming network (LBFN) (also equipped with an MRC). Some numerical simulations results have revealed that the TMA-based receiver exhibits, under certain conditions, an excellent trade-off between hardware and software complexity with respect to the performance obtained.
- There is still room for improving the beamforming performance (due to the correspondence between the number of harmonics exploited and the TMA efficiency) by exploring more appropriate shapes for the basic pulses (other than rectangular ones).
- It has been proposed and analyzed a novel family of TMAs –termed enhanced time-modulated arrays (ETMAs)– whose excitations are time modulated by sum-of-weighted-cosine (SWC) pulses rather than by those ones provided by on-off switches found in conventional TMAs.
- A method of synthesis of such ETMAs for harmonic beamforming has been developed. The simplicity of the method with respect to existing optimization methods for conventional TMAs is truly remarkable.
- Some possible hardware structures for the implementation of ETMAs have been studied and properly compared to those of both conventional TMAs and LBFNs.
- It has been shown that time modulation with periodic SWC pulses provides, when compared to conventional rectangular pulses, a larger flexibility to control the harmonic radiation patterns and, consequently, improves both the TMA power efficiency and the SNR at the receiver.

6.2 Future Work

The interplay between TMAs and digital communications still faces a number of challenges which are seen as future research lines. Among them, we highlight the following ones:

- The exploitation of TMAs at transmission. Up to now, the applications of TMAs in the area of digital communications has mainly focused on receiving TMAs. Hence, the performance of transmitting TMAs from a signal processing point of view, and in different scenarios, is still an unexplored research field. We propose two areas which certainly deserve further inspection: 1) the performance analysis of transmitting TMAs in multiuser scenarios, and 2) the feasibility of diversity transmission techniques with TMAs.
- The system performance with broadband signals. The current TMA literature exclusively focuses on narrowband signals. However, communications nowadays must unavoidably deal with broadband signals. The higher the bandwidth, the higher the switching frequency in the TMA, the wider the bandwidth at the radio frequency (RF) stage, and the higher the sampling rate at the analog-to-digital converters (ADCs). On the other hand, an analysis of the TMA behavior under frequency-selective fading still also remains unexplored.
- The beamforming design through the preprocessing of periodic pulses. More specifically, we propose a more accurate design of the periodic pulses in the frequency domain. The Fourier transform of a periodic pulse is a discrete spectrum with impulses at multiples of the time-modulation frequency and whose corresponding areas are 2π times the associated exponential Fourier series coefficients. Therefore, a simpler design by applying the Fourier series coefficients properties to preprocess conventional rectangular pulses before they are applied to the antenna elements could be possible.

Appendix A

Resumo da Tese

A.1 Introdución

A demanda continua de servizos móbiles cun grao crecente de capacidade robustez e mobilidade fan das comunicacións sen fíos o sector de máis rápida expansión hoxe en día dentro da industria das telecomunicacións. Como consecuencia, os cada vez máis limitados recursos radio han de ser explotados dun xeito intelixente e as antenas están chamadas a xogar un papel crucial. Neste sentido, as antenas intelixentes deben ser capaces de sentir e interpretar a súa contorna electromagnética e ter a habilidade de reconfigurar as súas características de radiación de tal xeito que se garanta, non só a calidade de servizo, senón a eficiencia enerxética do sistema ao cal pertence. Para lograr estes obxectivos, é preciso abordar o deseño dos sistemas radiantes con arranxo ao seguinte binomio:

- Múltiples disciplinas. Conxugando o deseño específico ou convencional de antenas con outras áreas do coñecemento como son o procesado do sinal, as comunicación dixitais, a propagación de ondas ou a enxeñaría de radio frecuencia (RF).
- Sustentable. Posibilitando novas tecnoloxías que permitan reducir o consumo enerxético e os custos asociados á implantación destes sistemas.

Os estándares de comunicación sen fíos actuais consideran técnicas de múltiples antenas [RENZO 2014; HEATH 2016; MÉNDEZRIAL 2016] para explotar a diversidade espacial, o multiplexado espacial e o conformado de feixe (máis coñecido polo termo en inglés *beamforming*) para acadar uns mellores niveis de fiabilidade e capacidade. Con todo, estas vantaxes son obtidas a expensas dun incremento da complexidade dos sistemas, que podería non ser asumible, e do tamaño axeitado dos dispositivos para satisfacer a demanda de mobilidade actual.

O concepto de agrupación de antenas moduladas temporalmente, máis coñecido pola súa sigla en inglés TMA (*time-modulated array*), é unha técnica multiantena que aporta notables vantaxes a nivel de simplificación do hardware.

A.2 Que é unha TMA?

Unha TMA é unha agrupación de antenas cuxo diagrama de radiación contrólase a través da modulación individual das súas excitacións mediante pulsos periódicos de duración variable. Na súa configuración máis simple, unha TMA baséase no acendido e apagado dos seus elementos radiantes empregando pulsos periódicos rectangulares implantados mediante interruptores de RF. Deste xeito, a rede de excitacións da agrupación gaña sensiblemente en simplicidade pois, en lugar de desprazadores de fase e amplificadores (caso das agrupacións convencionais), emprega interruptores.

A natureza non lineal desta operación orixina a aparición de diagramas de radiación nas frecuencias harmónicas $f_c + qf_0$, referidos na literatura como radiación de banda lateral (RBL), onde f_c é a frecuencia central ou de portadora e f_0 a frecuencia dos pulsos periódicos da modulación temporal ($q \in \mathbb{Z}$). Mediante esta técnica é posible modificar a magnitude (non así a fase) das excitacións correspondentes ó modo fundamental ($q = 0$) mediante a variación das duracións dos pulsos periódicos (τ_n) aplicados ós elementos da agrupación. Por outra banda, as excitacións correspondentes ós diagramas de harmónicos ($q \neq 0$), pódense modificar tanto en amplitude (variando τ_n) como en fase (variando os τ_n dos pulsos e/ou os instantes de acendido dos mesmos δ_n). Polo tanto, a RBL ou ben pode ser minimizada centrando o deseño no modo fundamental ou ben pode ser explotada de xeito beneficioso tal e como se explica seguidamente.

Características das TMAs

Os parámetros temporais que gobernan unha TMA (as duración dos pulsos τ_n e os instantes de acendido dos mesmos o_n) pódense optimizar para:

1. Explotar soamente o diagrama fundamental –na frecuencia de portadora f_c– co obxectivo de obter niveis de lóbulo lateral ultra-baixos á vez que se minimiza a RBL.
2. Explotar os diagramas de harmónicos, dotando á TMA de capacidades de gran utilidade e interese na contorna das antenas intelixentes.

Polo tanto, e de acordo co segundo punto, as TMAs van ser capaces de levar a cabo conformado de feixe (*beamforming*) adaptable, acomodando os diagramas de harmónicos á canle radio, combinando as súas correspondentes saídas e coa vantaxe de precisar unha única cadea de RF. Neste senso, o feito de prescindir de tantas cadeas de RF como compoñentes multitraxecto a explotar ofrece as seguintes vantaxes:

- Simplicidade hardware, co consecuente impacto no tamaño e custo do sistema.
- Consumo, tal e como se reflicte e cuantifica en publicacións recentes nas que ademais propóñense arquitecturas híbridas analóxico-dixitais para conformado de feixe. De feito, nunha implantación completamente dixital dunha rede de conformado de feixe lineal, o número de cadeas de RF precisas, L, debe ser igual ó número de antenas ou elementos da agrupación N. Na práctica, e con todo, é preferible unha relación $N \gg L$ por unha serie de razóns, sendo o consumo por cadea de RF un dos máis importantes.

- A inexistencia de inconvenientes relacionados coa sincronización, a coherencia de fase ou o acople entre diferentes cadeas de RF.

En resumo, a aplicación de pulsos periódicos ó nivel da antena ten o efecto de converter a diversidade espacial en diversidade en frecuencia, sendo suficiente unha soa cadea de RF para explotar a dita diversidade espacial.

A.3 Resumo do estado da arte

A.3.1 Orixe do concepto TMA

A idea pioneira de empregar a variable tempo coma un grao de liberdade adicional para controlar o diagrama de radiación dunha antena foi proposta por Shanks e Bickmore do Laboratorio de Microondas da Compañía Hughes Aircraft, California, en 1959 [SHANKS 1959]. Os autores introduciron teoricamente esta nova idea no deseño de antenas, e suxeriron varias posibilidades para a súa implantación física, como por exemplo, unha agrupación lineal cuxas excitacións eran moduladas por pulsos cadrados implantados con interruptores de ferrita. Con todo, os seus primeiros experimentos baseáronse nunha antena convencional de disco parabólico coa particularidade de que aplicaron á bucina primaria un movemento circular uniforme cunha frecuencia de 133 Hz. O resultado do experimento foi un comportamento multidiagrama da antena, obtendo, simultaneamente, un diagrama suma na frecuencia fundamental e un diagrama diferenza no harmónico de primeira orde.

En 1963, Kummer et al. –tamén da Hughes Aircraft– estenderon o concepto de "antena modulada temporalmente" ás agrupacións de antenas [KUMMER 1963], acuñando propiamente o termo TMA. Nos seus experimentos obtiveron diagramas con niveis de lóbulo lateral ultra-baixos mediante a inserción de interruptores de RF –programados con arranxo a unha secuencia temporal periódica predeterminada– na rede de excitacións dunha agrupación lineal de guía-onda con rañuras composta por 8 elementos e que traballaba na banda X. Kummer et al. constataron que canto maiores eran as melloras no nivel de lóbulo lateral ó aplicar modulación temporal, maiores eran tamén os custos na ganancia da antena. Polo tanto, é este traballo o que abre as portas a futuras investigacións que se enfocarán en minimizar a RBL á vez que melloran o nivel de lóbulo lateral a través da aplicación da técnica TMA.

A.3.2 Deseño de TMAs baixo a perspectiva (exclusiva) de antenas

A maioría dos traballos de investigación en TMAs desenvólvense baixo o punto de vista do deseñador de antenas. Máis concretamente, están centrados na síntese de diagramas de radiación coa forma axeitada. Neste resumo do estado da arte clasificaremos estes traballos segundo o tipo de diagrama sintetizado, é dicir, fundamental ou harmónicos.

Modo Fundamental

Malia que o desenvolvemento de métodos para minimizar a RBL representaba unha liña de investigación natural e inmediata, houbo que agardar ata comezos dos anos 2000 para que emerxeran os primeiros algoritmos de optimización [YANG 2002]. A razón foi que o deseño de sofisticados métodos necesarios para levar a cabo este tipo de optimización estaba intimamente vinculado ó desenvolvemento de ordenadores máis potentes. Xorde a partir desta situación unha eclosión de algoritmos sistemáticos capaces de optimizar o nivel de lóbulo lateral, a RBL, e incluso outras figuras de mérito simultaneamente [YANG 2005a; FONDEVILA 2004; FONDEVILA 2006; POLI 2010a; MANDAL 2011; MANDAL 2013]. Ademais destas solucións software, investigáronse solucións hardware para minimizar a RBL, baseadas en técnicas de subagrupacións [TONG 2011], o uso de elementos de ancho de banda fixo [TONG 2012b], ou no impacto das formas dos pulsos [BEKELE 2013].

En paralelo, outras investigacións introducían un novo grao de liberdade no proceso de síntese: os instantes de acendido –adicionalmente á duración– dos pulsos periódicos rectangulares aplicados ás excitacións da antena [TENNANT 2008; POLI 2010b; AKSOY 2012].

Por outra banda, aparte das configuracións xeométricas lineais, analizáronse e optimizáronse múltiples configuracións planas de TMAs [YANG 2005a; POLI 2010b; AKSOY 2014; TENNANT 2009].

A caracterización da ganancia e a eficiencia dunha TMA foi tamén un paso chave na investigación desta tecnoloxía. En particular, a identificación de dous tipos de eficiencia:

1. A eficiencia da rede de interruptores, que dá conta da fracción de tempo que os interruptores están apagados e, polo tanto, absorbendo ou disipando enerxía de xeito ineficaz. Así en [ZHU 2012b] danse solucións para mellorar esta eficiencia mediante o uso de interruptores de polo simple e dúas vías.
2. A eficiencia en potencia, que é a razón entre a potencia media radiada no modo fundamental (ou potencia útil) e a potencia media total radiada. A eficiencia total da TMA é o produto de ambas eficiencias [YANG 2004].

As TMAs foron tamén analizadas –exclusivamente dende o punto de vista das propiedades de radiación– para ser explotados en diferentes aplicacións, como por exemplo na supresión de interferencias e sinais non desexados incidentes na apertura da antena. Neste sentido, [POLI 2011a; ROCCA 2012b] estudaron a capacidade de síntese adaptativa de ceros ou nulos do diagrama de radiación das TMAs en escenarios variables no tempo. Outros exemplos son a aplicación de TMAs para a síntese dos denominados diagramas de potencia para amplas zonas de cobertura [YANG 2003; BALDERAS 2016] ou para aplicacións radar [LI 2009b; EUZIÈRE 2014].

Aparte de todas estas aplicacións, outras liñas de investigación céntranse no desenvolvemento de ferramentas de simulación para a análise rigorosa das non linearidades das TMAs como sistemas radiantes [MASOTTI 2013], ou do emprego de ferramentas existentes de

simulación de antenas a altas frecuencias para analizar o comportamento instantáneo e medio dunha TMA [YAO 2015a].

Diagramas de harmónicos

Como xa se comentou en liñas anteriores, a RBL non é necesariamente un fenómeno negativo, senón que pode ser explotado para mellorar as prestacións dunha TMA, dotándoa de capacidades propias das antenas intelixentes. Neste sentido, o primeiro traballo que introduce teoricamente a capacidade de escaneo de feixe (*beam-scanning*) dunha TMA débese a Shanks [SHANKS 1961], propiciando a aparición de posteriores investigacións con prototipos experimentais, como por exemplo [BOGDAN 2016b].

Por outra banda, a primeira análise de conformado de feixe adaptativo empregando os diagramas de harmónicos foi de carácter experimental, nun escenario de interferencia simplificado e considerando exclusivamente os harmónicos de primeira orde [LI 2010a]. Traballos posteriores amplían o escenario de interferencias e céntranse na síntese dos diagramas de radiación empregando diferentes técnicas ou estratexias [POLI 2011b; TONG 2012a; POLI 2014]. O direccionamento de feixe (*beam steering*) tamén é posible con TMAs [LI 2009a; TONG 2010], así como as súas aplicacións, destacando a procura e a estimación das direccións de chegada de sinais incidentes á agrupación (técnica máis coñecida pola súa sigla en inglés DOA, de *direction of arrival*) [LI 2010b; TENNANT 2010; HE 2015a].

As agrupacións reflectoras de antenas foron consideradas tamén para ser desenvolvidas empregando modulación temporal [WANG 2012; WANG 2014]. Unha agrupación reflectora de antenas moduladas temporalmente consiste nunha matriz de elementos dispersores que son iluminados ou alimentados a través dunha bucina, pero, en lugar de aplicarlles desprazadores de fase, emprégase a modulación temporal a través de interruptores, acadando a devandita agrupación funcións de direccionamento ou conformado de feixe.

Outro campo interesante de aplicación das TMAs é a transmisión de potencia sen fíos [MASOTTI 2016]. Neste caso, as características de conformado de feixe en tempo real das TMAs aprovéitanse seguindo un procedemento que consta de dous pasos: primeiro localízase o dispositivo a ser alimentado e, seguidamente, lévase a cabo unha transmisión directiva de potencia.

En investigacións recentes a filosofía TMA involúcrase en solucións híbridas máis complexas, contribuíndo á mellora das prestacións de todo o sistema de antenas. Exemplos nesta dirección son a aplicación de modulación temporal –en combinación coa modulación I/Q– a agrupacións en fase (*phased arrays*) de cara a xerar un escaneado de feixe exclusivamente nos harmónicos de orde positiva [YAO 2015b]. Tamén se considerou a modulación temporal, xunto con técnicas retrodirectivas, para sintetizar agrupacións de antenas de coapertura [YAO 2016b], e para obter diagramas de feixes invariantes no tempo e con gran resolución no espazo en agrupacións diversas en frecuencia [YAO 2016a].

A.3.3 Deseño de TMAs segundo a perspectiva do procesado do sinal

Tal e como se constata nas investigacións referidas anteriormente, na maioría dos traballos o diagrama fundamental e/ou os correspondentes harmónicos son manipulados de tal xeito que non se considera a interacción entre a técnica TMA e a natureza dos sinais enviados ou recibidos.

Así, e como punto de partida, é preciso atopar as restricións en frecuencia dos sinais. Especificamente, a relación entre a frecuencia da modulación temporal, o ancho de banda do sinal e a frecuencia de portadora que se debe satisfacer de cara a preservar a integridade dos sinais enviados/recibidos pola TMA. Estas restricións foron especificadas por Shanks e Bickmore [SHANKS 1959], e completadas por Brégains et al. [BRÉGAINS 2008], onde se derivan as fórmulas pechadas para a RBL e a eficiencia en potencia dunha TMA.

A transmisión de sinais de banda estreita moduladas en amplitude (AM) ou en frecuencia (FM) foi analizada teoricamente [LI 2009c] e, para o caso AM, tamén experimentalmente [ZHU 2013]. Outros casos específicos son o deseño dun receptor AM de canle dual [YAVUZ 2015], a transmisión de sinais moduladas linealmente en frecuencia [GUO 2015], ou a posibilidade de implantar funcións duais de radar e comunicacións [EUZIÈRE 2015; EUZIÈRE 2016].

As TMAs tamén se investigaron no contexto das comunicación seguras. Máis concretamente para transmitir sinais dependentes da dirección [ZHU 2014; ROCCA 2014; HANNAN 2016]. A idea baséase en xerar un nivel de RBL nulo nas direccións de interese e un alto nivel de RBL noutras direccións de cara a producir unha distorsión no sinal e polo tanto protexer a comunicación.

En [ZHU 2015] preséntase un primeiro estudo da relación sinal a ruído (máis coñecida pola súas sigla SNR, do inglés *signal-to-noise ratio*) nun sistema dotado dunha TMA en recepción que explota o modo fundamental e o primeiro harmónico positivo de cara a recibir dous sinais binarios modulados en fase (BPSK) considerando unha canle con ruído branco Gaussiano. As características multifeixe das TMAs foron tamén propostas para técnicas de multiplexación espacial [HE 2015c], aínda que as prestacións con sinais non foron analizadas. Traballos máis recentes céntranse no deseño hardware de TMAs aplicadas ó filtrado espacial de sinais [BOGDAN 2016a] e incluso á supresión de interferencias en comunicacións na banda de milimétricas [YASHCHYSHYN 2015].

A.4 Principais contribucións da tese de doutoramento

Esta tese de doutoramento é o resultado dunha investigación das TMAs dende un punto de vista que considera múltiples disciplinas, é dicir, non só dende unha perspectiva das posibilidades do seu diagrama de radiación, senón tamén dende a perspectiva do procesado do sinal, contemplando outras figuras de mérito como a eficiencia enerxética ou o nivel de

complexidade dos sistemas involucrados. Esta análise, cun carácter integral, xorde ó involucrar as TMAs no ámbito das comunicación dixitais. Neste sentido, ningunha das investigacións referidas no estado da arte fai un estudo en profundidade da interacción das TMAs con sinais de comunicacións dixitais.

A tese é unha análise teórico-matemática das aplicacións das TMAs en comunicacións dixitais e desenvólvese en catro etapas, cuxas contribucións poden sintetizarse en:

1. Análise matemática –nos dominios do tempo e da frecuencia– da posibilidade de transmitir sinais dixitais a través de TMAs, identificando as restricións para salvagardar a integridade do sinal e cuantificando a potencia radiada [MANEIROCATOIRA 2014a; MANEIROCATOIRA 2014b].
2. Caracterización da taxa de erro de bit dun sistema de comunicación dixital que incorpora unha TMA en recepción que explota o seu modo fundamental e considerando unha canle con ruído branco Gaussiano [MANEIROCATOIRA 2015a].
3. Estudo das prestacións dunha TMA –que explota os seus diagramas de harmónicos– para a recepción de sinais dixitais en canles con multitraxecto e esvaecemento [MANEIROCATOIRA 2017d; MANEIROCATOIRA 2015b].
4. Caracterización dun tipo de TMAs con mellores prestacións –ETMAs, sigla do termo en inglés *enhanced time-modulated arrays*– para o conformado de feixe (*beamforming*), empregando pulsos de suma de cosenos ponderados no lugar de pulsos rectangulares. Asemade, amósanse as vantaxes en termos de flexibilidade e eficiencia respecto ás TMAs convencionais [MANEIROCATOIRA 2017a; MANEIROCATOIRA 2016].

A.5 Principais conclusións

O emprego da variable tempo para controlar a forma do diagrama de radiación dunha agrupación de antenas presenta unha serie de atractivos, entre os que destaca a simplicidade de implantación da rede de excitacións do sistema radiante en comparación con outras solucións baseadas no control da amplitude e da fase con dispositivos convencionais (amplificadores e desprazadores de fase, respectivamente). A maioría dos traballos da literatura afondan na síntese de diagramas de radiación mediante a técnica de modulación temporal considerando a antena coma un ente illado. Esta tese afonda na interacción desta técnica coas comunicacións dixitais e, polo tanto, dando un enfoque integral e inclusivo ó deseño de TMAs. Así, os parámetros temporais da agrupación selecciónanse non só tendo en conta os requirimentos clásicos no deseño de antenas, senón que ademais xogan un papel chave nesta elección as figuras de mérito da comunicación dixital na que están involucradas.

Como punto de partida para o estudo desta interacción das TMAs cos sistemas de transmisión dixital considerase un escenario simple, no cal a TMA traballa no seu modo fundamental e transmite un sinal dixital modulado de xeito lineal, chegando ás seguintes conclusións:

- Identifícanse as restricións que permiten salvagardar a información contida nun sinal dixital modulado de xeito lineal e transmitido a través dunha TMA.
- Defínese a función de transferencia en potencia dunha TMA. Esta resposta en potencia da antena é función dos parámetros temporais da TMA e da súa xeometría.
- Cuantifícase a eficiencia en potencia da TMA nunha análise dual tanto no dominio do tempo coma no dominio da frecuencia.

Una vez demostrado que é factible, dende o punto de vista do procesado do sinal, a transmisión de sinais dixitais a través dunha TMA, procédese a analizar as prestacións do correspondente sistema dixital de comunicacións nun escenario simplificado, chegando ás seguintes conclusións:

- Caracterízase teoricamente a taxa de erro de bit dunha comunicación dixital con sinais moduladas de xeito lineal e que incorpora unha TMA en recepción, explotando o seu modo fundamental cun diagrama tipo pincel.
- As fórmulas pechadas que expresan a taxa de erro de bit permiten analizar e mostrar os beneficios da técnica TMA, é dicir, a reconfigurabilidade do diagrama de radiación namentres que se sintetizan niveis de lóbulo lateral ultra baixos, todo iso empregando unha rede de excitacións máis simple e cun impacto mínimo na taxa de erro de bit.

Con todo, as maiores potencialidades das TMAs en comunicacións sen fíos están inevitablemente relacionadas coa explotación dos diagramas de harmónicos. O conformado de feixe a través dos harmónicos dunha TMA emprégase para converter a diversidade espacial en diversidade en frecuencia. Asemade, pódese variar a forma dos diagramas de harmónicos mediante os parámetros temporais dos pulsos para acadar, por exemplo, ortogonalidade entre diagramas ou suprimir interferencias [LI 2010a; POLI 2011b; TONG 2012a; POLI 2014; BAROTT 2014]. En calquera caso, estes traballos de investigación non contemplan un aspecto crucial nas prestacións dun sistema de comunicacións: a eficiencia da TMA. Polo tanto, era necesaria unha análise máis ambiciosa, onde non fose suficiente co deseño da forma dos diagramas de harmónicos, senón que ademais se salvagardase a eficiencia da TMA, parámetro directamente relacionado coa relación sinal a ruído no receptor. Con esta motivación, decídese implicar ás TMAs en comunicacións multitraxecto con esvaecemento, considerando escenarios máis realistas, onde múltiples réplicas do sinal (atenuadas e retardadas) inciden na antena con arranxo ós diferentes ángulos do multitraxecto. As conclusións derivadas das investigacións neste novo reto son:

- Modélase un receptor de comunicacións sen fíos que consta dunha TMA que desenvolve un conformado de feixe non lineal seguido dun subsistema MRC (sigla que provén do termo inglés *maximum ratio combiner*) adicado a extraer a diversidade da canle a través da RBL do TMA.
- Derívanse fórmulas pechadas que expresan a taxa de erro de símbolo en función da relación sinal a ruído para o caso da transmisión de sinais dixitais modulados de xeito lineal sobre canles con diversidade tipo Rayleigh. Polo tanto, e de xeito salientable,

exprésase directamente a taxa de erro de símbolo deste receptor baseado en TMA en termos dos parámetros principais da TMA, constituíndo en si mesmo unha ferramenta fundamental para o deseñador.

- Desenvólvese un novo algoritmo de optimización para sintetizar o diagrama de radiación condicionado a unha arquitectura específica da rede de interruptores que permite maximizar a eficiencia total da TMA.
- Compáranse, a modo de referencia, as prestacións deste receptor baseado na técnica TMA, coas mostradas, por unha banda, por un receptor baseado en conformado de feixe lineal simple (e polo tanto sen explotar a diversidade da canle) e, por outra banda, coa ofrecida por un receptor que consta dunha rede de conformado de feixe lineal (tamén equipado cun MRC). Os resultados das simulacións numéricas mostran que o receptor TMA ten a mellor solución de compromiso entre prestacións e complexidade.

Ademáis, nestas investigacións detéctanse certas limitacións dos pulsos rectangulares cando o obxectivo é acadar un conformado de feixe flexible e eficiente mediante TMAs. Estas vulnerabilidades están directamente relacionadas coa resposta en frecuencia dos pulsos rectangulares: un ancho de pulso do lóbulo principal mínimo, un modesto nivel de lóbulo lateral (-13 dB) e unha caída asintótica lenta (primeira orde) dos lóbulos laterais. Este comportamento en frecuencia impón un compromiso entre o número de harmónicos a explotar e a eficiencia da TMA, e pon de manifesto que aínda hai marxe para a mellora de prestacións atopando novas formas de pulso –máis axeitadas que as rectangulares– para o conformado de feixe con TMAs. Consecuentemente, as novas investigacións nesta liña permiten concluír que:

- Proponse e analízase un novo tipo de TMA, acuñando o termo ETMA (do inglés *Enhanced TMA*), cuxas excitacións modúlanse temporalmente mediante pulsos suma de cosenos ponderados no lugar de pulsos rectangulares coma nas TMAs convencionais.
- Desenvólvese un método de síntese para as ETMAs aplicadas ó conformado de feixe. É destacable a súa simplicidade con respecto ós métodos de optimización sistemáticos necesarios para as TMAs convencionais.
- Discútense algunhas posibles estruturas hardware para a implantación de ETMAs e son comparadas tanto coas dos TMAs convencionais como cos correspondentes a agrupacións con redes de conformado de feixe lineais.
- Demóstrase que a modulación temporal con pulsos periódicos suma de cosenos ponderados proporciona unha maior flexibilidade para controlar os diagramas de radiación dos harmónicos e, en consecuencia, mellora tanto a eficiencia en potencia da TMA como a relación sinal a ruído en recepción en comparación cas TMAs convencionais baseadas en pulsos rectangulares.

Appendix B

List of Acronyms

ADC analog-to-digital converter
AM amplitude modulation
AWGN additive white Gaussian noise
ASK amplitude-shift keying
BER bit error ratio
BFN beamforming network
BPSK binary phase shift-keying
CSI channel state information
DAC digital-to-analog converter
DCS digital communication system
DOA direction of arrival
DC Dolph-Chebyshev
DSP digital signal processor
ESD energy spectral density
ETMA enhanced time-modulated array
FM frequency modulation
FSK frequency-shift keying
FT Fourier transform
HPBW half-power beamwidth
ISI inter-symbol interference
LB linear beamformer
LBFN linear beamforming network
LDM linear digital modulation
LFM linearly frequency modulated
MRC maximum ratio combining
MSLL maximum side-lobe level
NMLW normalized main-lobe width
NLOS non-line-of-sight

PDF probability density function
PSK phase-shift keying
PSO particle swarm optimization
QAM qauadrature amplitude modulation
RF radio frequency
RFC Rayleigh fading channel
RPDC Reconfigurable Power Divider/Combiner
SA simulated annealing
SER symbol error ratio
SIMO single input multiple output
SISO single input single output
SLL side-lobe level
SNR signal-to-noise ratio
SP3T single-pole triple-throw
SPDT single-pole double-throw
SPMT single-pole multiple-throw
SPST single-pole single-throw
SR sideband radiation
SWC sum-of-weighted-cosine
STA static array
TM time modulation
TMA time-modulated array
TMRA time-modulated reflector array
VGA variable gain amplifier

References

[AKSOY 2011] E. Aksoy and E. Afacan. "**Generalized representation of sideband radiation power calculation in arbitrarily distributed time-modulated planar and linear arrays**". *Proc. of Progress in Electromagnetics Research Symposium (PIERS 2011)*. Suzhou, China, 2011, pp. 368–371.

[AKSOY 2012] E. Aksoy and E. Afacan. "**Calculation of sideband power radiation in time-modulated arrays with asymmetrically positioned pulses**". *IEEE Antennas and Wireless Propagation Letters*, vol. 11, 2012, pp. 133–136. ISSN: 1536-1225.
DOI: 10.1109/LAWP.2012.2185916.

[AKSOY 2014] E. Aksoy and E. Afacan. "**An inequality for the calculation of relative maximum sideband level in time-modulated linear and planar arrays**". *IEEE Transactions on Antennas and Propagation*, vol. 62, no. 6, 2014, pp. 3392–3397. ISSN: 0018-926X.
DOI: 10.1109/TAP.2014.2311470.

[BALANIS 2005] C. Balanis. ***Antenna Theory: Analysis and Design***. 3rd. Wiley-Interscience, 2005.

[BALDERAS 2016] L. I. Balderas, A. Reyna, and M. A. Panduro. "**Time-modulated concentric ring antenna array for a wide coverage pattern**". *Proc. of 2016 IEEE International Symposium on Antennas and Propagation and USNC-URSI Radio Science Meeting (2016 IEEE AP-S & USNC-URSI)*. Fajardo, Puerto Rico, 2016, pp. 709–710.
DOI: 10.1109/APS.2016.7696063.

[BAROTT 2014] W. C. Barott and B. Himed. "**Time-modulated array pattern for sidelobe blanking in spectrometry and radar**". *IEEE Antennas and Wireless Propagation Letters*, vol. 13, 2014, pp. 1015–1018. ISSN: 1536-1225.
DOI: 10.1109/LAWP.2014.2323351.

[BEKELE 2013] E. T. Bekele, L. Poli, P. Rocca, M. D'Urso, and A. Massa. "**Pulse-shaping strategy for time modulated arrays –analysis and design**". *IEEE Transactions on Antennas and Propagation*, vol. 61, no. 7, 2013, pp. 3525–3537. ISSN: 0018-926X.
DOI: 10.1109/TAP.2013.2256096.

[BOGDAN 2016a] G. Bogdan, M. Jarzynka, and Y. Yashchyshyn. "**Experimental study of signal reception by means of time-modulated antenna array**". *Proc. of 2016 21st International Conference on Microwave, Radar and Wireless Communications (MIKON)*. 2016, pp. 1–4. DOI: 10.1109/MIKON.2016.7492030.

[BOGDAN 2016b] G. Bogdan, Y. Yashchyshyn, and M. Jarzynka. "**Time-modulated antenna array with lossless switching network**". *IEEE Antennas and Wireless Propagation Letters*, vol. PP, no. 99, 2016, pp. 1–1. ISSN: 1536-1225. DOI: 10.1109/LAWP.2016.2538463.

[BRÉGAINS 2008] J. C. Brégains, J. Fondevila-Gómez, G. Franceschetti, and F. Ares. "**Signal radiation and power losses of time-modulated arrays**". *IEEE Transactions on Antennas and Propagation*, vol. 56, no. 6, 2008, pp. 1799–1804. ISSN: 0018-926X. DOI: 10.1109/TAP.2008.923345.

[CHEN 2016a] J. Chen, X. Liang, R. Jin, J. Geng, C. He, and P. Li. "**Efficiency improvement for time modulated antenna arrays**". *Proc. of 2016 IEEE International Symposium on Antennas and Propagation and USNC-URSI Radio Science Meeting (2016 IEEE AP-S & USNC-URSI)*. Fajardo, Puerto Rico, 2016.

[CHEN 2016b] J. Chen, X. Liang, R. Jin, J. Geng, C. He, and P. Li. "**Efficiency improvement for time modulated antenna arrays**". *Proc. of 2016 IEEE International Symposium on Antennas and Propagation and USNC-URSI Radio Science Meeting (2016 IEEE AP-S & USNC-URSI)*. Fajardo, Puerto Rico, 2016.

[EUZIÈRE 2014] J. Euzière, R. Guinvarc'h, B. Uguen, and R. Gillard. "**Optimization of sparse time-modulated array by genetic algorithm for radar applications**". *IEEE Antennas and Wireless Propagation Letters*, vol. 13, 2014, pp. 161–164. ISSN: 1536-1225. DOI: 10.1109/LAWP.2014.2299285.

[EUZIÈRE 2015] J. Euzière, R. Guinvar'h, I. Hinostroza, B. Uguen, and R. Gillard. "**Time modulated array for dual function radar and communication**". *Proc. of 2015 IEEE International Symposium on Antennas and Propagation USNC/URSI National Radio Science Meeting*. Vancouver, BC, Canada, 2015, pp. 806–807. DOI: 10.1109/APS.2015.7304790.

[EUZIÈRE 2016] J. Euzière, R. Guinvar'h, I. Hinostroza, B. Uguen, and R. Gillard. "**Optimizing communication in TMA for radar**". *Proc. of 2016 IEEE International Symposium on Antennas and Propagation and USNC-URSI Radio Science Meeting (2016 IEEE AP-S & USNC-URSI)*. Fajardo, Puerto Rico, 2016, pp. 705–706. DOI: 10.1109/APS.2016.7696061.

[FONDEVILA 2004] J. Fondevila, J. C. Brégains, F. Ares, and E. Moreno. "**Optimizing uniformly excited linear arrays through time modulation**". *IEEE Antennas and Wireless Propagation Letters*, vol. 3, no. 1, 2004, pp. 298–301. ISSN: 1536-1225.
DOI: 10.1109/LAWP.2004.838833.

[FONDEVILA 2006] J. Fondevila, J. C. Brégains, F. Ares, and E. Moreno. "**Application of time modulation in the synthesis of sum and difference patterns by using linear arrays**". *Microwave and Optical Technology Letters*, vol. 48, no. 5, 2006, pp. 829–832.
DOI: 10.1002/mop.21489.

[GOLDSMITH 2005] A. Goldsmith. ***Wireless Communications***. Cambridge University Press, 2005. ISBN: 9780521837163.

[GUO 2015] J. Guo, S. Yang, Q. Zhu, and Z.-P. Nie. "**4D antenna arrays for LFM signal transmission**". *Proc. of 2015 IEEE International Symposium on Antennas and Propagation USNC/URSI National Radio Science Meeting*. Vancouver, BC, Canada, 2015, pp. 820–821.
DOI: 10.1109/APS.2015.7304797.

[GUO 2016] J. Guo, S. Yang, and Y. Chen. "**Efficient sideband suppression in 4d antenna arrays with multiple time modulation frequencies**". *Proc. of 2016 IEEE International Symposium on Antennas and Propagation and USNC-URSI Radio Science Meeting (2016 IEEE AP-S & USNC-URSI)*. Fajardo, Puerto Rico, 2016, pp. 699–700.
DOI: 10.1109/APS.2016.7696058.

[HANNAN 2016] M. A. Hannan, L. Poli, P. Rocca, and A. Massa. "**Pulse sequence optimization in time-modulated arrays for secure communications**". *Proc. of 2016 IEEE International Symposium on Antennas and Propagation and USNC-URSI Radio Science Meeting (2016 IEEE AP-S & USNC-URSI)*. Fajardo, Puerto Rico, 2016, pp. 695–696.
DOI: 10.1109/APS.2016.7696056.

[HE 2013] C. He, A. Cao, X. Liang, R. Jin, and J. Geng. "**Beamforming method with periodical amplitude modulation array**". *Proc. of 2013 IEEE Antennas and Propagation Society International Symposium (APSURSI)*. 2013, pp. 874–875.
DOI: 10.1109/APS.2013.6711096.

[HE 2015a] C. He, X. Liang, Z. Li, J. Geng, and R. Jin. "**Direction finding by time-modulated array with harmonic characteristic analysis**". *IEEE Antennas and Wireless Propagation Letters*, vol. 14, 2015, pp. 642–645. ISSN: 1536-1225.
DOI: 10.1109/LAWP.2014.2373432.

[HE 2015b] C. He, H. Yu, X. Liang, J. Geng, and R. Jin. "**Sideband radiation level suppression in time-modulated array by nonuniform period modulation**". *IEEE Antennas and Wireless Propagation Letters*, vol. 14, 2015, pp. 606–609. ISSN: 1536-1225.
DOI: 10.1109/LAWP.2014.2373639.

[HE 2015c] C. He, X. Liang, B. Zhou, J. Geng, and R. Jin. "**Space-division multiple access based on time-modulated array**". *IEEE Antennas and Wireless Propagation Letters*, vol. 14, 2015, pp. 610–613. ISSN: 1536-1225.
DOI: 10.1109/LAWP.2014.2373431.

[HEATH 2016] R. W. Heath, N. González-Prelcic, S. Rangan, W. Roh, and A. M. Sayeed. "**An overview of signal processing techniques for millimeter wave MIMO systems**". *IEEE Journal of Selected Topics in Signal Processing*, vol. 10, no. 3, 2016, pp. 436–453. ISSN: 1932-4553.
DOI: 10.1109/JSTSP.2016.2523924.

[KAY 1998] S. M. Kay. ***Fundamentals of Statistical Signal Processing, Detection Theory. Vol II***. 1st. Prentice Hall, 1998.

[KUMMER 1963] W. H. Kummer, A. T. Villeneuve, T. Fong, and F. Terrio. "**Ultra-low sidelobes from time-modulated arrays**". *IEEE Transactions on Antennas and Propagation*, vol. 11, no. 6, 1963, pp. 633–639.
DOI: 10.1109/TAP.1963.1138102.

[LI 2009a] G. Li, S. Yang, Y. Chen, and Z.-P. Nie. "**A novel electronic beam steering technique in time modulated antenna array**". *Progress In Electromagnetics Research*, vol. 97, 2009, pp. 391–405. ISSN: 1070-4698.
DOI: 10.2528/PIER09072602.

[LI 2009b] G. Li, S. Yang, and Z. Nie. "**A study on the application of time modulated antenna arrays to airborne pulsed doppler radar**". *IEEE Transactions on Antennas and Propagation*, vol. 57, no. 5, 2009, pp. 1579–1583. ISSN: 0018-926X.
DOI: 10.1109/TAP.2009.2016788.

[LI 2009c] G. Li, S. Yang, Z. Zhao, and Z.-P. Nie. "**A study of AM and FM signal reception of time modulated linear antenna arrays**". *Progress In Electromagnetics Research Letters*, vol. 7, 2009, pp. 171–181.
DOI: 10.2528/PIERL09030801.

[LI 2010a] G. Li, S. Yang, Y. Chen, and Z. Nie. "**A hybrid analog-digital adaptive beamforming in time-modulated linear arrays**". *Electromagnetics*, vol. 30, no. 4, 2010, pp. 356–364.
DOI: 10.1080/02726341003712608.

[LI 2010b] G. Li, S. Yang, and Z. Nie. "**Direction of arrival estimation in time modulated linear arrays with unidirectional phase center motion**". *IEEE Transactions on Antennas and Propagation*, vol. 58, no. 4, 2010, pp. 1105–1111. ISSN: 0018-926X.
DOI: 10.1109/TAP.2010.2041313.

[M K SIMON 2005] M. A. M. K. Simon. ***Digital Communication over Fading Channels***. 2nd. Wiley, 2005.

[MANDAL 2011] S. K. Mandal, R. Ghatak, and G. K. Mahanti. "**Minimization of side lobe level and side band radiation of a uniformly excited time modulated linear antenna array by using artificial bee colony algorithm**". *Proc. of 2011 IEEE Symposium on Industrial Electronics and Applications (ISIEA)*. Langkawi, Malaysia, 2011, pp. 247–250.
DOI: 10.1109/ISIEA.2011.6108708.

[MANDAL 2013] S. K. Mandal, G. K. Mahanti, and R. Ghatak. "**Differential evolution algorithm for optimizing the conflicting parameters in time-modulated linear array antennas**". *Progress In Electromagnetics Research B*, vol. 51, 2013, pp. 101–118.
DOI: 10.2528/PIERB13022710.

[MANEIROCATOIRA 2014a] R. Maneiro-Catoira, J. Brégains, J. A. García-Naya, and L. Castedo. "**On the feasibility of time-modulated arrays for digital linear modulations: a theoretical analysis**". *IEEE Transactions on Antennas and Propagation*, vol. 62, no. 12, 2014, pp. 6114–6122. ISSN: 0018-926X.
DOI: 10.1109/TAP.2014.2365827.

[MANEIROCATOIRA 2014b] R. Maneiro-Catoira, J. Brégains, J. A. García-Naya, and L. Castedo. "**Time-modulated arrays for digital communications**". *Proc. of IEEE International Symposium on Antennas and Propagation and USNC-URSI Radio Science Meeting (2014 IEEE AP-S and USNC-URSI)*. Memphis, Tennessee, USA, 2014, pp. 1760–1761.
DOI: 10.1109/APS.2014.6905206.

[MANEIROCATOIRA 2015a] R. Maneiro-Catoira, J. Brégains, J. A. García-Naya, and L. Castedo. "**Impact of time-modulated arrays on the BER of linear digital modulations**". *Journal of Electromagnetic Waves and Applications*, vol. 29, no. 16, 2015, pp. 2147–2154. ISSN: 0920-5071.
DOI: 10.1080/09205071.2015.1075908.

[MANEIROCATOIRA 2015b] R. Maneiro-Catoira, J. Brégains, J. A. García-Naya, and L. Castedo. "**Time-modulated arrays for digital communications in multipath scenarios**". *Proc. of 2015 IEEE International Symposium on Antennas and Propagation and North American Radio Science Meeting (2015 IEEE AP-S & USNC-URSI)*. Vancouver, BC, Canada, 2015, pp. 816–817. ISBN: 9781479978168.
DOI: 10.1109/APS.2015.7304795.

[MANEIROCATOIRA 2016] R. Maneiro-Catoira, J. Brégains, J. A. García-Naya, and L. Castedo. "**Time-modulated arrays with sum of weighted cosine pulses**". *Proc. of 2016 IEEE International Symposium on Antennas and Propagation and USNC-URSI Radio Science Meeting (2016 IEEE AP-S & USNC-URSI)*. Fajardo, Puerto Rico, 2016, pp. 697–698.
DOI: 10.1109/APS.2016.7696057.

[MANEIROCATOIRA 2017a] R. Maneiro-Catoira, J. Brégains, J. A. García-Naya, and L. Castedo. "**Enhanced time-modulated arrays for harmonic beamforming**". *IEEE Journal of Selected Topics in Signal Processing*, vol. 11, no. 2, 2017, pp. 259–270. ISSN: 1932-4553. DOI: 10.1109/jstsp.2016.2627178.

[MANEIROCATOIRA 2017b] R. Maneiro-Catoira, J. Brégains, J. A. García-Naya, and L. Castedo. "**Frequency-domain synthesis of time-modulated arrays**". *Proc. of 2017 IEEE International Symposium on Antennas and Propagation & USNC/URSI National Radio Science Meeting (accepted for publication)*. San Diego, California, USA, 2017.

[MANEIROCATOIRA 2017c] R. Maneiro-Catoira, J. Brégains, J. A. García-Naya, and L. Castedo. "**Time modulated arrays: from their origin to their utilization in wireless communication systems**". *Sensors*, vol. 17, no. 3, 2017. ISSN: 1424-8220. DOI: 10.3390/s17030590.

[MANEIROCATOIRA 2017d] R. Maneiro-Catoira, J. Brégains, J. A. García-Naya, L. Castedo, P. Rocca, and L. Poli. "**Performance analysis of time-modulated arrays for the angle diversity reception of digital linear modulated signals**". *IEEE Journal of Selected Topics in Signal Processing*, vol. 11, no. 2, 2017, pp. 247–258. ISSN: 1932-4553. DOI: 10.1109/JSTSP.2016.2609852.

[MANICA 2009] L. Manica, P. Rocca, L. Poli, and A. Massa. "**Almost time-independent performance in time-modulated linear arrays**". *IEEE Antennas and Wireless Propagation Letters*, vol. 8, 2009, pp. 843–846. ISSN: 1536-1225. DOI: 10.1109/LAWP.2009.2027452.

[MASOTTI 2013] D. Masotti, P. Francia, A. Costanzo, and V. Rizzoli. "**Rigorous electromagnetic / circuit-level analysis of time-modulated linear arrays**". *IEEE Transactions on Antennas and Propagation*, vol. 61, no. 11, 2013, pp. 5465–5474. ISSN: 0018-926X. DOI: 10.1109/TAP.2013.2279217.

[MASOTTI 2016] D. Masotti, A. Costanzo, M. D. Prete, and V. Rizzoli. "**Time-modulation of linear arrays for real-time reconfigurable wireless power transmission**". *IEEE Transactions on Microwave Theory and Techniques*, vol. 64, no. 2, 2016, pp. 331–342. ISSN: 0018-9480. DOI: 10.1109/TMTT.2015.2512275.

[MÉNDEZRIAL 2016] R. Méndez-Rial, C. Rusu, N. González-Prelcic, A. Alkhateeb, and R. W. Heath. "**Hybrid MIMO architectures for millimeter wave communications: Phase shifters or switches?**" *IEEE Access*, vol. 4, 2016, pp. 247–267. ISSN: 2169-3536. DOI: 10.1109/ACCESS.2015.2514261.

[MINICIRCUITS 2017] MiniCircuits. *MiniCircuits*. http://www.minicircuits.com. 2017.

[NUTTALL 1981] A. Nuttall. "**Some windows with very good sidelobe behavior**". *IEEE Transactions on Acoustics, Speech, and Signal Processing*, vol. 29, no. 1, 1981, pp. 84–91. ISSN: 0096-3518.
DOI: 10.1109/TASSP.1981.1163506.

[POLI 2010a] L. Poli, P. Rocca, L. Manica, and A. Massa. "**Handling sideband radiations in time-modulated arrays through particle swarm optimization**". *IEEE Transactions on Antennas and Propagation*, vol. 58, no. 4, 2010, pp. 1408–1411. ISSN: 0018-926X.
DOI: 10.1109/TAP.2010.2041165.

[POLI 2010b] L. Poli, P. Rocca, L. Manica, and A. Massa. "**Pattern synthesis in time-modulated linear arrays through pulse shifting**". *IET Microwaves, Antennas Propagation*, vol. 4, no. 9, 2010, pp. 1157–1164. ISSN: 1751-8725.
DOI: 10.1049/iet-map.2009.0042.

[POLI 2010c] L. Poli, P. Rocca, L. Manica, and A. Massa. "**Time modulated planar arrays - analysis and optimisation of the sideband radiations**". *IET Microwaves, Antennas Propagation*, vol. 4, no. 9, 2010, pp. 1165–1171. ISSN: 1751-8725.
DOI: 10.1049/iet-map.2009.0379.

[POLI 2011a] L. Poli, P. Rocca, G. Oliveri, and A. Massa. "**Adaptive nulling in time-modulated linear arrays with minimum power losses**". *IET Microwaves, Antennas Propagation*, vol. 5, no. 2, 2011, pp. 157–166. ISSN: 1751-8725.
DOI: 10.1049/iet-map.2010.0015.

[POLI 2011b] L. Poli, P. Rocca, G. Oliveri, and A. Massa. "**Harmonic beamforming in time-modulated linear arrays**". *IEEE Transactions on Antennas and Propagation*, vol. 59, no. 7, 2011, pp. 2538–2545. ISSN: 0018-926X.
DOI: 10.1109/TAP.2011.2152323.

[POLI 2014] L. Poli, T. Moriyama, and P. Rocca. "**Pulse splitting for harmonic beamforming in time- modulated linear arrays**". *International Journal of Antennas and Propagation*, vol. 2014, no. 1, 2014, pp. 1–9. ISSN: 1687-5869.
DOI: 10.1155/2014/797590.

[PRABHU 2014] K. M. M. Prabhu. ***Window Functions and their Applications in Signal Processing***. 1st. CRC Press, Taylor & Francis Group, 2014.

[PROAKIS 2008] J. G. Proakis. ***Digital Communications***. 5th. McGraw-Hill, 2008.

[RENZO 2014] M. D. Renzo, H. Haas, A. Ghrayeb, S. Sugiura, and L. Hanzo. "**Spatial modulation for generalized MIMO: challenges, opportunities, and implementation**". *Proceedings of the IEEE*, vol. 102, no. 1, 2014, pp. 56–103. ISSN: 0018-9219.
DOI: 10.1109/JPROC.2013.2287851.

[ROCCA 2012a] P. Rocca, L. Poli, and A. Massa. "**Instantaneous directivity optimisation in time-modulated array receivers**". *IET Microwaves, Antennas Propagation*, vol. 6, no. 14, 2012, pp. 1590–1597. ISSN: 1751-8725.
DOI: 10.1049/iet-map.2012.0400.

[ROCCA 2012b] P. Rocca, L. Poli, G. Oliveri, and A. Massa. "**Adaptive nulling in time-varying scenarios through time-modulated linear arrays**". *IEEE Antennas and Wireless Propagation Letters*, vol. 11, 2012, pp. 101–104. ISSN: 1536-1225.
DOI: 10.1109/LAWP.2012.2183849.

[ROCCA 2014] P. Rocca, Q. Zhu, E. T. Bekele, S. Yang, and A. Massa. "**4-D arrays as enabling technology for cognitive radio systems**". *IEEE Transactions on Antennas and Propagation*, vol. 62, no. 3, 2014, pp. 1102–1116. ISSN: 0018-926X.
DOI: 10.1109/TAP.2013.2288109.

[ROCCA 2016] P. Rocca, G. Oliveri, R. J. Mailloux, and A. Massa. "**Unconventional phased array architectures and design methodologies — a review**". *Proceedings of the IEEE*, vol. 104, no. 3, 2016, pp. 544–560. ISSN: 0018-9219.
DOI: 10.1109/JPROC.2015.2512389.

[SHANKS 1959] H. Shanks and R. Bickmore. "**Four-dimensional electromagnetic radiators**". *Canadian Journal of Physics*, vol. 37, no. 3, 1959, pp. 263–275.
DOI: 10.1139/p59-031.

[SHANKS 1961] H. Shanks. "**A new technique for electronic scanning**". *IRE Transactions on Antennas and Propagation*, vol. 9, no. 2, 1961, pp. 162–166. ISSN: 0096-1973.
DOI: 10.1109/TAP.1961.1144965.

[SIMON 1998a] M. K. Simon and M.-S. Alouini. "**A unified approach to the performance analysis of digital communication over generalized fading channels**". *Proceedings of the IEEE*, vol. 86, no. 9, 1998, pp. 1860–1877. ISSN: 0018-9219.
DOI: 10.1109/5.705532.

[SIMON 1998b] M. K. Simon and D. Divsalar. "**Some new twists to problems involving the gaussian probability integral**". *IEEE Transactions on Communications,* vol. 46, no. 2, 1998, pp. 200–210. ISSN: 0090-6778.
DOI: 10.1109/26.659479.

[SKLAR 2001] B. Sklar. ***Digital Communications***. 2nd. Prentice Hall, 2001.

[STEYSKAL 1983] H. Steyskal. "**Simple method for pattern nulling by phase perturbation**". *IEEE Transactions on Antennas and Propagation*, vol. 31, no. 1, 1983, pp. 163–166. ISSN: 0018-926X.
DOI: 10.1109/TAP.1983.1142994.

[TENNANT 2008] A. Tennant and B. Chambers. "**Control of the harmonic radiation patterns of time-modulated antenna arrays**". *Proc. of 2008 IEEE Antennas and Propagation Society International Symposium*. San Diego, CA, USA, 2008, pp. 1–4.
DOI: 10.1109/APS.2008.4619900.

[TENNANT 2009] A. Tennant and B. Chambers. "**Time-switched array analysis of phase-switched screens**". *IEEE Transactions on Antennas and Propagation*, vol. 57, no. 3, 2009, pp. 808–812. ISSN: 0018-926X.
DOI: 10.1109/TAP.2009.2013448.

[TENNANT 2010] A. Tennant. "**Experimental two-element time-modulated direction finding array**". *IEEE Transactions on Antennas and Propagation*, vol. 58, no. 3, 2010, pp. 986–988. ISSN: 0018-926X.
DOI: 10.1109/TAP.2009.2039301.

[TONG 2010] Y. Tong and A. Tennant. "**Simultaneous control of sidelobe level and harmonic beam steering in time-modulated linear arrays**". *Electronics Letters*, vol. 46, no. 3, 2010, pp. 201–202. ISSN: 0013-5194.
DOI: 10.1049/el.2010.2629.

[TONG 2011] Y. Tong and A. Tennant. "**Reduced sideband levels in time-modulated arrays using half-power sub-arraying techniques**". *IEEE Transactions on Antennas and Propagation*, vol. 59, no. 1, 2011, pp. 301–303. ISSN: 0018-926X.
DOI: 10.1109/TAP.2010.2090484.

[TONG 2012a] Y. Tong and A. Tennant. "**A two-channel time modulated linear array with adaptive beamforming**". *IEEE Transactions on Antennas and Propagation*, vol. 60, no. 1, 2012, pp. 141–147. ISSN: 0018-926X.
DOI: 10.1109/TAP.2011.2167936.

[TONG 2012b] Y. Tong and A. Tennant. "**Sideband level suppression in time-modulated linear arrays using modified switching sequences and fixed bandwidth elements**". *Electronics Letters*, vol. 48, no. 1, 2012, pp. 10–11. ISSN: 0013-5194.
DOI: 10.1049/el.2011.2378.

[TSE 2005] D. Tse and P. Viswanath. ***Fundamentals of wireless communication***. Cambridge University Press, 2005.

[WANG 2012] Y. Wang and A. Tennant. "**Time-modulated reflector array**". *Electronics Letters*, vol. 48, no. 16, 2012, pp. 972–974. ISSN: 0013-5194.
DOI: 10.1049/el.2012.1893.

[WANG 2014] Y. Wang and A. Tennant. "**Experimental time-modulated reflector array**". *IEEE Transactions on Antennas and Propagation*, vol. 62, no. 12, 2014, pp. 6533–6536. ISSN: 0018-926X.
DOI: 10.1109/TAP.2014.2362129.

[WANG 2016] Y. Wang, F. Lin, and A. Tennant. "**Increasing the energy efficiency of time-modulated reflector-arrays using double layer designs**". *Proc. of 2016 10th European Conference on Antennas and Propagation (EuCAP)*. Davos, Switzerland, 2016, pp. 1–5.
DOI: 10.1109/EuCAP.2016.7481629.

[YANG 2002] S. Yang, Y.-B. Gan, and A. Qing. "**Sideband suppression in time-modulated linear arrays by the differential evolution algorithm**". *IEEE Antennas and Wireless Propagation Letters*, vol. 1, no. 1, 2002, pp. 173–175. ISSN: 1536-1225.
DOI: 10.1109/LAWP.2002.807789.

[YANG 2003] S. Yang, Y.-B. Gan, and T. P. Khiang. "**A new technique for power-pattern synthesis in time-modulated linear arrays**". *IEEE Antennas and Wireless Propagation Letters*, vol. 2, no. 1, 2003, pp. 285–287. ISSN: 1536-1225.
DOI: 10.1109/LAWP.2003.821556.

[YANG 2004] S. Yang, Y. Gan, and P. Tan. "**Evaluation of directivity and gain for time-modulated linear antenna arrays**". *Microwave Optical Technology Letters*, vol. 42 2, 2004, pp. 167–171.
DOI: 10.1002/mop.20241.

[YANG 2005a] S. Yang, Y.-B. Gan, A. Qing, and P. K. Tan. "**Design of a uniform amplitude time modulated linear array with optimized time sequences**". *IEEE Transactions on Antennas and Propagation*, vol. 53, no. 7, 2005, pp. 2337–2339. ISSN: 0018-926X.
DOI: 10.1109/TAP.2005.850765.

[YANG 2005b] S. Yang, Z. Nie, and F. Yang. "**Synthesis of low sidelobe planar antenna arrays with time modulation**". *Proc. of 2005 Asia-Pacific Microwave Conference Proceedings*. Vol. 3. Suzhou, China, 2005, pp. 1–3.
DOI: 10.1109/APMC.2005.1606682.

[YAO 2015a] A. M. Yao, W. Wu, and D. G. Fang. "**Efficient and effective full-wave analysis of the instantaneous and average behaviors of time-modulated arrays**". *IEEE Transactions on Antennas and Propagation*, vol. 63, no. 7, 2015, pp. 2902–2913. ISSN: 0018-926X.
DOI: 10.1109/TAP.2015.2421943.

[YAO 2015b] A. M. Yao, W. Wu, and D. G. Fang. "**Single-sideband time-modulated phased array**". *IEEE Transactions on Antennas and Propagation*, vol. 63, no. 5, 2015, pp. 1957–1968. ISSN: 0018-926X.

[YAO 2016a] A. M. Yao, W. Wu, and D. G. Fang. "**Frequency diverse array antenna using time-modulated optimized frequency offset to obtain time-invariant spatial fine focusing beampattern**". *IEEE Transactions on Antennas and Propagation*, vol. 64, no. 10, 2016, pp. 4434–4446. ISSN: 0018-926X.
DOI: 10.1109/TAP.2016.2594075.

[YAO 2016b] A. M. Yao, W. Wu, and D. G. Fang. "**Study on reconfigurable coaperture antenna arrays based on time-modulation and retrodirective techniques**". *IEEE Transactions on Antennas and Propagation*, vol. 64, no. 5, 2016, pp. 1713–1724. ISSN: 0018-926X.
DOI: 10.1109/TAP.2016.2540660.

[YASHCHYSHYN 2015] Y. Yashchyshyn, K. Derzakowski, P. R. Bajurko, J. Marczewski, and S. Kozłowski. "**Time-modulated reconfigurable antenna based on integrated S-PIN diodes for mm-Wave communication systems**". *IEEE Transactions on Antennas and Propagation*, vol. 63, no. 9, 2015, pp. 4121–4131. ISSN: 0018-926X.
DOI: 10.1109/TAP.2015.2444425.

[YAVUZ 2015] Y. Yavuz, M. Karahan, and E. Aksoy. "**A dual channel AM receiver structure in 4D arrays**". *Proc. of 2015 IEEE International Symposium on Antennas and Propagation USNC/URSI National Radio Science Meeting*. Vancouver, BC, Canada, 2015, pp. 804–805.
DOI: 10.1109/APS.2015.7304789.

[ZHU 2012a] Q. Zhu, S. Yang, L. Zheng, and Z. Nie. "**Design of a low sidelobe time modulated linear array with uniform amplitude and sub-sectional optimized time steps**". *IEEE Transactions on Antennas and Propagation*, vol. 60, no. 9, 2012, pp. 4436–4439. ISSN: 0018-926X.
DOI: 10.1109/TAP.2012.2207082.

[ZHU 2012b] Q. Zhu, S. Yang, R. Yao, and Z. Nie. "**Gain improvement in time-modulated linear arrays using SPDT switches**". *IEEE Antennas and Wireless Propagation Letters*, vol. 11, 2012, pp. 994–997. ISSN: 1536-1225.
DOI: 10.1109/LAWP.2012.2213292.

[ZHU 2013] Q. Zhu, S. Yang, R. Yao, M. Huang, and Z.-P. Nie. "**Unified time- and frequency-domain study on time-modulated arrays**". *IEEE Transactions on Antennas and Propagation*, vol. 61, no. 6, 2013, pp. 3069–3076. ISSN: 0018-926X.
DOI: 10.1109/TAP.2013.2253538.

[ZHU 2014] Q. Zhu, S. Yang, R. Yao, and Z. Nie. "**Directional modulation based on 4-D antenna arrays**". *IEEE Transactions on Antennas and Propagation*, vol. 62, no. 2, 2014, pp. 621–628. ISSN: 0018-926X.
DOI: 10.1109/TAP.2013.2290122.

[ZHU 2015] Q. Zhu, S. Yang, P. Rocca, and Z. Nie. "**Signal-to-noise ratio and time-modulated signal spectrum in four-dimensional antenna arrays**". *IET Microwaves, Antennas Propagation*, vol. 9, no. 3, 2015, pp. 264–270. ISSN: 1751-8725.
DOI: 10.1049/iet-map.2014.0199.